Capstone Project Report:

Design and Manufacture of a Cross-Flow Helical Tidal Turbine

Josh Anderson   Bronwyn Hughes   Celestine Johnson

Nick Stelzenmuller   Leonardo Sutanto   Brett Taylor

In cooperation with Adam Niblick and Eamon McQuaide

Supervised by: Alberto Aliseda and Brian Polagye

June 14, 2011

Contents

List of Figures

Abstract

The Mechanical Engineering Department at the University of Washington is developing a hydrokinetic turbine as a power source for oceanographic monitoring equipment with the aim of significantly reducing the present power source system costs. For this purpose a helical-blade cross-flow turbine (Gorlov turbine) will be utilized to power batteries connected to an array of oceanographic instruments requiring 20 W of continuous electrical power. The 1 m height by 0.75 m diameter turbine device will operate at depths of about 100 m in Puget Sound, Washington. This ongoing project entails design selections and engineering for the turbine device, the supporting framework, and the energy conversion system. Due to limited availability of published literature on about Gorlov turbine design details, scale model testing of three devices was used to select a four bladed turbine with a, 0.3 solidity ratio for the helical turbine configuration. Design selections and engineering analysis were used to identify the turbine blade material as a composite made up of fiberglass and vinyl ester resin; the framework spoke material as 5086 aluminum; and a blade-spoke attachment design using titanium bolts. The first set of blades was constructed, but, due to method inaccuracies, will need to be fabricated again after a review of the construction process. The aspects of the overall project presented in this report are: tidal turbine background and hydrodynamics, details pertaining to the Gorlov turbine design, model testing details, analytical modeling for design selections, the blade manufacturing process, framework and spoke details, and economic and social considerations.

1 Introduction

1.1 Tidal Energy

The gravitational pull of the Sun and the Moon on the oceans produces a predicable rise and fall in sea level. Coastal bathymetry can translate this regular rise and fall into tidal currents, for example the filling and draining of tidal estuaries as the tides rise and fall. Areas of the world with large tidal ranges and appropriate coastline geometry see significant tidal currents that occur at predictable intervals. Some of the energy in this flow can be extracted by tidal turbines placed in the flow, in a way closely analogous to wind power. The power in the flow is $\frac{1}{2}\rho A U^3$ where A is the area perpendicular to the flow that is swept by the turbine, ρ is the density of the fluid, and U is the free-stream velocity of the fluid. Water is approximately 1000 times denser than air, and so the power in flowing water is proportionately greater than the power in wind. Additionally, tidal currents are predicable, a key attribute often missing from other renewable energy resources such as wind and solar energy. Tidal energy has three primary obstacles to large-scale development. The first is the inherent limits of the resource—sites with large current velocities are relatively rare world-wide, and because power is proportional to U^3 slower tidal currents are not suitable for energy extraction. The second is the extremely harsh nature of the operating environment. Corrosion, biofouling, lack of easy access to the turbines, and the expense of undersea cabling pose large engineering challenges. The third obstacle to development is the lack of knowledge of environmental effects of tidal energy projects. Areas of high quality tidal resource are often sensitive marine ecosystems that are heavily protected. Research to understand the effects of

tidal turbine and tidal energy extraction on the environment is ongoing.

1.2 Project Background

Puget Sound in Washington State has tidal energy potential that is currently being investigated by the Northwest National Marine Renewable Energy Center (NNMREC) and Snohomish Public Utility District [1] . This research attempts to characterize energy extraction potential at specific sites and the effects of tidal energy extraction on the environment. As part of this research program a number of oceanographic instruments that measure current velocity, acoustic signals, temperature, etc., as well as the associated data storage and batteries, have been deployed on a fiberglass tripod at various locations on the sea bottom. This tripod with instruments, known as a Sea Spider, is deployed for months at a time. The key factor limiting both deployment time and instrument sampling rate is instrument battery life. Batteries are a large expense, and retrieving and redeploying the Sea Spider in order to change the batteries is an even larger expense. The high cost of electricity due to the cost associated with the batteries, in addition to the availability of the tidal current, makes a small scale tidal turbine mounted on the Sea Spider an attractive option. A tidal turbine on the Sea Spider could charge a small battery bank during periods of tidal current above the cut-in speed of the turbine (0.5-1 m/s)—extending Sea Spider deployment times and allowing increased instrument sampling rates. The capstone design project described in this report is the desig and manufacture of a helical cross-flow tidal turbine to achieve this goal.

1.3 Hydrodynamics of Cross-Flow Turbines

Due to the relatively recent interest in tidal energy conversion, comprehensive theoretical analysis methods for turbine behavior in water are yet to be developed. Methods presently employed include application of wind turbine analysis techniques; information available on marine propellers [11]; analysis used in the aeronautical industry for foil shape lift and drag considerations, for example the XFoil computer program; and various Computational Fluid Dynamic (CFD) tools, for example Fluent as discussed by Antheaume et. al. [9]. These analytical tools have merit as valuable approximations and can offer some well founded fundamentals.

Wind turbine analysis typically starts by applying mass balances, energy balances (in the form of Bernoulli's equations) and momentum equations. With a number of simplifying assumptions this can result in the well known Betz limit for efficiency of 59% and the equation for the power generated per unit cross-sectional area of the turbine $P = \frac{1}{2}\rho v(u^2 - v^2)$ where P is the power; ρ is the fluid density; v is the fluid velocity at the turbine; and u is the fluid velocity upstream of the turbine, as presented by Garrett and Cummins [15]. This result is based on the pressure difference caused by the turbine in the fluid flow, with optimal turbine interference clearly somewhere in the range between no interference and total blockage by the turbine. Garrett and Cummins conclude "...it not being possible to derive a general result for the maximum value."[15], and consequently alludes to the limits of applying wind turbine analysis to tidal turbines. These limits are due to the fundamental difference that "...tidal power generation requires both head and current."[15], and, as listed by Batten et al, "Particular differences entail changes in Reynolds number, different stall characteristics and the possible
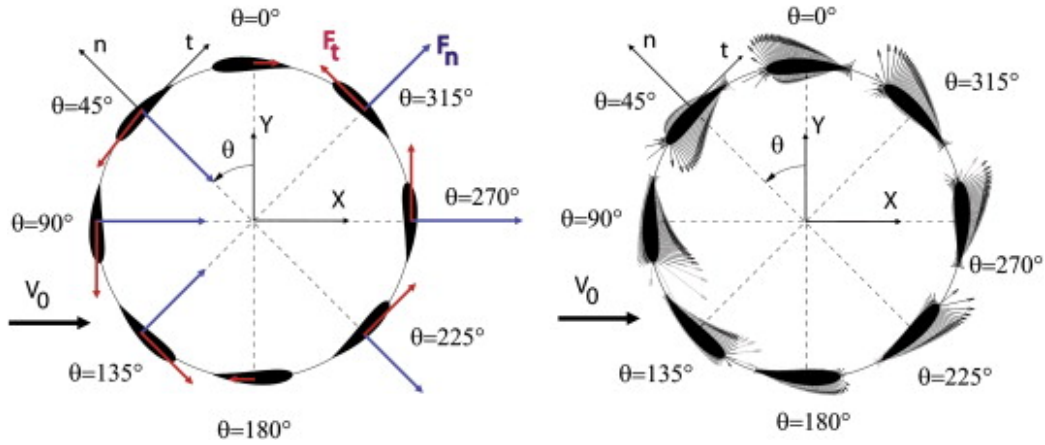
Figure 1: Schematics of forces and pressure vectors on an airfoil in a cross flow turbine. From Zanette et. al. [28]

occurrence of cavitation."[11]. The Blade Element Momentum (BEM) theory is a method of analysis that divides the turbine blades into segments that can each be approximately assessed in a 2D fluid flow. The sum of all these segments is then used to characterize the 3D turbine. Although this does include simplifications, this approach is typically the basis of CFD models that can be modified by empirically identified inaccuracies. In the case of a cross turbine flow device, such as the Darrieus or Gorlov turbines, this approach offers engineering insight as the blades move through a full rotation. Figure 1 show graphically the principal behind applying this method to quantify the blade elements' hydrodynamics.

The hydrodynamics of each blade segment in the cross flow turbine is assessed with reference to a number of parameters, some of which are:

1. The tangential velocity which is equal to the product of the radius and angular velocity.

2. The relative velocity (V_r) which is the vector sum of the tangential

velocity and the fluid flow upstream of the turbine.

3. The tangential force.

4. The axial force (F).

5. The lift force (L) which is a vector perpendicular to the relative velocity.

6. The drag force which is a vector parallel to the relative velocity.

7. The angle of attack (α) which is the angle between the chord line of the blade element and the relative velocity.

8. The rotational angle (θ) which is the angular position of the blade element on the circumference.

Use of BEM for cross flow analysis does not accurately account for interactions by all the blade elements nor, obviously, describe the overall performance of a finite length, structurally supported tidal turbine. Consul et al. acknowledges the complications of cross flow turbine analysis stating that "...aside from blade characteristics; profile, incidence, surface roughness, and incident flow conditions; free-stream profile, turbulence, yaw angle and surface waves, the performance of a cross-flow turbine is governed by six non-dimensional groups; Reynolds number, tip speed ratio, Froude number, blockage ratio, solidity and the number of blades itself."[13]. Some of these criteria are not included in the BEM analysis, and the research into the influence of solidity presented in this paper is achieved using the CFD package Fluent. Further description of the tip speed ratio, solidity and the number of blades is included in the discussion on the Gorlov turbine in section 2.
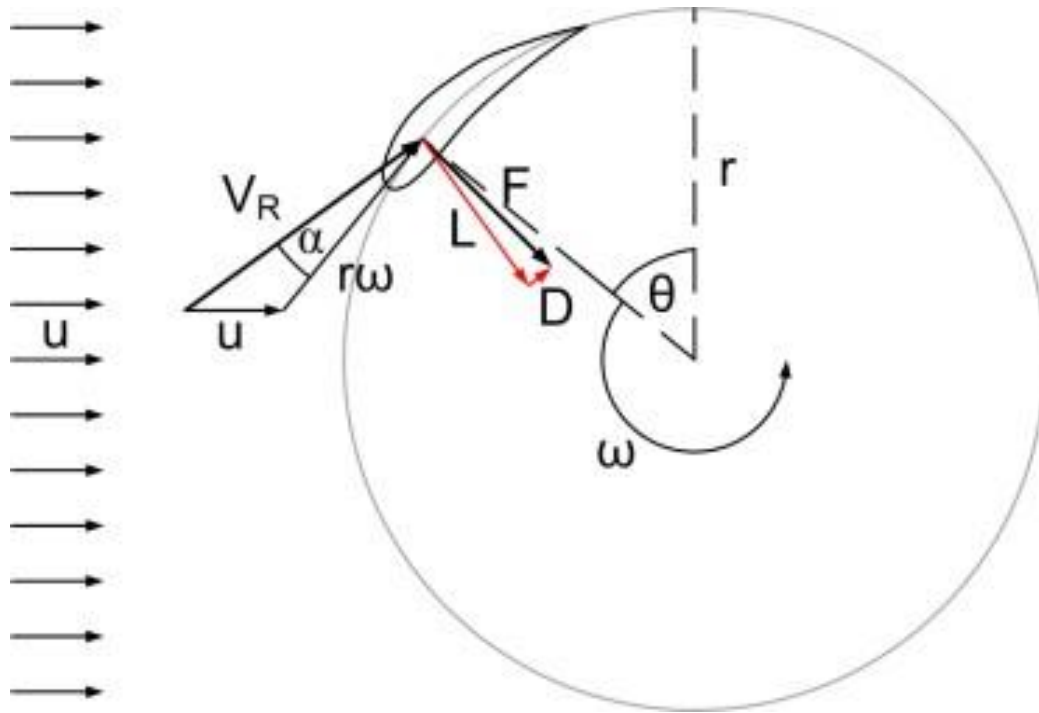
Figure 2: Schematic of lift, drag, and relative velocities [3]

Lastly, research for this project included consideration of cavitation issues with review of the Wang, D et al. report [27]. Although cavitation concerns are reduced by the depth at which the turbine will be operating, the research did reveal the possibility of vibration induced cavitation, even at relatively slow operating speeds. This emphasizes the importance of diligent engineering to restrict vibrations in the device.

2 Helical Cross-Flow (Gorlov) Turbine Design

The Gorlov helical turbine was presented by Alexander Gorlov in the 1990's as an improvement on the Darrieus turbine. Both designs are vertical axis devices with the feature of unidirecitional rotation in all fluid flow orientations. This is an advantage for our application where deployment methods do not easily facilitate control of the device's functioning orientation and tidal flow directions are not necessarily confined to bidirectional patterns. The Gorlov design was chosen for this project after a review of various tidal turbine designs. This review can be found in Appendix A.

2.1 Efficiency

The Gorlov helical turbine is also an extension of the Darrieus design in that it uses the contribution of a lift force on the rotating blades for energy conversion. This mechanism allows the rotational velocities of the turbine to potentially exceed the free stream velocity of the fluid, unlike a strictly drag force turbine. The efficiency of a turbine to produce power is directly related to this relative speed by $\eta = \frac{T \cdot \omega}{\frac{1}{2} \rho V^3 A}$ where T is the torque produced by the turbine; ω is the angular velocity of the turbine; A is the frontal area of the turbine presented to the free stream flow; ρ is fluid density; and V is free stream velocity. The advantage of higher rotational velocities implies that the Gorlov design can have efficiency values that are adequate to produce the power needed given the size constraints for this project. Available research into the hydrodynamics of this emerging device's design is limited, but of the four reliable sources found, empirically determined maximum turbine

16

Table 1: Turbine efficiencies for current speeds from V=0.6-1.4 m/s, various blade types, and helical angles. From Shiono et. al. [25]

Blade Type	Helical Angle	Efficiency (%)				
		V=0.6	V=0.8	V=1.0	V=1.2	V=1.4
H4	43.7	11.6	13.7	14.7	15.8	17.8
H4-50	50.0	13.3	15.3	16.3	17.8	18.9
H4-60	60.0	17.1	19.1	19.7	21.7	24.4

efficiencies attained values between 24.4% [25] and 39% [22]. The lower end of this range is presented by Shiono, Suzuki and Kiho in their paper titled "Output Characteristics of Darrieus Water Turbine with Helical Blades for Tidal Current Generations" [25]. This report compares a range of six helical turbine configurations where solidity, chord length, height, degree of the blade's inclination, and free stream velocity are variables. A straight bladed Darrieus turbine was also included in the experimental process to quantify relative general performance characteristics of interest. The turbines were standardized to a 0.3 m diameter and either 0.3 m, 0.374 m, or 0.544 m in height. Three turbine efficiency curves are published: One of the blade configurations in various free stream velocities; one of various percentages of solidity in 1.0 m/s water velocity and blade inclination angle of 43.7 degrees; and one of various blade inclination angles in 1.2 m/s and with solidity of 0.4.

Table 1 shows the range of efficiencies found for the set of experiments using a solidity of 0.4. Values start from 11.6% through to the maximum efficiency attained by the helical shaped blades of 24.4%. The 39% value for maximum efficiency referred to above is found in a report on research conducted by Verdant Power LLC and GCK Technology Inc. in 2005. These experiments involved analysis of 3 bladed helical turbines 1 m in diameter and 2.5 m

tall with chords of 0.14 m and blade inclination angle of 67 degrees. The turbines were exposed to various free water velocities and loading conditions. This report also investigated the impact on performance of adjacent turbines and a downstream turbine for array configurations. The maximum turbine efficiencies in various flow rates were calculated using what is termed "peak practical power point", the value of maximum power output from a curve fit for each water velocity. The results ranged from 18.6% to the highest values at 38.8% for 0.66 m/s flow and 28% for 1.33 m/s flow. The behavior of the efficiency values at different water velocities was noted to have these two maxima which it is proposed could be explained by critical blade interferences in the turbine.

In the report Gorlov prepared for the DOE in 1998 he claims an efficiency value of "about 35%" for a 3 bladed, 24" diameter by 34" height turbine in free water flow of 5 ft/s [17]. This report does not offer many details or insight into variations in efficiency under varying circumstance.

The last resource used to indicate the potential efficiencies for the Gorlov helical turbine is research conducted in the Uldolmok channel, Korea titled "Evaluation of Helical Turbine Efficiency for Tidal Current Power Plant base on In-situ Experiment" [18]. This research included testing a 3 bladed helical turbine of diameter 2.2 m and height 2.5 m to record RPM; torque and current velocity. Like the Verdant-GCK Technologies research, the peak power point was identified for efficiency calculations using a curve fit to the data. The paper states that "it does not seem that to assume 35% as the power coefficient for 3 bladed turbine is unreasonable"[18] although later reduces this slightly to a more conservative 30% which is closer to the tabulated values shown in Figure 3. These discrepancies are not explicitly explained in the report so for purposes of our project the 28.6% efficiency

18

Type \ Velocity (m/s)	1.5	1.7	1.9	2.1	average
3-blade turbine	29.9 %	29.1 %	29.8 %	25.7 %	28.6 %
6-blade turbine	24.9 %	22.7 %	23.5 %	22.4 %	23.4 %

Figure 3: Turbine efficiencies at peak power points for three and six bladed turbines, as various free stream velocities. From Han et. al. [18]

value was considered most credible.

2.2 Starting Performance

The fundamental modification Gorlov has made to the Darrieus design is to distribute the blade cross sectional areas in the horizontal plane evenly around the circumference of the horizontal plane of the cylinder. This is achieved by the blade's positions being determined by a helix that, between the total number of blades, completes one revolution of the circumference of the turbine. At any one time as the turbine rotates there is a blade cross section located and acting relative to the fluid flow at each position around the horizontal circle. This has a significant impact on two main characteristics of the Gorlov turbine compared to the Darrieus turbine: The self starting performance and torque behavior. Self starting ability at low water velocities is a primary concern for this project. The turbines will be deployed with limited monitoring facilities typically in tidal flows of less than optimum velocities. The turbine system would be significantly simplified if no prompting electric start was needed and more effective if utilization of the valuable battery power is avoided. The Gorlov turbine design is advantageous because by always having a section of a blade orientated at all positions relative to the fluid flow the possibility for self starting is maximized. This feature is

included in the list of benefits of the helical design in the Gorlov-DOE report although was not realized in the Verdant-GCK Technology research. In the Verdant-GCK Technology experiments for a generator assembly the gearing and associated transmission system resulted in requiring hand cranking to start the turbine. The report acknowledges this was an unexpected restriction and suggests that possibly the relatively low solidity, 0.14, "...may be too low to be optimal for maximizing C_p..."[22]. Generator cogging also may have played a role in preventing the system from self-starting. In the gearing recommendations section of this report an automatic electric start is suggested as most practical and reliable.

2.3 Torque Behavior

Decreasing the fluctuations in torque as the turbine spins is the second significant advantage that the Gorlov helical design has over the Darrieus design. This property is due to the even blade section distribution described above. Shiono includes analysis comparing torque trends as the various turbine configurations rotate [25]. In the figure below the dampened fluctuations of the helical turbines are clearly evident compared to the 'S' trend of values attained by the Darrieus design turbine.

The primary advantages of reduced torque fluctuations are more power production, less vibration and lower cyclical stress. The durability and reliability of the tidal turbine device will be severely undermined if the project does not include consideration of these engineering concerns. From the Gorlov-DOE report: "Another important characteristic of hydraulic turbines which actually triggered the present research is their oscillation and vibration under the load. Oscillation of the turbine causes not only fluctuation of the
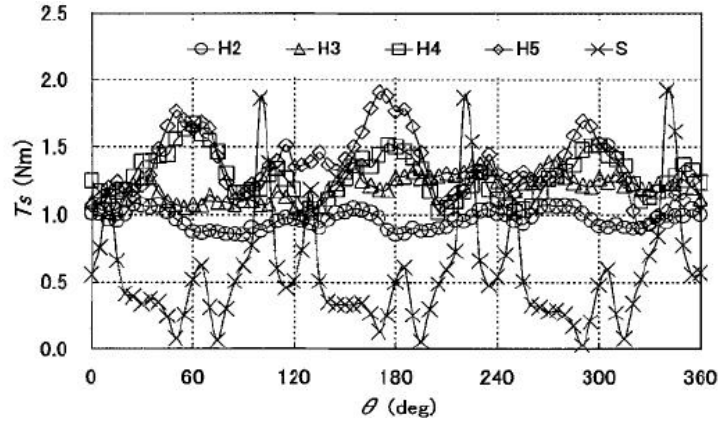
Figure 4: Starting torque characteristics (V=1 m/s,$\phi = 43.7$ degrees) From Shiono et. al. [25]

electric power, but it also leads to the fast failure of mechanical parts and joints in the turbine-generator-transmission chain."[17]. Although the report refers to identifying no vibrational issues in their helical turbine testing, no data analysis of this mechanism is presented. It should also be noted that although the torque is more evenly distributed in the rotating plane it "rides" up or down the blades in the vertical plane in a cyclical manner that is not inherent in the Darrieus design. This dynamic vertical loading needs to be accommodated for in a durable support structure design.

2.4   Tip Speed Ratios

The natural tip speed ratios of the Gorlov helical turbine were found to fall within the range from 2 to 2.5 in all resources used, except Shiono et al. found the range to be just below 1 to 2.5 [25]. If this lower range is considered to be for not quite optimized circumstances and ignored, the tip speed ratio range of 2 to 2.5 can be used to predict possible expected angular velocities

for our turbine using the relationship $\lambda = \frac{R\omega}{V}$ where λ is the tip speed ratio; R is the turbine radius; ω is the angular velocity and V is the free stream water velocity.

2.5   Dimensions

The Gorlov helical turbine has a number of dimensions to describe the device.

1) Height, h, of the cylinder defined by the turbine blades

2) Diameter, d, of the cylinder defined by the blades

3) Number of blades, n

4) Type of foil

5) Chord length, C

6) Blade inclination angle, ϕ, from the horizontal, where $\phi = tan^{-1}(nh\pi d)$

7) Solidity, σ, defined as $\sigma = nC\pi d$

The helical turbine design described in this report has a diameter of 0.7 m and a height of 1 m. This geometry was based on the turbine efficiency calculations detailed in Appendix G, the drag force and tipping moment calculations detailed in Appendices E and F, and the restrictions due to Sea Spider geometry. Inspection of either the solidity or blade inclination angle equations above demonstrates the connected relationships between the remaining dimensions. The papers reviewed provided some insight into the impact of these dimensions on turbine performance. The Shiono et al. research provides the most extensive attention to the roles of relative dimensions with experiments that are tailored to evaluate the impacts of solidity and blade inclination angle. They found that, "... the starting torque can be largely

affected by solidity rather than by blade inclination angles."[25] and that increasing either the solidity or inclination angle improved the performance of the turbines tested. For the purposes of this project it is worth noting from the graphs presented that higher solidity turbines attained their peak efficiency at lower tip speed ratios. As we anticipate the project turbine will be operating predominantly in slow tidal speeds the tip speed ratios expected will be low accordingly and so keeping the solidity reasonably high could be of benefit.

Between the other three reports referred to here, blade inclination angles varied from 47.3 degrees in the Uldolmok experiments to 65 degrees in the Verdant-GCK technology tests, and solidities used were 0.132 for the Uldolmok device; 0.279 for the Gorlov-DOE turbine and 0.14 for the Verdant-GCK Technologies tests. The Verdant-GCK Technologies report comments that this solidity value could be blamed for the problems with self starting encountered in their experiments [22]. In view of the possible dimensions we could consider for this project, Table 2 was put together to demonstrate the relative impact of dimensional parameters. The equations used were those listed above.

2.6   Additional Comments

The Gorlov-DOE report includes quantifying the effect of "turbine resistance" when comparing the Gorlov helical turbine to the Darrieus turbine design. Turbine resistance is described as the extent to which the turbine alters the flow streams so that the water "...simply avoids the turbine without producing any useful work..."[17]. Tables and graphs are presented that demonstrate the superior performance of the helical bladed turbine based

Table 2: Various combinations of helical angle, turbine dimensions, and solidity

ϕ(degree)	n	h (m)	d (m)	C (m)	σ
43.68	3	0.75	0.75	0.15	0.191
51.85	3	0.8	0.6	0.15	0.239
58.37	3	0.85	0.5	0.15	0.286
47.5	3	0.8	0.7	0.15	0.205
51.85	4	0.75	0.75	0.12	0.204
59.5	4	0.8	0.6	0.12	0.255
65.2	4	0.85	0.5	0.12	0.306
55.5	4	0.8	0.7	0.12	0.218

on measuring the "water head", the water crest formed on the water surface immediately upstream of the turbine. This is the only resource reviewed that refers to this characteristic as an assessment method for turbine performance. The Verdant-GCK Technologies report includes detailed mechanical descriptions and recommendations pertaining to gearing, resistances, bearings, etc. Considering the mechanical problems encountered by this project, this resource offers a worthwhile guide of how not to engineer these components, or at least a "beware" list.

2.7 Scale Model Testing

2.7.1 Model Testing Motivation

Previous sections have reviewed the literature on helical tidal turbines, and an attempt was made to summarize the relevant parameters and the relationships between them. However the helical bladed vertical axis tidal turbine is a relatively new design, and the literature is far from complete. We felt

that building and testing scale models before we built the full size turbine would give us a deeper understanding of this type of turbine, and allow us to have some confidence in the performance of the full size turbine. Among the questions we sought to resolve:

1. The effect of helical angle on the performance characteristics of the turbine

2. The effect of the number of blades on the performance characteristics of the turbine

3. The effect of solidity of the turbine, defined by the following equation:

$$\sigma = \frac{Bc}{2\pi r}$$

4. The effect of "overwrap", or the continuing of a helix of one blade past the point where the next blade begins.

After considering previous work [25], we determined that the area and overwrap of the turbines would be held constant across all tests, providing a control baseline for the model evaluation. This eliminated Parameter 4 from testing, but reduced the complexity of the model manufacturing process considerably.

The NACA 0018 airfoil is a symmetric airfoil having an 18% width-to-thickness ratio. Researchers have previously used this airfoil [25] and it was felt that it provided a good balance of structural support and performance. Solidity was chosen to be relatively high—0.3—for turbines #1 and #2 because we wanted to maximize starting torque. Shiono et. al. found that a solidity of 0.4 produced the highest efficiencies[25], but other researchers

Table 3: Parameters of proposed scale models to be tested in the flume. Courtesy of Adam Niblick

	Turbine 1:	Turbine 2:	Turbine 3 (contingent):	Turbine 4 (contingent):
Change:	Baseline	4 blades, 60 helix	Low solidity	10% Over-wrap
Blade type:	NACA 0018	NACA 0018	NACA 0018	NACA 0018
Number of Blades:	3	4	3	3
Blade tilt:	0	0	0	0
Solidity Ratio:	0.3	0.3	0.15	0.3
Chord length (cm)	6.28	6.126	4.712	8.954
Diameter (meters)	0.2	0.26	0.3	0.285
Aspect Ratio:	1	1.36	1	1.1
Height (meters)	0.286	0.35	0.3	0.31
Swept Area (m^2)	0.0572	0.092	0.0901	0.0894
Helix Angle (degrees)	43.7	60	43.7	43.7
Blockage ratio (flume area 840 sq in)	10.50%			
Overwrap (%)	0	0	0.00%	10.00%
Central shaft:	No	No	No	No
End support:	Radial Arms	Radial Arms	Radial Arms	Radial Arms
Contingency:	Test	Test	Test if turbines 1 and 2 result in low C_p	Test if problems with torque oscillation from 1, 2 and 3.

have demonstrated good results with lower solidity turbine; a solidity of 0.3 was chosen as a compromise value. Turbine #3 had a solidity of 0.15, which was chosen in order to test the effect of solidity directly between turbines #1 and #3. Turbine #2 was designed to compare the performance of a 4 bladed turbine with a 3 bladed turbine of equal solidity (turbine #1). Unfortunately the aspect ratio is necessarily different between turbines #1 and #2, which complicates interpretation of the results. The scale of the turbine was chosen to maintain as small a blockage ratio as possible through the flume in order to closely replicate free-stream conditions. It was our desire to remain at less than 10% of the wetted flume area. The width of the flume is 29 inches, or 0.76 meters. The depth of the water in the flume is 0.6 m when flowing, giving a wetted area of 0.456 m^2. Therefore, the turbine was fabricated with a 0.04 m^2 swept area. The aspect ratio of the turbine was to remain 1:1 for Turbine #1 and #3. The resulting values for the size of the airfoil are shown in Table 3.

2.7.2 Model Material Selection

There was considerable discussion about the optimal material to use for the model blades. It was our desire that the blades be as uniform as possible (free from defects) and also as consistent as possible between the different blades. Consideration was given to several different types of material, including solid wood, laminated wood, cast aluminum, machined aluminum, cast bronze, solid PVC, laminated PVC, PVC cut from a section of pipe, and solid ultra-high weight polyethylene. Table 4 below summarizes these options.

Table 4 also indicates some of the various reasons why different materials were abandoned during our selection:

Table 4: Summary of material options for model turbine blades

Material	Comments	Disposition
Solid Wood	Difficult to maintain isotropic structure due to grain structure of wood	Not Used
Laminated Wood	Labor-intensive but cheap. Difficult to maintain uniformity	Not used; we did make some test sections
Cast Aluminum	Difficult to realize; Equipment not available	Not used
Machined Aluminum	Expensive	Used to make 10 blades.
Cast Bronze	Difficult to realize; Equipment not available; Very expensive	Not used
Solid PVC	Cheap, but difficult to locate material; concerned about chattering during manufacture & Not used	
Laminated PVC	Cheap, but labor-intensive	Not used; some laminates were constructed but failed during machining
PVC from pipe	Cheap, concerned about chattering during manufacture	Not used; pipe acquired for free
Solid UHMW	Difficult to locate material; concerned about strength of material	Not used

- It was our desire to keep the cost of the modeling as low as possible to remain within our budget for the project, which eliminated metal casting as an option.

- Wood was considered, but concern about the non-isotropic grain structure, and therefore the strength of the material, outweighed greater availability and lower cost.

- Fabrication of a wood-laminate blade was attempted, but was too time consuming and not precisely replicable enough for our purposes.

- Solid PVC and solid UWHM PE were considered but were not available for a reasonable price.

- Laminated PVC was attempted: we glued several sheets of $\frac{1}{4}$ inch PVC together to form a stack 4 inches wide and 3 inches tall; however, the adhesive did not withstand the machining process, and the stack failed. It was also decided that the process was too labor-intense for the number of blades needed.

We were eventually able to locate billet aluminum in the dimensions required for a reasonable price, and selected this material for the prototype blades. Aluminum provided a high-strength blade which would not deflect under load. The blades were cut from solid billets of 6061-T6 aluminum in a Haas 3-axis CNC machining center by Eamon McQuaide. Figure 5 shows the blades in different stages of the machining process. Discussion was held about the blade attachment scheme, specifically if a solid circular disk was to be used or if a discontinuous spoke system would work better. We had difficulty quantifying the effect of skin friction that would be inherent in a solid disk, and there was some question about out-of-plane forces on the discs

Figure 5: Images of the blades during manufacture

Figure 6: Turbine #1 constructed (left) and mounted in the gantry (right)

that would increase thrust, and thereby friction, in the shaft bearings. It was therefore decided that the blades would be held with discontinuous spokes made also from aluminum.

2.7.3 Flume Description

The University of Washington Aeronautical Engineering department is in possession of a moderately-sized test flume, which we were able to use for our prototype tests. The flume consisted of a rectangular glass section approximately 8 ft long and 29 inches square. Water was pumped through the flume by a centrifugal pump to induce flow, which would achieve a maximum value of 0.8 meters per second. The pump was controlled by a variable frequency drive, allowing substantial control of the flow rate through the flume, and therefore of the water velocity. Direct measurements of volumetric flow rates were not taken; however, velocity of the water was the primary variable of interest. This was directly measured with an immersed Acoustical Doppler Velocimetry (ADV) device, which provided the velocity in the flume in real time.

In order to mount the test turbines in the flow, a gantry was constructed over the top of the flume to provide mechanical restraint during the test. The gantry was built to avoid contact with the glass walls of the flume to prevent damage to them. Additionally, the frame was kept to a minimal profile in the water to reduce stray turbulence around the turbine, which could confound the test results. A sketch of the frame, gantry, and model turbine is shown in Figure 8.

2.7.4 Test Gantry Description

The gantry and turbine supports were built from mild steel. The top section of the gantry was made of 3"-square box tubing just larger than the width of the flume. The $1\frac{1}{4}$" $\times \frac{1}{4}$" angle-iron cross members provide sideways strength to the frame. We constructed the A-frame uprights from 3" $\times \frac{1}{4}$"
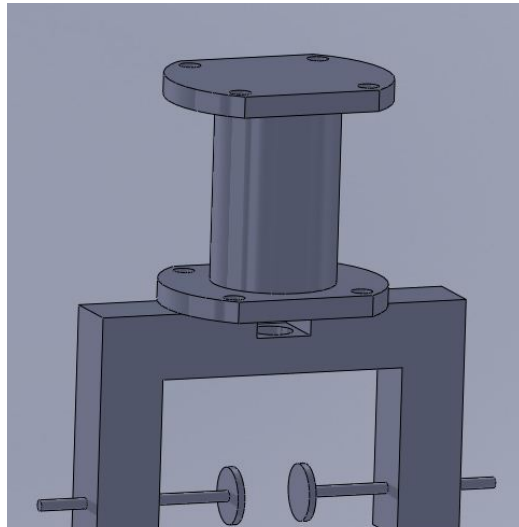
Figure 7: A rendering of the torque cell used for testing

flat steel. Channel iron 2" wide by 1" high provided the supports for the turbine, top and bottom. The upper frame was welded to provide rigidity, as were the A-frames, which were then bolted together to allow for disassembly of the frame. The frame was primed and painted with an oil-based enamel to reduce corrosion of the steel during immersion in the flume. The turbine was mounted inside the frame as shown in Figure 8, and a torque cell and rotation encoder were attached to the top of the turbine shaft. A sketch of the torque cell is shown in Figure 7. A LabVIEW DAQ suite was used to acquire torque and velocity data.

2.7.5   Testing of the Prototype Turbines

The following parameters were to be tested across the three different turbines:

- Starting torque of the turbine

- Maximum no-load rotational speed
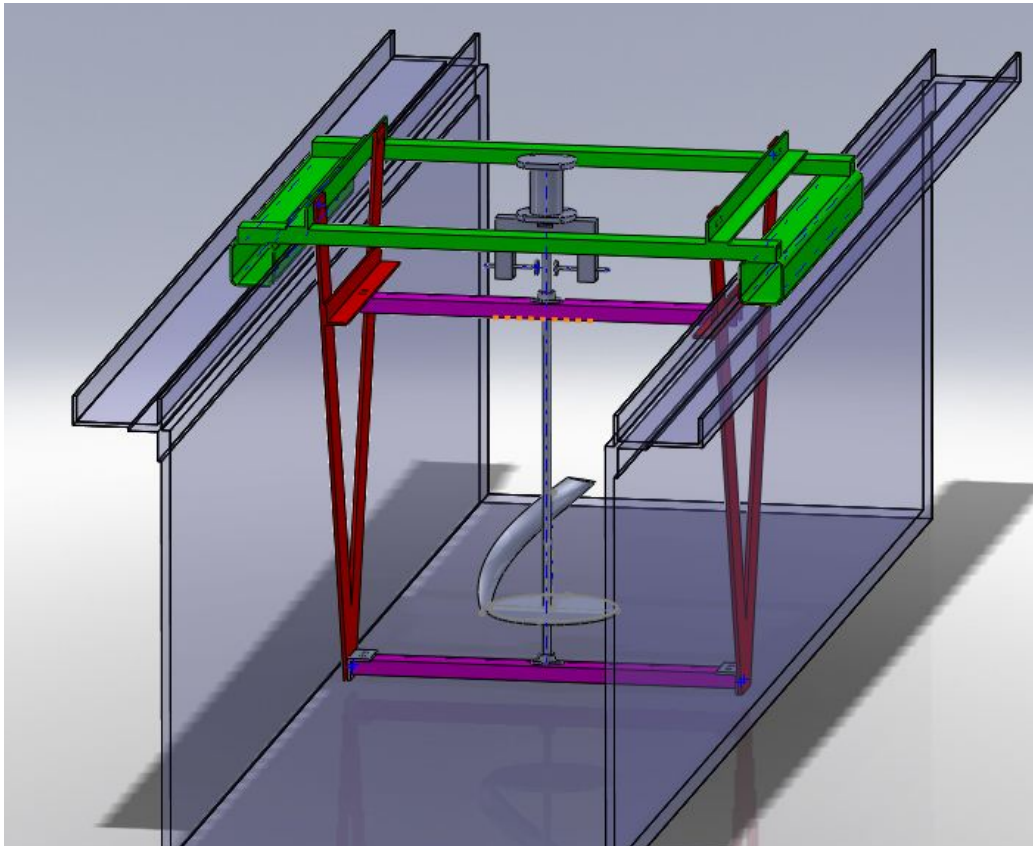
Figure 8: The test flume with turbine and gantry mounted in place

- Orientation of highest torque

- Coefficient of power (turbine efficiency)

The torque cell directly measured torque transmitted through the turbine shaft; the rotation encoder provided angular velocity data. Maximum starting torque could be measured by increasing the braking force applied to the shaft until the turbine was prevented from rotating, while maximum no-load rotation was measured by reducing the braking force applied to the turbine shaft to zero and recording the speed of the turbine. Multiplying the angu-

33

Table 5: No-load test results tested at 0.8 m/s

Test:	No-Load Rotational Velocity	
Turbine #1:	150.9 RPM	15.8 rad/sec
Turbine #2:	181.0 RPM	19.0 rad/sec
Turbine #3:	32.7 RPM	3.4 rad/sec

lar velocity by the torque developed will yield the power developed by the turbine:

$$P_{turbine} = T\omega$$

The coefficient of power developed in the turbine was measured indirectly. Equation 1 below gives the power available in the flowing water:

$$P_{flow} = \frac{1}{2}\rho A V^3 \tag{1}$$

The power output of the turbine is given by:

$$P_{turbine} = \frac{1}{2}\rho A V^3 C_p = P_{flow} C_p \rightarrow C_p = \frac{2\omega T}{\rho A V^3}$$

This coefficient of power must be corrected for the non-trivial blockage of the turbine in the flume; however, problems were encountered in the acquisition of results that precluded any corrections.

2.7.6 Modeling Results

Maximum free-stream rotation was easily measured with the velocity encoder, and results are shown below in Table 5

In measuring torque, however, we encountered problems acquiring reliable data from the DAQ suite, as the torque cell measurements were extremely

noisy. Investigation determined that the torque cell available to the team had a measurement range of 0-200 inch-pounds of torque, which converts to approximately 23 newton-meters of torque. The minimum resolution of the cell was 1% of full scale, which was 2 in-lb or 0.23 Nm.

We first considered Turbine #1. To provide a baseline, we initially estimated a conservative C_p value for the turbine of 10%. Given a swept area of 0.04 m^2, a density of 1000 $\frac{kg}{m^3}$, and a water velocity of 0.7 $\frac{m}{s}$, we can solve for the expected torque output of the turbine:

$$T = \frac{\frac{1}{2}C_p\rho A V^3}{\omega} = \frac{\frac{1}{2}(0.1)(1000\frac{kg}{m^3})(0.04\ m^2)(0.7\ \frac{m}{s})^3}{15.8} = 0.04\ Nm$$

This measurement is much less than the resolution of the torque cell, which substantially reduces the reliability of the data available from it. We concluded that acquiring a torque cell of the appropriate range was necessary to continue testing of the prototype turbine models. However, with time running out in the quarter and a limited budget, the decision was made to use the turbine that produced the highest no-load rotation, which was Turbine #2.

The torque cell relied upon the application of braking torque to the turbine to produce a torque measurement. However, the braking system provided with the torque cell did not perform as we had intended. The rubber brake shoes generated a sticky and unstable torque on the shaft, such that torque could not be adjusted appropriately without stopping the rotation.

We also experienced problems with aluminum oxides and hydroxides forming on the unpainted surfaces of the turbine blades. The existence of these corrosion products substantially reduced the speed at which the turbine would rotate. Unfortunately, removing them required removal of the turbine from

35

the test apparatus, which was a time consuming and tedious process. Corrosion of the shaft bearings, resulting in increased rotational drag was also a problem, but this was mitigated by installation of a point-type bearing at the underwater shaft connection.

2.7.7 Future Work

Helical cross-flow turbines are a relatively new technology, and a substantial amount of research is still needed to investigate and understand their operation and properties. Substantial characterization can be done with the turbines we have made this quarter. The foremost priority is to acquire instrumentation that is of appropriate resolution. A torque cell with a range of 0-5 Nm would be much more useful. Additionally, an upgraded brake system is needed to more appropriately apply torque restraint to the turbine. We recommend an eddy current-type brake, which will provide a stable amount of torque on the turbine. Development of such a brake was considered this quarter, but the complexity of such a device and time required for construction did not allow us to proceed.

The flume at the University of Washington has a maximum water speed of 0.8 m/s, which is too slow to fully characterize the capabilities of the turbine models. Testing them in a location with water speeds of at least 1.5 m/s will allow a full series of testing in the proposed operating range, and should be included in future work.

As seen in the figures above, the turbines were all designed with a drive shaft extending fully through the blades. It is possible that removal of this shaft will increase the performance of the turbine by eliminating the turbulent wake generated by the shaft— this wake may interfere with the flow around the

blades and reduce lift, therefore reducing efficiency. Construction of a new shaft bearing system and shaft-turbine connection is underway to investigate this possibility.

2.8 Turbine Blade Manufacturing

2.8.1 Machining from a solid block

Preliminary investigation of manufacturing methods for the full size turbine blades led us to consider machining them out of a solid block of material. The material required to make a 1 m long blade for a turbine with a diameter of 0.7 m is 30 cm x 17 cm x 106 cm [1]. This amount of aluminum costs many thousands of dollars—prohibitively expensive for this project. The amount of material required for this method could be substantially reduced if thinner material was welded together in a "blank" of the appropriate shape. These welds would have to be very strong, and may or may not be possible; this option was not investigated in detail.

2.8.2 Casting

Cast aluminum or bronze was briefly considered as a manufacturing option for the turbine blades. Large ship propellers with similar geometry (long and thin, with tapered edges) are cast out of bronze, so there is some experience in industry from which to learn. An informal quote was obtained from a local casting company [2]: with some tooling provided to them they would cast a turbine blade from aluminum for approximately $600. We decided to not

---

[1]This calculation is for a three bladed turbine with a blade helical angle of 43.7 degrees

[2]Pentz Cast Solutions, www.pentzcastsolutions.com

cast the turbine blades because of a negative experience by Verdant Power [22] with cast aluminum blades, and because composites offered a potentially cheaper option. Casting may be an attractive option for future projects of this kind, especially if multiple turbines will be manufactured.

3 Composite Blade Manufacturing

Building the full size turbine blades from composite materials was chosen for three reasons:

- Mechanical (strength, toughness, etc)

- Corrosion resistance in salt water

- Cost and feasibility

Research was done into various manufacturing process and material options, the results of which are presented below.

3.1 General Process

The overall approach for composite construction is to prepare a shaping tool to which the laminate matrix can be formed. This may either be the positive (called male or plug) or negative space (female) of the product. The fibers of the laminate are selected for the appropriate engineering requirements: The options are extensive but include fiber weave pattern, weight and orientation. Laminates with various criterions can be selectively located in the tool for localized strength. The fibers are bonded by a matrix material such as

one of the thermoset resins epoxy, phenolics, polyesters and vinylesters [1]. For hand lay-up for composite construction two methods prevail: The catalyzed matrix material is applied during the lamination process or the matrix material is previously impregnated into the fibers and requires catalyzation by heat and pressure. Prepreg, the latter process, is also called the autoclave process due to the instrument used to provide these conditions. When the catalyzed matrix is applied directly, resin curing requirements need to be observed. Although vacuum bagging and heating may be used to assist the curing process, many resins do not necessarily require these conditions. The lamination design may also include a core or less structurally crucial volume. The use of cores can lower the cost and weight of the end product, but is totally insufficient to replace the necessary structural volume. Diligent attention should be given to all material requirements, like mixing ratios, solvents, application and stipulated durations, to produce an uncompromised composite product.

3.2 Process options

3.2.1 Plug or male mold

To apply this method to fabricating the helical turbine blades a male form would be CNC machined that is shy of finished dimensions. Carbon fiber laminate would then be bonded to the plug/ core to add structural strength and make up the dimension deficit. The dimensions and shape of our blades make this approach very challenging. According to a composite boat foils builder, Russell Brown, if the plug is made of a material that does not contribute to the blade strength, like foam, it needs to be small enough to leave sufficient volume for composite fiber laminate. (If the laminate is too

thin it will just crack and leave no integrity to the blade.) In our case, the reduced center volume would leave a form that is very difficult to control without an additional mold. The plug/core could be made of fiberglass or laminated hardwood that can hold its shape better and contribute to structural strength, thus allowing a thinner composite fiber laminate. The work involved preparing these materials and then to machine each of the plugs seems inefficient compared to using one female mold repeatedly.

3.2.2 Two-sided female mold

A two-sided female mold is typically used repeatedly so CNC machining of the tool is done once. The blade form would be split along the foil chord length line to obtain optimum draft angles, most effective vacuum-bagging or resin flow orientation and maximize adhesion surfaces in a split mold cure, as explained below. The mold can be used in two ways: The laminates can be placed in the molds in such a manner that the two sides are clamped together before curing, or the laminates are divided between the two halves to cure separately and glued together later. The first method necessitates strong, rigid molds, aluminum is best, to withstand repeated clamping pressures. This was the approach used for previous turbine blades in other projects [3]. The laminate lay-up on the leading edge of the blades can be smoothly integrated by a "wrapping" orientation of the fibers with excess cloth at the trailing edge. This produces a desirable structural and aesthetic lay-up. The second approach with two-sided molds is to apply laminations that are slightly proud to each half of the tool, vacuum-bag, cure, route each side flush to the molds, and then glue the sides together. Mold material for this method can be slightly inferior to the first approach, but must still provide a rigid,

vacuum-bagging platform. Gluing the two halves introduces the possibility of seam lines on the leading edge. This can be addressed by building a rebate strip into the leading edge of the molds so that a length of specified width composite tape may be applied over the seam and faired in with finishing.

3.2.3   One-sided mold

The one-sided mold would be used repeatedly to build blades that are formed in the mold on one side and "over built" on the other. The laminates could be designed to closely approximate the final form with a "wrapping" technique used for the leading edge and a pseudo core of short fibers around broad full width cloth. The lamination would be vacuum-bagged, cured and then the second side CNC machined into shape. The orientation and use of unidirectional fiber will facilitate no structural compromise with the machining process [2]. The exposed composite fibers will be coated with epoxy resin.

3.2.4   Mold materials

To fabricate the molds in house we could use foam that is machined to the tool shape and then sealed with epoxy. Foam is more fragile than some other mold materials but with care would be adequate for the low number of iterations we need. The epoxy provides a surface on which to apply non-stick wax and hold a vacuum for vacuum-bagging. The foam would either be free or of relatively low cost. Mold coating and waxing costs could be in the $30 to $60 range.

3.3　Laminate options

3.3.1　Prepreg

The advantages of using prepreg are the predicable ratio of fiber to matrix in the end product("usually have more than 60% fiber volume fraction."[23]), the parts are very stiff and strong, and the lay-up is clean relatively easy. Disadvantages are the cost (more than regular carbon fiber) and the mold requirements for autoclave exposure.

3.3.2　Wet lay-up

According to Mazumdar in his book "Composites Manufacturing", one of the advantages of wet lay-up is it is a simple and versatile process [23]. The molds do not have to be as sophisticated as for prepreg and the autoclave is unnecessary. The main disadvantage can be that the fabricator's lack of skill in fiber and resin application impacts the final product.

3.3.3　Core

Cores can be made of many materials from totally non-supportive (students doing a similar project used an air bladder in their lay-up resulting in a hollow core) to foams and honeycombs, or solid. Using some form of core would reduce unnecessary cost for the blade construction. The most appropriate core material needs to bond and be compatible with the composite laminate, and easily conform to the blade shape.

3.4 Fabrication method selected

3.4.1 Mold fabrication

The mold construction method selected for this project was the one-sided mold, as described above. Reasons for this choice included consideration of a limited project time frame, avoiding having to glue two separate halves of the blades together, avoiding reliance on the busy University of Washington machinists to schedule fabricating a mold, and the offer by Turn Point Design to construct the tool surface with graphite blocks at no extra cost. Turn Point Design is a Port Townsend based fabrication shop that has extensive experience with this method of composite manufacturing. The mold construction was contracted out to Turn Point Design who received a SolidWorks mold file developed by our team. This file was engineered so that it could be used for both the mold machining and blade machining by hiding one surface of the blade during mold construction.

3.4.2 Composite materials

The composite materials we have chosen to construct the turbine blades are e-glass (fiberglass) in a wet lay-up with vinyl ester resin. Fiberglass was selected, rather than carbon fiber, because it provides adequate strength for our requirements at reasonable cost, and does not pose the galvanic corrosion issues associated with carbon fiber. The wet lay-up process avoids higher mold fabrication costs (according to Brandon of Turn Point Design, mold costs are doubled for a mold that must stand 350° F instead of 250° F, and quadrupled for a mold that must withstand 450° F) and reliance on access to the autoclave for prepreg cure. Vinyl ester resin was selected for the

composite matrix for two main reasons. This curing reaction of this resin is less exothermic than epoxy and thus allows for a single step lay-up process for the 2.97 cm maximum thickness blades. Consultation with a Gudgeon Brothers technician, Tom Pollock, confirmed that a 3 to 4 step process may be required for epoxy. Reducing the number of lay-up steps is desirable due to a tight project timeline. Secondly, in material performance research conducted by Anderson Ogg, a graduate student at the University of Washington, it was found that exposure to 9 months submersion in seawater at a depth of 150 m had a less detrimental effect on a composite of vinyl ester resin than one of epoxy resin. In addition to these reasons to use vinyl ester resin, this product is less expensive than epoxy.

3.4.3 Laminate choice

The fiber laminates used in the turbine blades will need to resist forces from a number of directions. The analysis of these loads is presented in detail in section 5. Research identified the need to use predominantly unidirectional fibers with a 25-30% biaxial component. Although this laminate design could be achieved by combining 3 layers of unidirectional cloth with a layer of biaxial, 45-45, we were able to locate a triaxial, knitted fiberglass cloth that achieves this proportion in each layer. The 22 oz triaxial cloth is manufactured as a stitched, single layer $\pm$ 70% weight unidirectional fibers and $\pm$ 30% weight biaxial fibers. This meant our lay-up process involved simply orienting the unidirectional fibers along the length of the blades and adding sufficient layers. In addition to the triaxial cloth we selected to use 2 mm coremat, a flexible, fiberglass core cloth, to build up the inner 6-8 mm of the thicker sections of the blades. The coremat was replaced by triaxial cloth for

the last 5 cm at each blade end to provide stronger attachment points. The inclusion of a core material in the blade laminate was verified by consultation with Paul Bieker of Bieker Boats. Bieker is a very experienced composites designer (for example, the last two Oracle America's Cup vessels) who found in his back of the envelope analysis that we were "way over building" the blade if it was solid fiberglass. Although we do not want to jeopardize the performance of the blades, we have decided that a modest addition of core material will not compromise meeting the requirements of the blades.

4 Turbine Blade Fabrication

A one-sided mold was manufactured by Turn Point Design, a Port Townsend based shop with extensive composite fabrication experience. This mold was made from many small block of graphite that had been glued together, then glued to a MDF base. Graphite has the advantage of being an effective heat sink, which reduces the risk of the composite overheating when the resin cures. The inner half of the blade profile was cut into the graphite block based on a SolidWorks model of the blade geometry. Four small, short dowels were attached to the corners of the MDF base to allow precise realignment of the mold when the blades are being machined. The mold was delivered to the University of Washington Mechanical Engineering shop, and our team made five blades between May 30 and June 4, 2011.

The first step after getting the mold into place was to coat the mold with three layers of epoxy to seal and smooth the surface. Several layers of mold wax was applied after the epoxy to make the blade more likely to detach after lay-up is complete. After the final layer of wax had hardened a layer of polyvinyl

alcohol (PVA) was applied to the mold as another release mechanism. A coat or two of wax and PVA were applied before each layup to ensure release from the mold. While the PVA was being applied and drying, other people were cutting out the fiberglass layers. The cutting schedule is listed in below in Table 6. The cutting schedule was determined by fitting dry material into the mold up to the chord line. This material was mirrored on the top half of the blade, with a few extra layers of fiberglass added to ensure the top surface was overbuilt. Figure 10 shows members of the team doing a dry run with the material in the mold. After the initial layup, the 4A, 4B, 14A, and 14B layers were added and cut out of biaxial fiberglass as it was discovered that more material would be required. The lettered order was only the core material, so A was after 9 and J was before 10.The core material was generally cut in a different location than the fiberglass because the core material would snag strands of the fiberglass and fray it. In order to avoid excessive handling of the fiberglass and the risk of fraying, it was decided to use a different ordering system to avoid reshuffling the order several times for a single layup. After the material was cut it was labeled with small pieces of tape and stacked in the order it will be used. Figure 9 shows members of the group cutting out the fiberglass layers.

Figure 9 shows members of the group cutting out the fiberglass layers.

The material was wetted out on mylar covered plywood; plastic squeegees were used to work the resin into the fiberglass and scrape the excess off. After the fiberglass was fully saturated with resin, and the excess resin was removed, the strips of material were placed into the mold, where laminating rollers were used to eliminate air pockets. There is a slight deviation in this procedure after the core has been completed. Thin beads of resin thickened with silica were squeezed on to the edges of the coremat to smooth the sharp

Table 6: Material cutting schedule

Fiberglass Width (cm)	Layup Order	
16		20
16		19
15.5	1	18
15.5	2	17
15.25	3	16
15	4	15
15	4A	14B
15	4B	14A
14.5	5	14
14	6	13
14	7	12
13	8	11
12	9	10

Core Width (in.)	Layup Order	
4	A	J
3.5	B	I
3	C	H
2.5	D	G
2	E	F

Figure 9: Cutting Fiberglass Layers

Figure 10: Putting Layers in Mold

corner made by the edge of the coremat, and reduce the chance of an air pocket there. Short filler strips of fiberglass mat were added on either side of the core material, because the core material is shorter than the normal strips of fiberglass. After these short pieces of mat were built up to the same height as the core material, the process goes back to putting fiberglass strips onto the mold.

Once all of the material has been put into place it is covered with peel ply, two layers of breather material, and then vacuum sealed using vaccum bagging and vaccum bagging tape. In Figures 11 and 12 below the completed layup is shown before and after the vacuum pump has been activated. After initially securing the vacuum seal material and attaching the pump, significant time

Figure 11: Completed Layup with Initial Covering

Figure 12: Vacuum Sealed Layup

Figure 13: Completed Blade

was spent listening for and securing leaks. Once no more leaks were detected, the blade was left for approximately 24 hours to cure. A blade that has been cured and removed from the mold is shown below in Figure 13.

The wet lay-up process for the turbine blades was messy and labor intensive. After some practice our team was able to complete one blade in slightly less than one hour. The process required six people: two were wetting out material, two were laminating material onto the mold, one was mixing resin, one was assisting with the lamination, preparing the thickened resin, etc. After approximately 20-30 minutes the first batch of resin was starting to get very tacky, which means the at least half of the blade is partially cured before the lay-up was complete. This limits the effectiveness of the vaccum bagging in drawing away excess resin and ensuring good consolidation of the blade. This wet lay-up process probably cannot be easily sped up, due to the limitation of having to carefully place 30+ strips of material into the model and roll them out. Each blade made by this process consumed approximately $1\frac{1}{2}$ -2 gallons of resin.

After five blades had been made (one was made as a practice/spare) the mold and the blades were returned to Turn Point Design so the top surface of the blade could be machined. During the machining of the first blade it was discovered that an error in the lamination schedule had resulted in the core material extending all the way up to the top surface of the blade. Additionally, the core material extended to the ends of the blades, even though it was intended to by extend only to within 5 cm of the blade ends. Due to the asymmetry of the lamination after machining the blade distorted significantly (sprang back) after it was released from the mold. There does not appear to be a way to use these blades for the turbine, and so we have determined that new blades will have to be fabricated.

The error in the lamination schedule seems to have resulted from an inaccurate estimation of the *wetted* thickness of the fiberglass and coremat—because the lamination schedule was developed using dry material we underestimated

the thickness of each layer, pushing the whole stacking sequence out. This would not have been a problem if there was only fiberglass in the lamination (it would have been simply far more overbuilt then intended), but because there was a core material this error resulted in severe asymmetry.

Future work will include developing a resin infusion process for making the next set of blades. The resin infusion process will allow us to place all of the dry material in the mold and and then add the resin to the material quickly—eliminating the problem of the blade partially curing during the process. This will allow the use an all-fiberglass lamination schedule without the time/heat concerns that led us to use coremat originally. Resin infusion is a more complicated process; care and practice will be required to produce a quality blade. Test laminations should be fully evaluated (cross-sectioned, etc.) before all four blades are made.

5 Turbine Spokes and Spoke/Blade Connections

5.1 Spokes

The turbine blade generate lift and drag forces from the incident water current, and transmit the resultant torque through the spokes to the central shaft. The spokes are also responsible for structurally supporting the turbine blades, and preventing blade twisting, vibration, and vertical movement. The spokes should perform these functions at a minimal cost in rotational drag, which directly affects turbine efficiency.

A flat circular disk was first proposed as a spoke design. A circular disk has
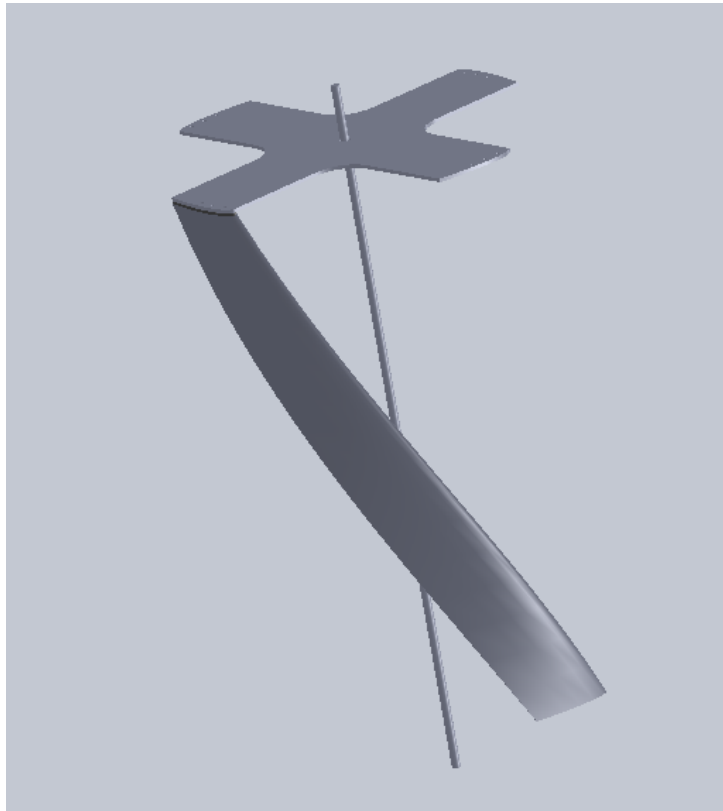
Figure 14: Rendering of the turbine as designed, with only one blade and spoke shown for clarity

the advantage of not presenting a frontal area to the tangential component of the flow. However, it was felt that the disadvantage caused by the large boundary layer drag caused by the large planform area of the disk was of greater concern. This spoke design was not modeled or tested, and may be of interest for further testing to quantify this planform drag vs frontal drag question.

Having eliminated the circular disk there were the following design decisions:

- Spoke material

- Spoke width

- Spoke thickness

- Spoke/blade connection detail

5.1.1 Spoke material

The key material properties considered when choosing the spoke material were strength and resistance to corrosion. The turbine will operate in highly corrosive environment, and the corrosion resistance of various materials and combinations of materials was carefully studied in the course of this design process. Details of this review are presented in Appendix B. Spoke material selection was focused on two classes of material:

- Composites, which provide excellent corrosion resistance, and can be quite strong

- Metals, of which anodized 5086 marine grade aluminum became the clear choice after other metals were proved either too expensive or ferrous, which could interfere with any instruments mounted on the Sea Spider that utilize a magnetometer to determine heading (e.g., Doppler profilers).

The large uncertainty regarding the loading on the spokes, the relative uncertainty and lack of experience associated with designing with composites, and ease of manufacturing led us to choose the anodized 5086 aluminum over composite materials. It was felt that the increased risk of corrosion associated with aluminum could be mitigated by anodizing and careful surface treatment. Additionally, corrosion tests conducted on material coupons mounted

on the Sea Spider show that 5086 aluminum has a far slower rate of corrosion than 6061 aluminum, even without a protective coating. A general reduction in uncertainty associated with using aluminum was considered prudent for the first iteration of the turbine design.

5.1.2   Spoke width

The width of the spokes was chosen to be equal to the chord length, which means the spokes completely cap the ends of the blades. Future iterations of the design may be able to reduce boundary layer drag slightly by reducing this spoke width, but because of the uncertainty surrounding the loading on the blades we decided that the small cost in drag was worth the increased blade support this spoke width will provide.

5.1.3   Spoke thickness

The thickness of the spokes represents the frontal area that is presented to the tangential component of the flow, and is therefore important to minimize in order to minimize rotational drag on the turbine. The forces on the blade have been modeled, and the results presented in section 5.3. A high level of uncertainty is present in this analysis however, because we know the flow is significantly more complicated than this very simplified model considers. Additionally, turbulent flow conditions, corrosion, and lack of symmetry in fabrication may all contribute to unanticipated loading or weakened parts. In order to satisfy the project goal of high reliability we had to choose the spoke thickness conservatively, even though a thicker spoke reduces overall turbine efficiency.
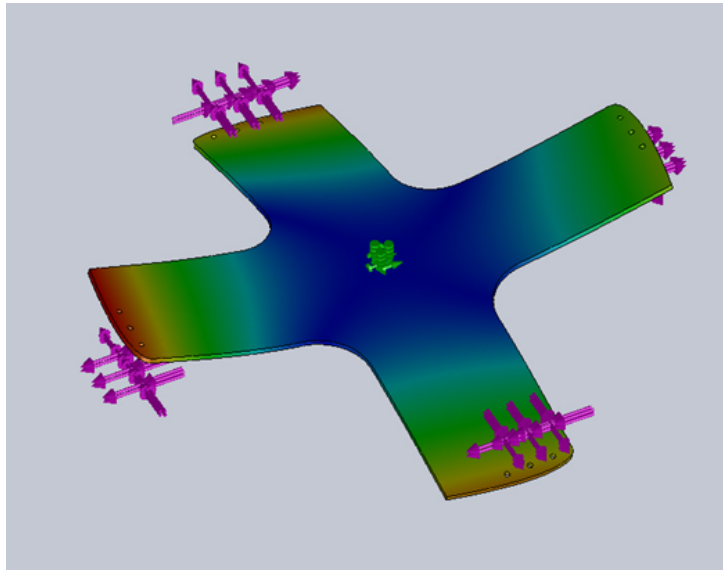
Figure 15: Image from stress analysis of spoke, performed in SolidWorks Simulation

Based of the forces on the blades as modeled in section 5.3, stress analysis performed in SolidWorks Simulation shows a large factor of safety for 5/16" 5086 aluminum spokes. This analysis should be confirmed before fabrication to recheck the results.

5.2   Spoke/blade connection detail

In designing the turbine blade attachment, we began by developing a list of 11 potential concepts compatible with either metal or composite spokes. Sketches of these concepts are shown in Figures 16 and 17. The list of potential attachment methods was less constrained with this approach, and meant that the spoke material of the optimum attachment designs could be considered in conjunction with the spoke material selection process.

Metal Spoke Options

Concept A

Construct the blade with metal tab protruding from the end of the bolt attachment to a metal spoke.
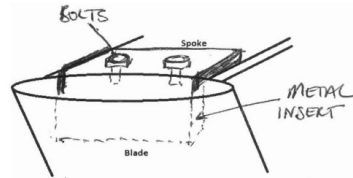
Concept C

Build in a composite extrusion on the ends of the blade for bolting to a metal spoke.
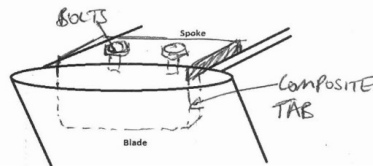
Concept E

Use threaded inserts in the blade to attach the blade to a metal spoke.
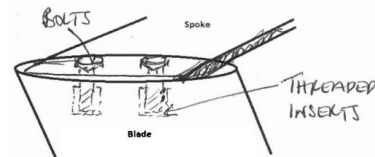
Concept H

Fabricate a metal sleeve on the end of the metal spoke that receiveds the blade and is bolted.
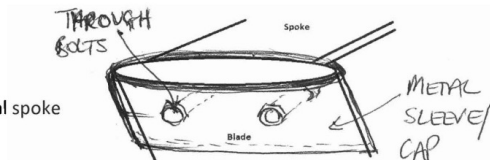
Concept I

Fabricate a metal. L-shape bracket on the end of a metal spoke and bolt the blade to this.
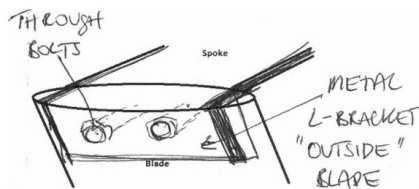
Concept J

Fabricate a metal, L-shaped bracke on the end of a metal spoke that is received in a slot on the end of the blade and is through bolted.

Figure 16

57
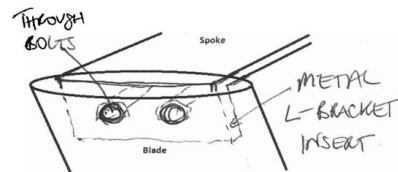
Composite Spoke Options

Concept B

Construct the blade with a metal tab protruding from the end for a bolt attachment to a metal spoke.
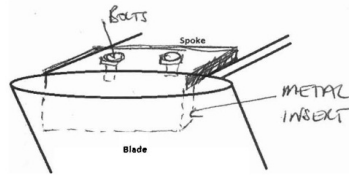
Concept D

Build in a composite extrusion on the ends of the blade for bolting to composite spoke.
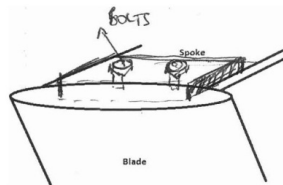
Concept F

Fabricate the blade and spoke as one piece in composite materials.
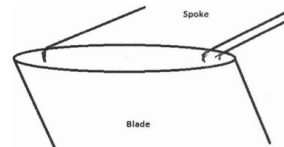
Concept G

Glue and tape the blade to a composite spoke.
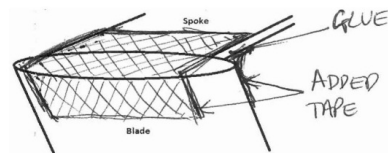
Concept K

Fabricate a composite, L-shaped bracket on the end of a composite spoke that is received in a slot on the end of the blade and glued in place.

Figure 17

58
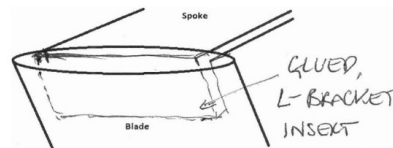
Table 7: Criteria for Weighted Decision Matrix

Criteria	Weight
Strength of the connection	22%
Corrosion resistance	22%
Hydrodynamics	17%
Ease of maintenance and repair	13%
Ease of manufacturing	13%
Cost of fabrication	9%
Environmental impacts	4%

The design options were assessed using seven primary design criteria in a weighted decision matrix. The criteria we identified characterize engineering, hydrodynamic and logistic concerns generated from the design requirements. The weighted values assigned to each criterion were the result of prioritizing agreed upon by the team, shown in Table 7.

These criteria and the eleven concept options were entered into a decision matrix. A ranking of 0 to 5 was used to determine the success of compliance for each concept to each criterion. This ranking process was conducted as a collaborative exercise by the team. The results of our decision matrix are in Table 8

The use of this decision matrix led to two designs that we considered to be equally good. These were concepts E and K, the metal spokes bolted to the fiberglass blades using threaded inserts, and the carbon fiber spokes connected to the fiberglass blades via a bonded slot-and-tab, respectively. The key advantage to the carbon fiber spoke is the resistance to corrosion, and the key advantages to the metal spoke is ability to disassemble, low risk, and low cost. After further discussion, that included spoke material considerations (see section 5.1.1), we decided that the metal spoke option would be the best fit for the project. Specifically, this decision was based on

Table 8: Final Weighted Decision Matrix

Criteria	Weight	Concepts										
		A	B	C	D	E	F	G	H	I	J	K
Strength of connection	5	5	4	3	4	5	5	3	4	3	4	5
Corrosion	5	2	3	2	4	3	5	5	2	2	2	5
Hydrodynamics	4	3	3	3	3	4	5	4	3	2	3	4
Maintenance/repair	3	4	3	4	3	4	0	2	5	5	4	1
Manufacturing	3	3	2	3	3	3	0	2	2	5	3	3
Cost	2	3	3	3	3	3	0	4	2	5	2	3
Environmental	1	5	3	5	3	3	1	2	4	5	4	1
Total		25	21	23	23	25	16	22	22	27	22	22
Weighted Total	**115**	**79**	**71**	**69**	**79**	**86**	**71**	**78**	**71**	**78**	**71**	**85**

the following basis:

1. It was felt that corrosion in the metal spokes could be avoided if the metal surfaces were carefully treated.

2. The team felt that it was important to be able to easily disassemble the spokes and blades.

3. Designing with carbon fiber presented several uncertainties regarding tear-out strength, buckling delamination, and the effect of prolonged seawater exposure. While some literature exists that study these factors, it was felt that using this material would create greater overall risk of failure than if a metal spoke was used.

4. The slightly larger dimensions associated with using metal spokes was not significant enough to impact overall hydrodynamic performance.
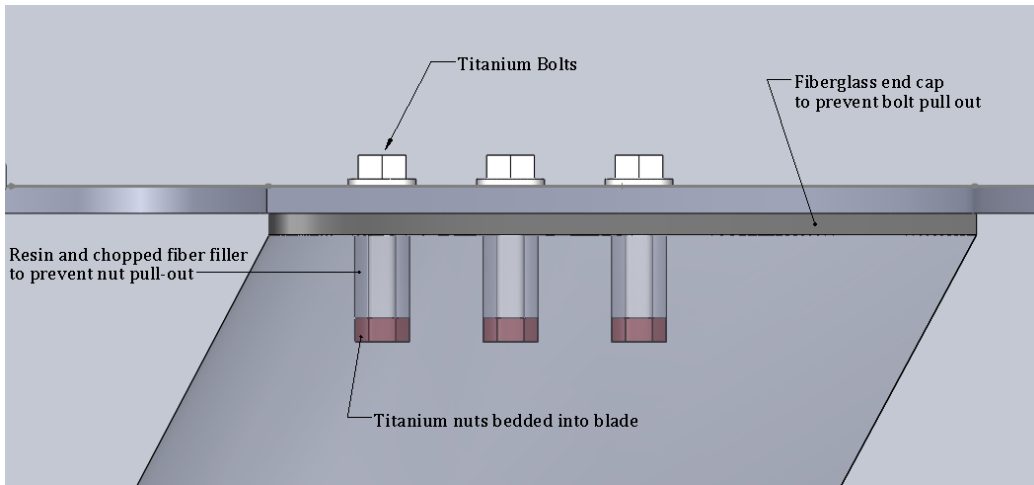
Figure 18: Cut-away side view of bolt/blade connection

5.2.1 Description of the final spoke design

A schematic of the final design is shown in Figure 18. For this design, the metal spoke material was chosen to be 5086 aluminum. The 5086 aluminum was deemed strong and stiff enough for the forces it will encounter, and anodizing and marine paint will provide sufficient corrosion resistance. Additionally, securing the bolts in the blade required special consideration. We initially considered two possibilities:

1. Laying up inserts into the composite blade during its fabrication

2. Adding inserts after blade fabrication

Manufacturing difficulties with these approaches led us to propose gluing nuts into holes drilled into the blades, as shown in Figure 18. Back-filling resin and chopped fibers in the space between the nut, the bolt and the top surface of the blade will provide sufficient resistance to prevent bolt pull-out. As an added precaution against bolt pull-out, we propose adding a thin layer

61

of fiberglass between the spoke and the blade, to be added after the nuts are in place. A potential drawback of this design is that the nuts will be permanently set into the blades, which prohibits replacement if they become corroded. For this reason we will use nuts and bolts made of titanium, which has an extremely high resistance to corrosion. Each blade end will be secured by three, $\frac{1}{4}$" $\times$ $1\frac{1}{2}$, titanium bolts. Although we considered using only two bolts, the size of the blade end areas allows the use of three bolts, resulting in more distributed loading and margin for single bolt failure.

5.3   Bolt force analysis

The design described in section 5.2.1 uses 3 quarter-inch titanium bolts for the spoke to blade connections. In an effort to make sure that the bolts have a large enough diameter, such that failure of the turbine will not occur from the bolts being sheared, the following analysis was carried out. In this force analysis V_r, the relative velocity of the water, will be strictly a sum of v_w the free-stream velocity vector and ωr or the tangential velocity vector that results from the turbine spinning. We will assume that λ, the tip speed ratio, is 2 and the free-stream velocity is 3 m/s. Therefore, ωr is 6m/s as is laid out in Figure 19.

The values for α, V_r, and Re were tabulated for every 4° of θ, the angle position around the blade, which is also the angle between the chord and v_w. These values we tabulated and calculated in Excel, with the subsequent C_L and C_D values obtained from XFoil and then the calculated F_L and F_D values, found using the following common equations:

$$FL = CL\rho V_r \frac{2C(dh)}{2}$$
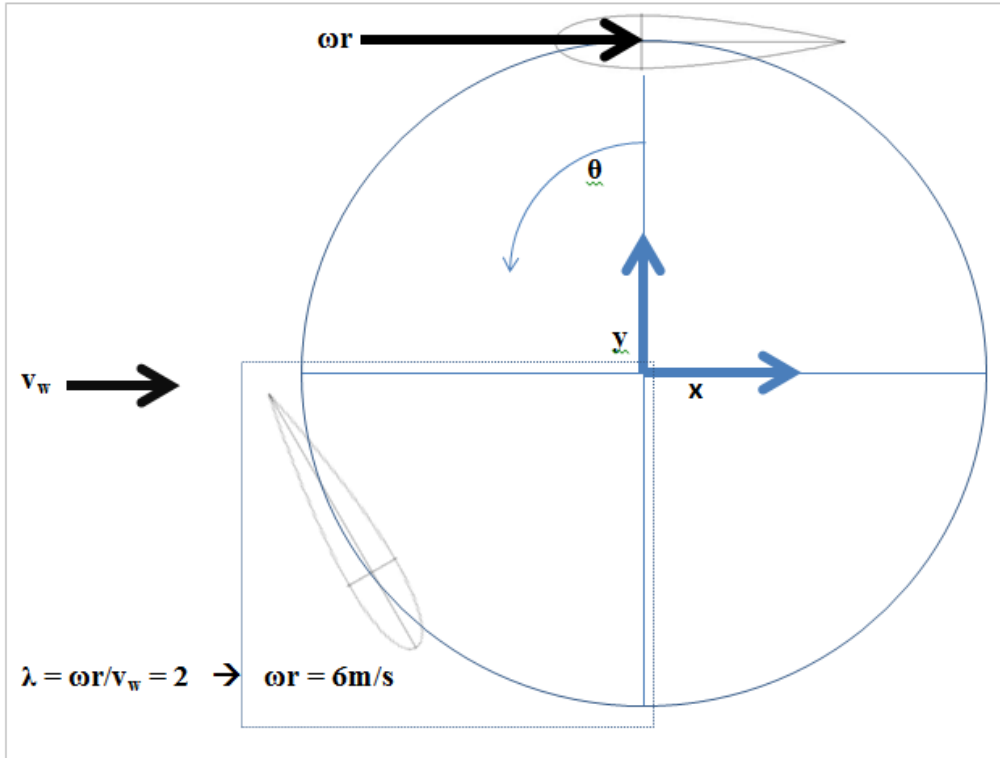
Figure 19: Velocity vector illustration for bolt diameter analysis

$$FD = CD\rho V_r \frac{2C(dh)}{2}$$

$$\text{Where} \frac{H}{\frac{2\pi r}{B}} = \frac{dh}{\frac{4°\pi r}{180°B}} \rightarrow dh = \frac{H4°}{360°} = 0.011\ m$$

C is the chord length, 0.165 m and $\rho = 1025\ \dfrac{kg}{m^3}$

The angle of F_L and F_D in the x-y plane is found from γ which is shown in Figure 20. γ is the angle between V_r and v_W and is the same as the angle between V_r and the x-axis. Quite simply, the lift force is orthogonal to V_r and the drag force is in the same direction as V_r. Now F_x and F_y are found

using the following equations:

$$F_x = F_L sin(180° - \gamma) + F_D sin(90° - \gamma)$$

$$F_y = F_L cos(180° - \gamma) + F_D cos(90° - \gamma)$$

The angle in parenthesis is from the y-axis. After the forces of each 4° blade section had been translated into the x-y plane, the forces for 90° segments were summed at each 4° interval. The 90° segment that had the largest force was found to be from around 256° to around 344°; a perfect 90° was not calculated because of an initial decision to use 4° intervals. This maximum blade force was 1472 N in magnitude or 1001 N in the x direction and 1079 N in the y direction. This translates to 245 N per bolt as F', the direct shear translated to the bolts.

To find the location in the x-y plane for F_x and F_y centers shown in Figure 21 the F_x and F_y forces were summed until the sum was about half of the total for the 88° section. The sum of the F_x forces on this 88° section is termed $F_{max}X$, and the sum of the F_y forces is termed $F_{max}Y$. The angle that $F_{max}X$ was centered at was at 294° in the x-y plane and $F_{max}Y$ was centered at 308°. In an attempt to simplify the calculations a new coordinate system is set to be 0,0 at the leading pressure center of the blade, where it is assumed the leading bolt will be, as shown in Figure 21. In this new coordinate system the location of $F_{max}X$ and $F_{max}Y$ are located at (s,t) = (13.5 cm, 27.6 cm) and (6 cm, 19.6 cm) respectively. The moment in the x-y or s-t planes that was a result of these forces not being centered on this blade was very small and added no more than 5 N to the shearing of the bolts. It was determined using the data in Appendix B that a bolt diameter of 0.25 inches will allow for a factor of safety of more than 10 in static loading. Such
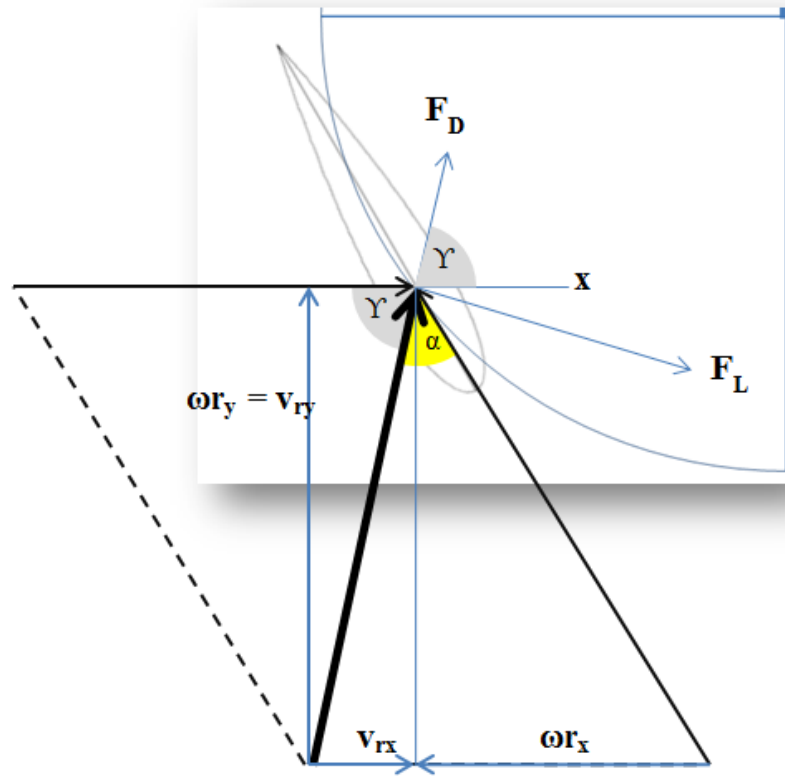
Figure 20: Velocity Vector Addition

a high factor of safety assuming the lowest yield strength for titanium would surely be safe from fatigue.

The area center for the 6 bolts centered 3cm apart was calculated to be
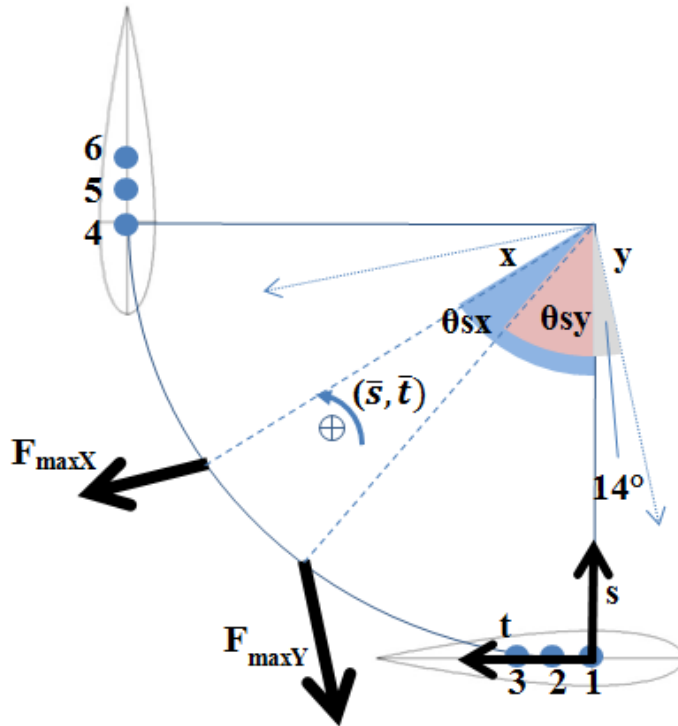
Figure 21: Maximum Blade Force Center and translated s-t plane

$(\bar{s}, \bar{t})=$(19 cm,19 cm), using the following location points for each bolt center.

$$(s,t) = \begin{cases} (0,0) & @\ 1 \\ (0,3) & @\ 2 \\ (0,6) & @\ 3 \\ (35,35) & @\ 4 \\ (38,35) & @\ 5 \\ (41,35) & @\ 6 \end{cases}$$

In order to have more confidence in this calculation it seemed prudent to calculate the torque of this dynamic system. This torque neglects the induction

factor and assumes a perfect hydrofoil at a turbine that is not deep enough to feel a change in sea water density or viscosity. For this analysis we once again translate to a new coordinate system that is centered at the pressure center of NACA 0018 hydrofoil, as shown in Figure 4. This is useful for our helical turbine in that all 360° degrees that were calculated above exist at all times as the turbine spins. Using the following equations and data listed in Appendix A, the sum of the forces in the γ direction can be multiplied by the radius to determine the torque.

$$\chi = \sum F_i sin\theta_i$$
$$\gamma = \sum F_i cos\theta_i$$
$$\theta_L = \alpha - 90°$$
$$\theta_D = \alpha$$

The torque was calculated to be about 520 N-m, yielding a coefficient of power of a 0.92, which is very unrealistic. However Linear Momentum Theory (LMT) predicts a reduction of incident fluid speed due to blockage of the flow by the turbine. For a turbine operating at the Betz limit this reduction factor (called induction factor in LMT)is$\frac{1}{3}$. If we use an induction factor of $\frac{1}{3}$ as an initial estimate of the reduction of incident flow speed,then we find have a more realistic coefficient of power of 0.27.

6 Turbine Frame Design

The preliminary design of the frame structure for the turbine and Sea Spider is shown by Figure 24. The primary design goal was to create a strong structure that is able to provide support to the helical turbine that will be
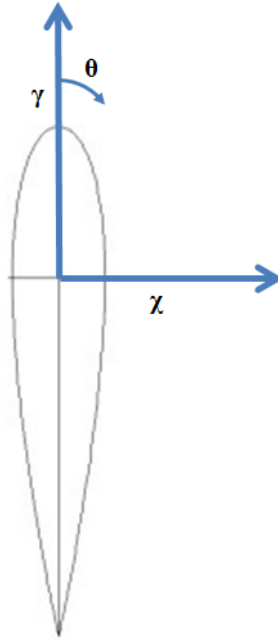
Figure 22: Skematic of the $\chi - \gamma$ coorindinate system that is referenced from the foil chord line

installed at the center shaft. Additionally, this frame structure will be used to offer some space for the Sea Spider's oceanographic instruments. In this frame analysis, two different faces of the frame will be used to calculate the deformation of the frame due to axial force of the ocean currents, since the orientation of the sea spider are unknown once it is being deployed in Puget Sound. The analysis that is being done in this section is assuming that the ocean currents speed of 3.5 meter per second, and the axial force that corresponds to the currents speed is approximately 4800 N. [3]. This represents the worst-case scenario for which we are designing.

The analysis of the frame was done with SimulationXpress from SolidWorks.

---

[3]See appendix E for details of the drag calculations
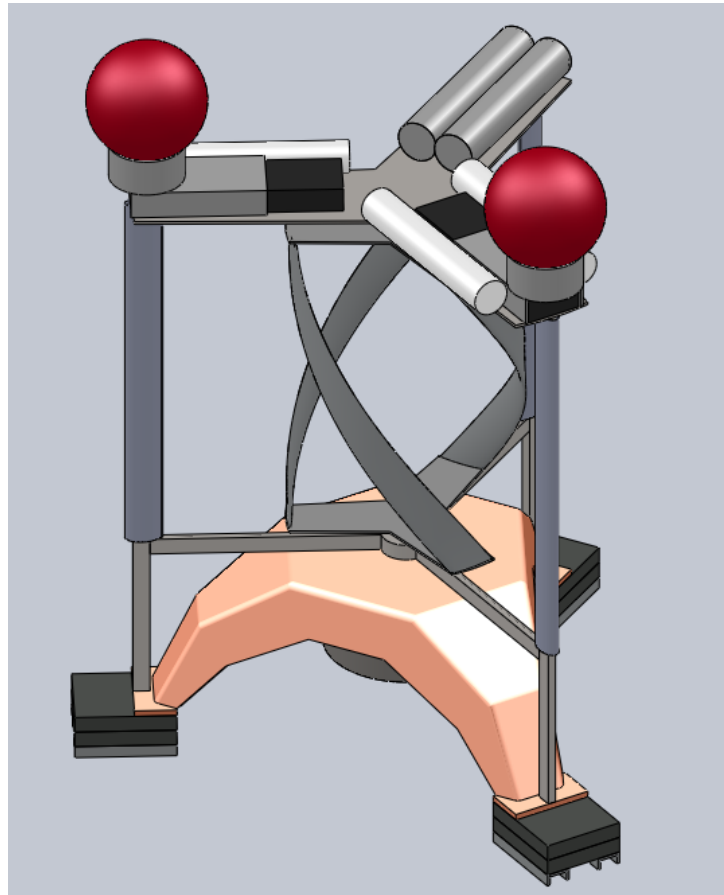
Figure 23: CAD model of the Sea Spider with the initial design of the turbine and turbine frame.

Furthermore, in this analysis, the material assigned to the frame is Stainless Steel (ferritic). Figure 25 below displays one of the three-dimensional models of the frame under an applied load. The green arrows in the Figure show the fixtures applied to keep the part from moving when loads are being applied, and the purple arrows simulate the applied loads on the frame. Overall, the results in Figure 25 show high safety factors, with the exception of a critical part in the center shaft that might cause failure, and the lowest factor of
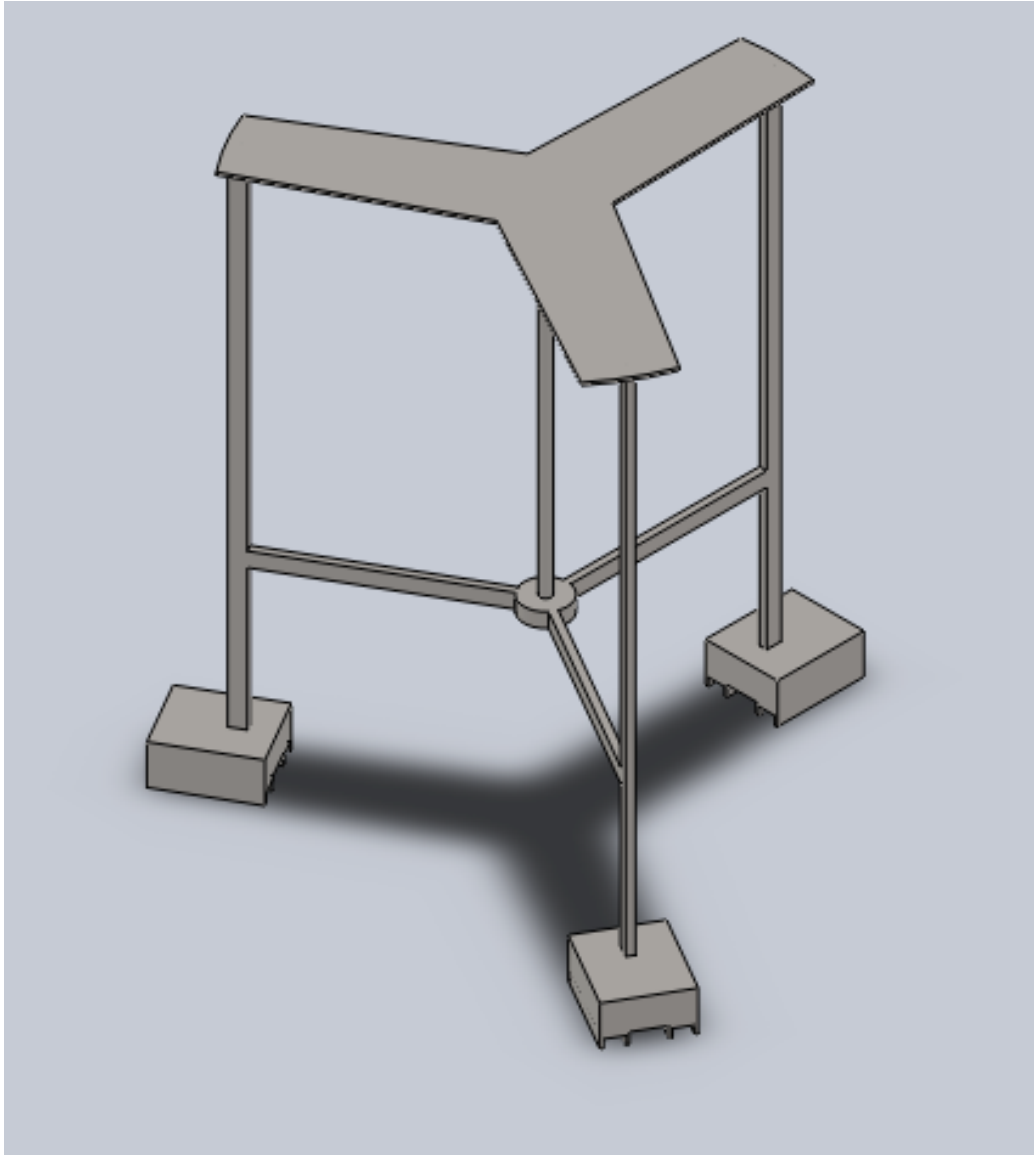
Figure 24: Preliminary design of the frame structure

safety in this case is 1.326. The analysis of the frame from a different face is shown in Figure 26. In this face, the same thing happens as the previous case, the critical part is located in the central shaft where the turbine is going to be attached. However, the lowest factor of safety is only 0.846 which means some improvements need to be made to overcome deformation due to the loads applied. Some points to take away from this analysis is that the bottom section of the frame is stronger in comparison to the top section of the frame; therefore one way to help prevent deformation is by adding structural beams to the top section. At this point, this is enough analysis to approximate how this frame behaves under the ocean currents, even though several assumptions have been made to illustrate the oceans condition, such as the axial force on the turbine, the speed of the ocean currents, and the material that is used to build the frame. More complete analysis with the whole turbine and sea spider is needed to see how everything is going to behave as a whole.

6.1   Proposed Manufacturing

Due to time and financial constraints, constructing the frame was not possible at this time. In the initial analysis of the frame, it was decided that stainless steel would be appropriate. After learning more about how stainless steel corrodes in the ocean, it was deemed an inappropriate material from which to make the frame. The frame would likely be constructed out of 5086 marine grade aluminum . Another consideration when designing for manufacturing is that the forces applied in this simulation could be comparative to the forces applied to turbine blades. The force used in these simulations were not updated since those forces were investigated.
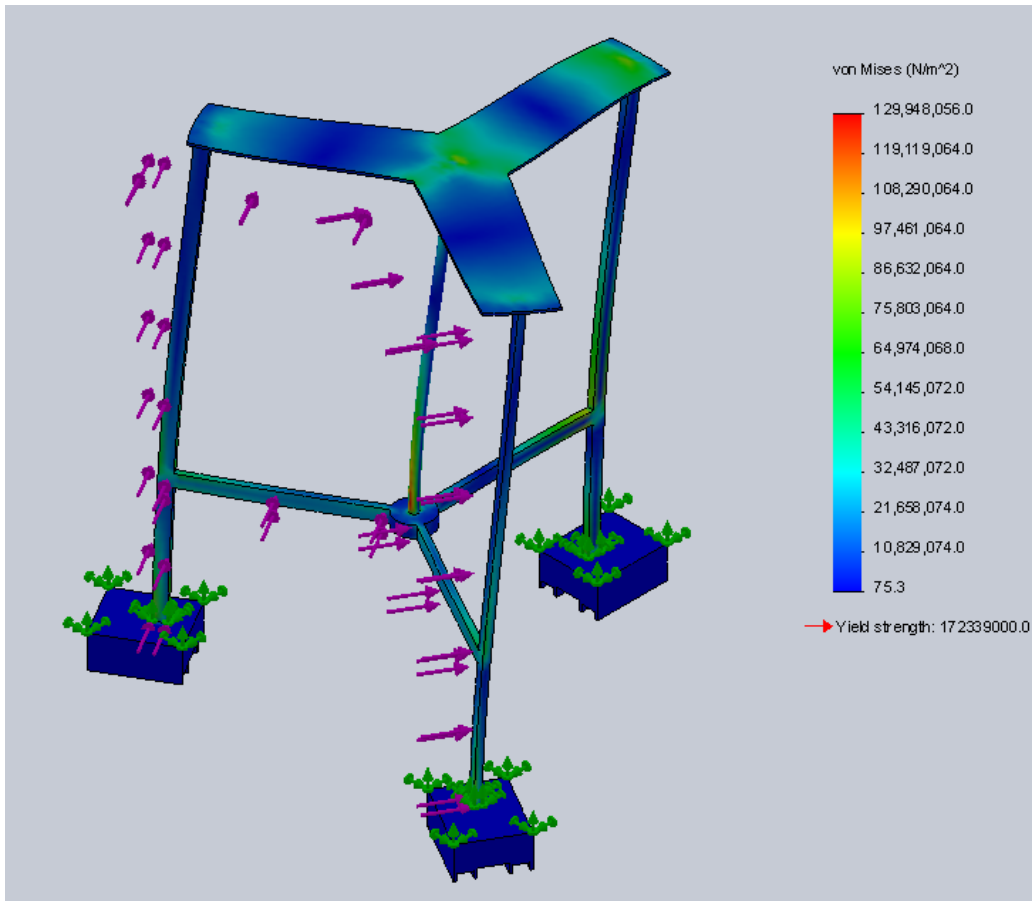
Figure 25: Preliminary design of the frame under loading, orientation 1

6.2 Bearings

A key component of the design will be the bearings used to mount the central shaft to the frame of the support structure. The bearings must be durable, be able to support the bending moment of the shaft and turbine. Price will also be considered when deciding upon the type of bearings. Several types of bearings have been considered, including sleeve, ball/roller, and mounted bearings. Images of each are shown in Figure 27. Sleeve bearings work by allowing low friction rotation between the bearing and the shaft. This is
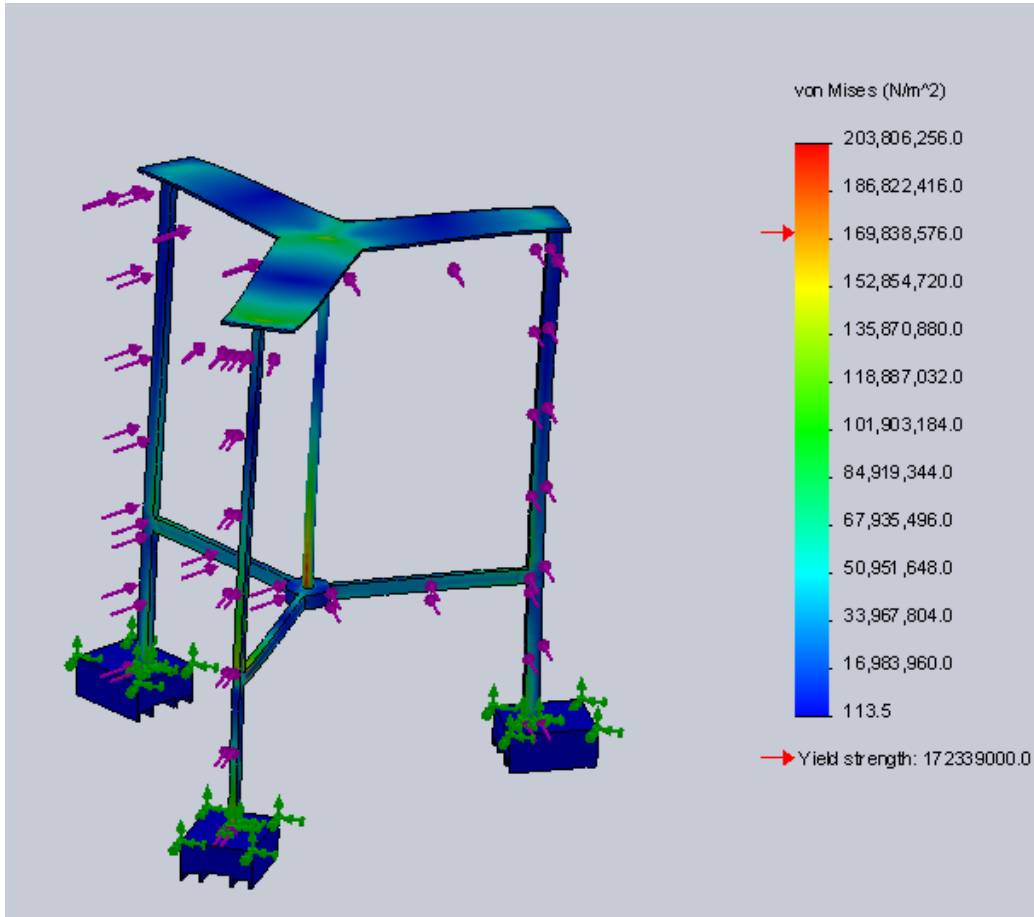
Figure 26: Preliminary design of the frame under loading, orientation 2

(a) Sleave Bearing   **(b)** Ball Bearing   **(c)** Mounted Bearings

Figure 27: Three styles of bearings [5]
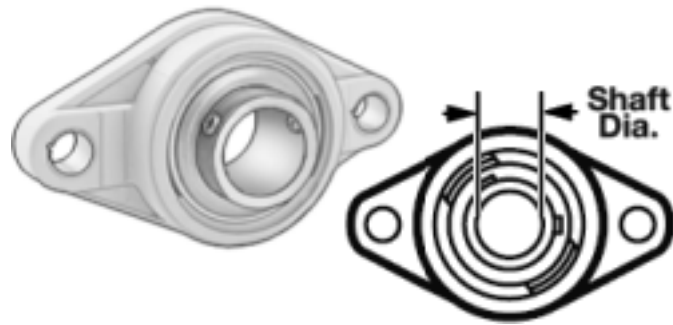
Figure 28: Mounted bearing type to be used for turbine shaft

generally aided by a lubricant. Water lubricated polymer sleeve bearings are an example of this type of bearing that may be suitable for this application, and deserves further investigation. Ball bearings use metal balls to reduce the friction even further. There are several types of ball bearings, including open, flanged, double sealed, double shielded, and extended inner ring [6]. The most appropriate ball bearings for this project are the double sealed ball bearings because they keep sea water out while keeping the lubricant inside with the ball bearings. Roller bearings have similar properties to ball bearings, however they use cylinders instead of balls to reduce friction. Roller bearings typically have higher load capacities than ball bearings, making them ideal for high load cases.

Mounted bearings consist of the aforementioned bearing types, but installed with a flange or plate. This flange makes installing the bearings much easier and allows them to be mounted to surfaces easily [1]. Initial cost comparisons of each type of bearing revealed that the majority of roller bearings were too expensive, being in the $500 and above range. After comparing the prices of several different bearing types, it was decided that a standard mounted double sealed bearing is the best choice of bearings. The price ranges between $55 and $65, depending on the shaft diameter, while having a relatively easy

installation and attachment to the frame. Figure 28 shows a picture of a standard mounted bearing.

7   Economics

This project is partially motivated by the current cost of replacing batteries on oceanographic equipment. The battery cost itself is not a trivial figure, but the cost of operating a boat to go out to the equipment and service it is substantial, in many cases comparable to the cost of all other elements in the experimental campaign. By designing a turbine to attach to the equipment, the plan is to reduce the frequency of trips out to the equipment, as well as the need to replace the batteries as often. This would be achieved by having rechargeable batteries that would be kept charged by the tidal turbine during the times of fast current, and would supply the instruments during the times of slow current. Another economic consideration for this project arises from the material choices made of the turbine. Choosing the material of the blades, central shaft, and bearings all are relevant and cost related.

During the project period discussed in this report we were fortunate enough to receive a Capstone Project Funding award of $2500. This money has been used towards the blade manufacturing process, specifically, contracting Turn Point Design to fabricate a molding tool (quoted at about $1800), and acquiring materials for the composite construction. To date, the cost of mold tool fabrication is about $1600 and the composite costs are about $800. Although this spending is within the available funding, the project finances have been severely altered by needing to re-fabricate the blades. This major obstacle will mean that an estimated additional $200-$300 for machining the

blades at Turn Point Design, and $500-600 in composite materials is needed to progress with the blade manufacturing. In all the design selections made in this report economic considerations were significant. The team has identified the following costs for recommended designs as they are implemented:

1. Approx. $300 for the 5086 aluminum for the spokes.

2. Approx.$70 for the 24 $\frac{1}{4}$" $\times$ $1\frac{1}{2}$" titanium nuts and bolts of the blade-spoke attachment.

3. Approx. $55-65 for each bearing.

4. Costs associated with the structural framework and central shaft have yet to be established.

8   Risk and Reliability

Since this project is focusing on tidal turbine, there are few health and safety concerns that directly affect the user. The design and the implementation of the turbine should address more on marine life and their ecosystems that will be cover in the next sections. One thing that might need consideration is regarding the turbine maintenance. This turbine need to have occasional maintenance in order to work properly by fixing any corrosion damage, adding more lubricant, and coatings to stay the advances of biofouling, since the turbine constantly working and subject to harsh environment condition. This might become problematic if we do not design the turbine properly for easy maintenance. However, the choice of cross-flow helical turbine might be helpful in the way that it has smoother torque than any other turbine,

which in result reduces the chance of cavitation, vibration, and less frequent maintenance [24].

Throughout the design process we have kept in mind the project goal of high reliability. Conservative estimates of forces, corrosion, and efficiency have been used in the process in an attempt to reduce the possibility of turbine failure in service.

9 Social, Environmental, and Ethical Considerations

9.1 Societal Effects

Finding new ways to generate power has been a main concern of our society for quite some time. Tidal energy offers an alternative to coal and oil energy production that neither diminishes earth's resources nor produces any harmful byproducts that cause adverse effects on the environment. This represents an advantage for tidal turbines to aid future generations in meeting their energy needs while maintaining the health of the environment. The deployment of tidal turbines at a certain location might also have a local effect impact on the people who live in the nearby area, such as local tribes who practice traditional fishing and crabbing, commercial fishing and crabbing operations, and also people who dive for the purpose of recreation. However, since the goal of our project is to build a small scale micro-power tidal turbine that will be used only to power underwater research instruments, we predict the impact to local communities to be negligible or nonexistent.

9.2 Environmental Effects

Tidal energy is a form of renewable source of energy which does not result in any gas emissions responsible for global warming or acid rain associated with fossil fuel generated electricity. Even though tidal energy is a clean type of energy, there are still potential impacts on the environment to varying degrees that we need to consider when we designing our tidal turbine. One of the important issues is the issue of fish mortality as they encounter spinning turbine blades. Another issue that we need to consider is the issue of chemical pollution to the marine environment due to necessary coatings and lubrication for antifouling and to control corrosion. Therefore, the use of nontoxic chemicals is crucial. Lastly, as the turbine rotates, it will produce noise. This might affect the marine environment such as migration patterns of fish and marine mammals. The choice of a turbine design that generates smooth torque curve and therefore produces less vibration and noise will mitigate this impact somewhat.

9.3 Ethical Considerations

In any engineering project, every aspect of the product design, implementation, and disposal needs to be ethical. Our priority in designing the tidal turbine is reliability. The turbine needs to be reliable, since it will be deploy in hostile environment for a long time and without any communication with the surface until the turbine and oceanographic instruments are retrieved. Additionally, the accelerated corrosion experienced in salt water plays a major role in the durability of a device, while erosion is possibly more influential on tidal current converters, as carefully profiled rotor blades and hydrofoils will operate less efficiently once their surfaces become scratched, pitted and

generally tarnished. Similarly, bio-fouling and marine growth on rotor blade surfaces, hydrofoils or even ducting will also cause disruption to the flow of water around these surfaces and reduce the operating efficiency of the device. Therefore, we will ensure that the turbine is built out of good quality materials and parts, and that it is assembled with skill and care. The considerations for the marine life are also accounted in every aspect of our turbine design and implementation. These considerations include the fish mortality and chemical pollution to marine environment discussed in previous sections. We will consider the use of nontoxic lubricants, corrosion and biofouling coatings, regardless the cost.

10   Conclusion

We have described the design and partial fabrication of a helical vertical axis tidal turbine. This turbine was designed to be part of a system for the production of 20 W (average) of electricity, to be used to power oceanographic instruments as part of a tidal energy site characterization research project. We surveyed the tidal turbine literature, especially regarding the helical vertical axis turbines. This literature was examined closely to understand the relationships between key turbine design parameters and turbine performance. Questions involving these parameters were examined by the fabrication and testing of three turbine scale models, which were tested in a flume. The tests were not conclusive, but based on preliminary results a turbine design was selected. Turbine blade manufacturing options were explored and a process and materials were chosen. Five full size turbine blades were manufactured from fiberglass and vinyl ester resin in a one-sided mold wet lay-up process that involved overbuilding the top half of the blade, then

machining it to shape. During the blade machining an error in the lamination schedule was discovered; the fabricated blades were deemed unusable.

Forces on the blades were modeled using Blade Element Momentum theory, and the results of this analysis was used to design the turbine spokes and spoke/blade connections. Preliminary design work was performed on the support frame. Economic, ethical, and environmental issues regarding this project were discussed.

A   Survey of Tidal Turbine Concepts

A.1   Transverse Horizontal Axis Water Turbine

The transverse horizontal axis water turbine, or "lawnmower turbine", is one of the initial designs that was considered. A lawnmower turbine is essentially a Gorlov turbine turned on its side. The lawnmower turbine operates similarly to the Gorlov turbine, however the orientation when lowered into the ocean is important, since the turbine will not work if it is not properly aligned with the current. To correct for this orientation issue, some way to passively align the turbine would be required. It was decided that a vertical axis Gorlov turbine would be a better fit for this situation.

A.2   Vortex Induced Vibration Aquatic Clean Energy (VIVACE)

The VIVACE system [12] makes use of vortex induced vibrations, VIV, exhibited by cylinders placed in tidal streams to generate electric power. The VIV phenomena has been well documented as a problematic feature in many engineering systems, but the VIVACE system is designed to harness this energy. The converter is made of a long cylinder placed perpendicular to the flow stream and supported on both ends by springs. The springs relay the kinetic energy to a generator system that then produces electricity. The authors' concept is to deploy numerous such devices stacked at prescribed distances apart in a rectangular "power plant" [12]. Researchers have included both laboratory and mathematical models in the analysis resulting in a reported experimental efficiency of 22% at flow velocity of 1.5 m/s.

The report includes the "Design particulars of six different scales of the VI-VACE converter"[12]. The "Micro" scaled device is stated as producing 76.1 Watts per module. Although this power output meets the 20 Watts required for our project (assuming continuity with most calculations in the report made for 1.5 m/s tidal stream), the dimensions of this converter would be 0.1 m diameter by 2 m length. The dimensions are larger than is appropriate for our application but theoretically could be altered by the minimum correlation length recommended in the report to an aspect ratio of 7. This would produce a marginally effective system that would require consideration of multiple modules and the implied mechanical complications.

One of the main concerns with use of this design for our project is orientation. Efficient operation of the device assumes a particular orientation to tidal flow direction that is hard to ensure in our application. The design described in the report does not offer a simple aligning method in varying flow directions but is proposed for predictable bidirectional flow locations. The system would be at the margin of applicability for our required efficiency so the potential of these added losses or adjustments is risky. The report also refers to the necessity to tailor the total system damping, spring stiffness and oscillating mass role for specific depth deployment which would be difficult to predict for our more versatile device. The overall system includes a number of parts in a complicated configuration that could foul, fault or break, and an awkward attachment profile for the Sea Spider. Lastly, there is very limited available literature or experimental references to VIV tidal converters to adequately engineer from for our project.

Figure 29: Artist rendering of a Horizontal Axis Tidal Turbine

A.3   Horizontal Axis Turbines

The Horizontal Axis Tidal Turbine (HATT) was a turbine design considered for this project. As the name implies, the rotor of this turbine rotates about a horizontal hub in exactly the same way as modern wind turbines, shown in Figure 29. This type of turbine has several attractive features, including:

- A long and favorable track record in the wind industry, and continued support in the marine energy industry [11], [22])

- High extraction efficiency, with realistic energy conversion from kinetic energy in the tidal stream to rotational energy in the turbine of approximately 45% [11], [10]

- Well-documented numerical simulations of turbine performance [11]
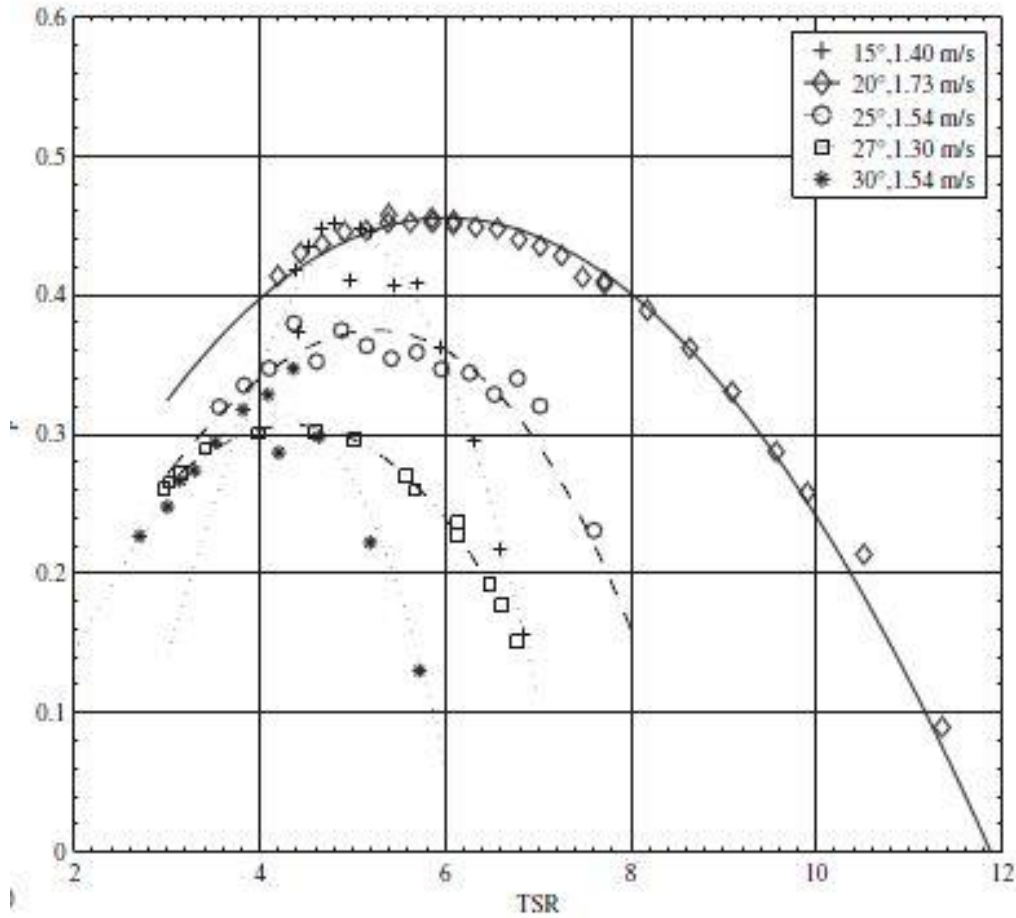
Figure 30: Horizontal Axis Tidal Turbine Efficiency as a function of Tip Speed Ratio for various blade geometries and water speeds

- Reasonably accessible blade manufacturing techniques, and highly accessible performance predictions based on blade element momentum theory.

A variety of horizontal axis turbine designs were considered, including the no-hub design of Open Hydro [7] and the more conventional design of Marine

84

Swept Area	1.0 m^2
Efficiency	40%
Current Speed	1.4 m/s
Extracted Power	561W

Current Turbines [4]. Most literature we considered was focused on turbines with a three-blade aerodynamically shaped rotor. Batten, et al, give general performance expectations for a three-bladed turbine [11], and their simulations are confirmed by testing performed in a cavitation tunnel and tow tank [10]. These tests also investigated differing yaw angles and studied cavitation of the blades. Bahaj et. al. [10] shows the performance of such a turbine tested in a cavitation tunnel at various speeds. Efficiencies between 35-45% were demonstrated. Table 1 shows a summary of the power generation capability of such a turbine at moderate efficiencies and current velocities. It was assumed that a HATT designed for the purpose of small-scale power production would be a three-blade type with a swept area no larger than 1 m^2 and located as close to the deck of the Sea Spider as possible to reduce the overall overturning moment placed on the frame. The blades would be formed into an appropriate airfoil shape as was determined to be most suitable for our flow and performance needs, including the need to self-start the rotation of the turbine. The blades would be a fixed-pitch design. Cavitation was not considered a significant design consideration for this rotor. Hydrodynamic pressure at the depths at which the turbine would operate is great enough to largely eliminate all vapor pocket formation.

There are disadvantages to this turbine as well, however, the most prominent being the inability of the turbine to adapt to a reversing tidal flow. Current velocity profiles in Puget Sound are somewhat chaotic, not allowing the turbine to be purely bi-directional in design. The rotational axis of the turbine
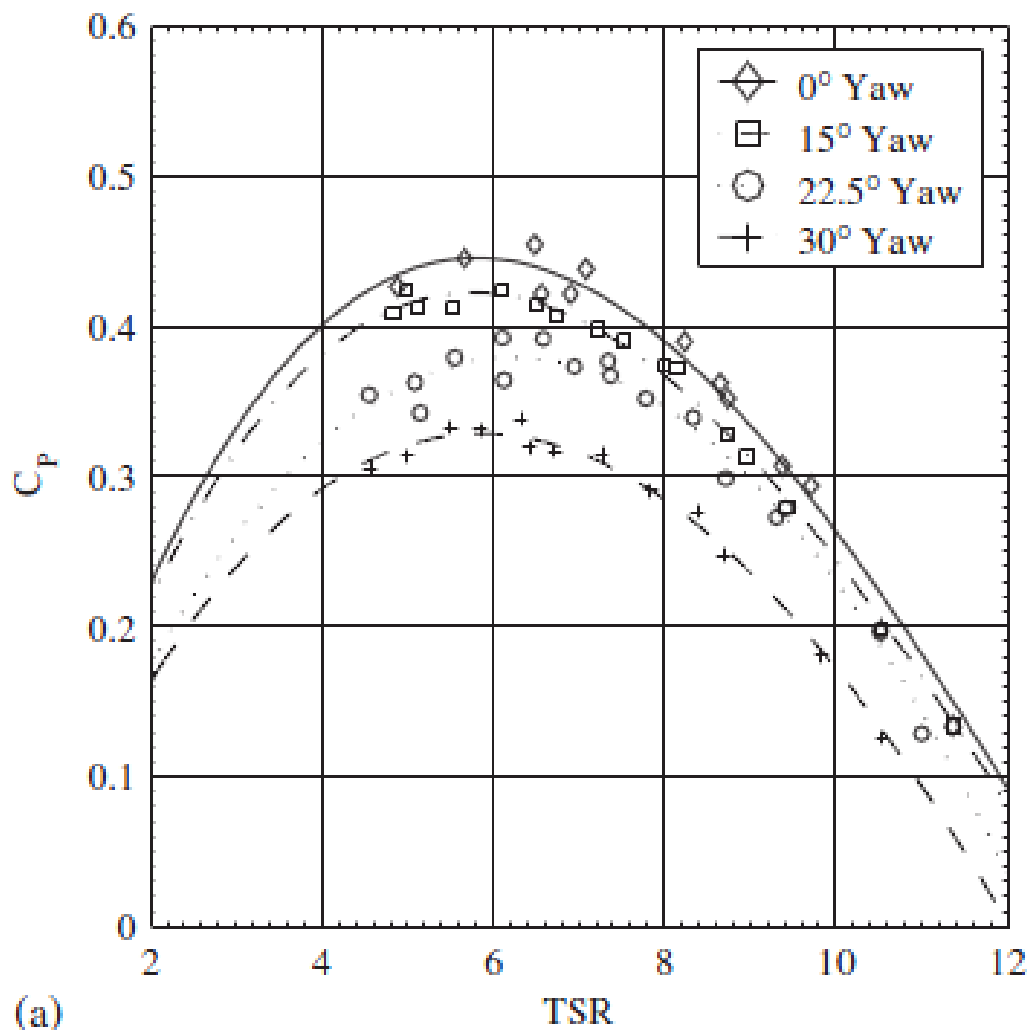
Figure 31: HATT Efficiency as a function of Tip Speed Ratio for various yaw angles

must ideally be parallel to the current velocity vector for optimum power extraction, with not insignificant degradation in performance as the angle (yaw) between the axis and velocity vector is increased [10]. Theoretically, a downwind-type turbine should automatically orient itself into the direction of the ambient current, and an upwind-type turbine could be oriented with a vane-type system. The challenging aspect of the design is then the transmission of electrical energy from the horizontal rotational axis of the rotor to the vertical rotational axis of the nacelle and pylon. Commercial manufacturers have used slip rings to provide electrical contact, or they have limited the extent of rotation to allow conventional wiring to pass through the pylon without undue torsion. Hydraulic drive systems were attempted by wind turbine manufacturers but were never perfected. Passive yaw systems have been demonstrated by Verdant [8], and active yaw controls for wind turbines have been enormously successful. Nonetheless it was decided that designing and implementing any such yaw control system would be beyond the scope of this project. Additionally, the entire turbine assembly, including the generator, mounting frame, transmission and rotor, must be built to work singularly with a HATT system, unlike vertical axis turbines which could potentially have some interchangeability among parts. This would have the effect of reducing the scalability and flexibility of our construction choices as the project progresses. The HAWT concept remains a promising avenue of research and much development is being done with it on commercial tidal energy projects. However, it was determined that the design was too complex and that unforeseen complications could significantly impair the development of our turbine.

A.4 Achard Turbine

The Achard Turbine is a variant of the "squirrel cage" type of cross flow turbine. Instead of three or four vertical blades, the Achard design is composed of three vertical blades arranged in a delta shape, as seen in Figure 32. The delta wing blade is designed to smooth the torque spikes characteristic of the vertical blade turbine. Torque spikes are characteristic of cross flow turbines because as the airfoil moves around the axis of rotation it moves through areas of high lift/low drag and areas of high drag/low lift. For vertical blade turbine the whole blade moves through these areas at the same time, causing periodic torques spikes. The delta wing of the Achard turbine—like the helical cross flow turbine—attempts to ameliorate this problem by spreading the blade around the angle of rotation. The tip of the delta blade moves into a high drag area first, while the tips of the blade are still in a low drag area; this acts to smooth the torque spikes.
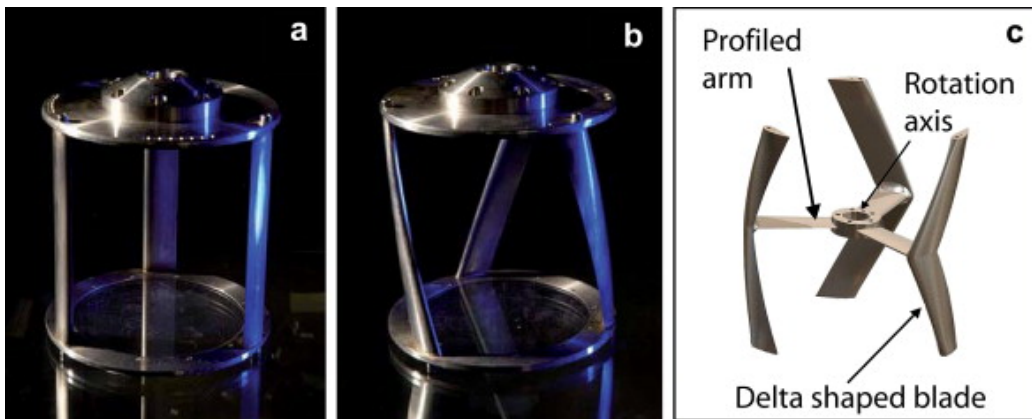
Figure 32: The squirrel cage style cross flow turbine (a), a helical cross flow turbine (b), and the Achard turbine (c). From Zanette, et. al. [28]

Numerical models have been used to characterize the performance of the Achard turbine [16] [9], but there is no published experimental data for

h!
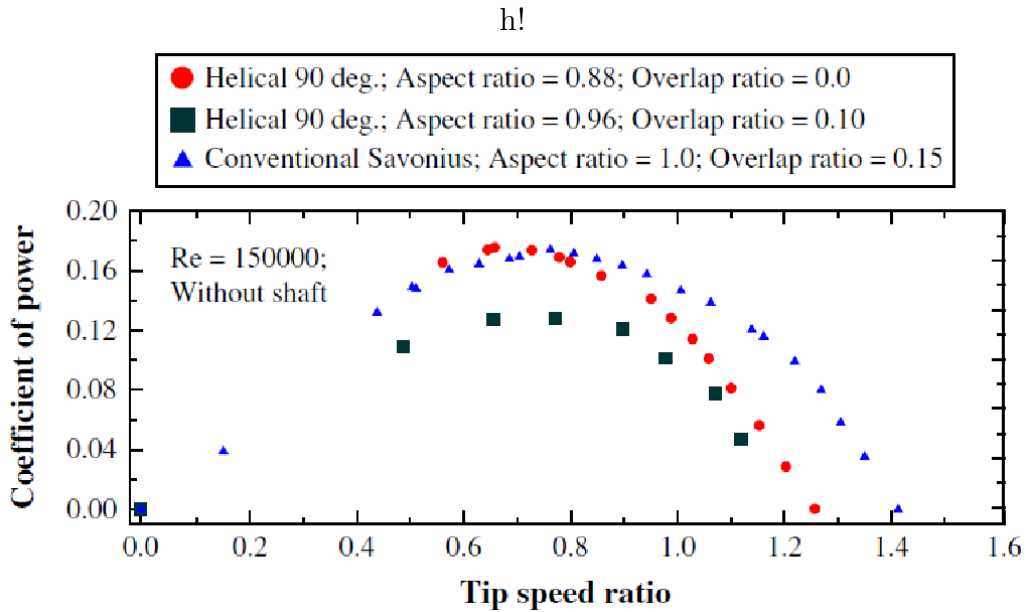
Figure 33: Coefficient of power for a helical Savonius as a function of λ [20]

Achard turbine efficiency at this time. The Achard design is a promising concept, but we decided that some experimental results were a minimum criteria for a turbine design in the context of this project.

A.5 Twisted Savonious Turbines

The Savonius is primarily a drag turbine; it does not rely on lift from an airfoil. The primary advantage in using drag forces to rotate the turbine is the high starting torque. The primary disadvantage is the low C_p, as seen in Figure 33. Adding buckets to the Savonius tends to reduce the C_p, however twisting the buckets with a helical angle has been shown to increase Cp. Interestingly a 10% overwrap of the helical angle decreased C_p again. The highest efficiency of a wind tested helical Savonius was still only 0.17[20]. This is below our minimum requirement for C_p .

A.6   Tesla Turbine

Nikola Tesla invented a little known bladeless rotor back in 1913. This turbine is bladeless, which is thought to be desirable for reducing the chance of debris snagging in the rotor or fish being struck. The Tesla rotor is a stack of evenly spaced disks that rotate due to shear forces on the disks by a fluid flowing perpendicular to the rotor's axis. Recent test efficiencies increase with rpm and max out around 0.2 and 0.25 [19]. Even though these efficiencies are desirable, the Tesla has a very low track record and the fully submerged/bidirectional version could prove to be a very complicated design. It was for this reason this rotor idea was dismissed.

A.7   Lift/Drag Hybrid Turbines

The lift-drag hybrid type of turbine was investigated as a potential solution to the self-starting problem of Darrieus turbines. The primary form of the hybrid turbine is a Darrieus-Savonius hybrid. Existing wind literature on the subject was consulted. The idea is to take a self-starting drag-type turbine and convert it into a high efficiency lift-type turbine after it has started. The problem is that the Savonius turbine becomes a drag on the system, limiting efficiency. This was shown by Yusaku Kyozuka for several configurations of Darrieus-Savonius hybrids [21]. The best-case scenario for a hybrid turbine is to reach the efficiency of the Darrieus turbine. This is an attractive scenario, however in every paper the researchers were unable to reach the Darrieus efficiency, and could only approach it. In some cases, this is considered acceptable to compensate for self-starting problems. Kyozuka showed the best results, however the hybrid tested was only able to reach 33% efficiency, compared to 43% of a solo Darrieus. This turbine was tested in a circulating
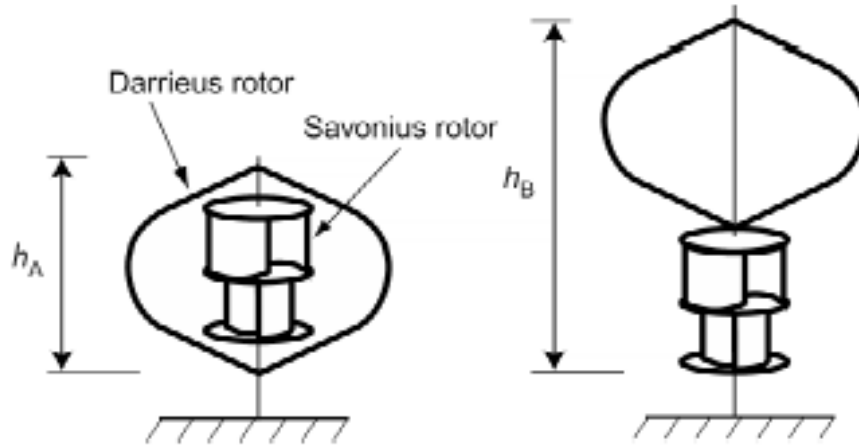
Figure 34: Schematic drawings of two Darrieus-Savonious hybrid turbines

water channel, but no indication of the blockage ratio was given. Another consideration is that there are no velocities given during the results, only tip speed ratios. The turbine is also not rotating freely, but the rotational speed is being controlled.

Another test was conducted in that paper, this time in a tow tank. The reported efficiencies dropped significantly for similar tip speed ratios. The hybrid turbine dropped to around 17% efficiency while the Darrieus dropped to 24% efficiency. Wakui tested different configurations of the Darrieus-Savonius hybrid [26]; the different configurations consisted of having the Savonius inside and outside of the Darrieus, as shown in Figure 34.

The coefficient of power from these tests was 13% and 15%, respectively [26]. These turbines were considered unacceptable because they were below the cutoff of 20% efficiency for the turbine.

B   Corrosion

Seawater is a highly corrosive environment for most commonly available metallic materials, due to high electrolyte content and the presence of oxidizing species. Corrosion of parts on the turbine is therefore an important consideration in the design process. There are multiple mechanisms of corrosive attack that may be present in the seawater environment, and consideration of the most damaging forms must be given in order to produce a reliable turbine. The primary mechanisms we are concerned about are:

- General corrosion, which is the slow attack of exposed surfaces

- Galvanic corrosion, due to contact between dissimilar metals

- Crevice corrosion, which is due to a chemical concentration gradient between different parts of a material

B.1   General Corrosion

General corrosion is the same mechanism as rusting of iron in air or water. Metal ions are dissolved by moisture in the air or by an electrolyte and oxidize to form corrosion products on the surface of the material. This mechanism is not of significant concern, since we can use materials in our turbine which resist general attack. Type 5086-T6 marine-grade aluminum is quite resistant to oxidation in a seawater environment, so from a corrosion standpoint, we propose to use this material for exposed flat surfaces on the turbine. Nickel alloys, titanium alloys, and stainless steels are also quite resistant to general corrosion in seawater, but are unreasonably expensive or may interfere with

Table 1
GALVANIC SERIES
In Flowing Seawater

Alloy		Voltage Range of Alloy vs. Reference Electrode*
Magnesium	**Anodic or Active End**	-1.60 to -1.63
Zinc		-0.98 to -1.03
Aluminum Alloys		-0.70 to -0.90
Cadmium		-0.70 to -0.76
Cast Irons		-0.60 to -0.72
Steel		-0.60 to -0.70
Aluminum Bronze		-0.30 to -0.40
Red Brass, Yellow Brass, Naval Brass		-0.30 to -0.40
Copper		-0.28 to -0.36
Lead-Tin Solder (50/50)		-0.26 to -0.35
Admiralty Brass		-0.25 to -0.34
Manganese Bronze		-0.25 to -0.33
Silicon Bronze		-0.24 to -0.27
400 Series Stainless Steels**		-0.20 to -0.35
90-10 Copper-Nickel		-0.21 to -0.28
Lead		-0.19 to -0.25
70-30 Copper-Nickel		-0.13 to -0.22
17-4 PH Stainless Steel †		-0.10 to -0.20
Silver		-0.09 to -0.14
Monel		-0.04 to -0.14
300 Series Stainless Steels ** †		-0.00 to -0.15
Titanium and Titanium Alloys †		+0.06 to -0.05
Inconel 625 †		+0.10 to -0.04
Hastelloy C-276 †		+0.10 to -0.04

Figure 35: Galvanic Series in Flowing Seawater

oceanographic equipment. Where type 5086 aluminum is not available, anodized type 6061-T6 aluminum will be used instead. Anodizing of aluminum is an electrochemical chemical process in which a layer of aluminum oxide is formed on the surface of the metal. This oxide layer is reasonably resistant to corrosion, strongly adherent, and will hold up acceptably in a saltwater environment [14].

B.2 Galvanic Corrosion

When dissimilar metals are brought into close proximity within an electrically conductive environment, such as seawater, an electrical potential will

develop between the two materials. Depending on the composition of the two materials, the potential may be quite high or quite small. The "nobility" of a metal is a measurement of how strong this electric potential is—highly noble metals present a strong positive potential, while highly active metals exhibit a strong negative potential. This potential is commonly measured against a reference electrode made from a specialized alloy. Measurements are reported on a chart known as the galvanic series, shown in Figure 35. Of the two metals in contact, the metal that is more active and less noble (the anode) will corrode while the cathode remains undamaged. The reactions occurring are as follows (in neutral environments such as seawater):

- At the anode, the metal oxidizes to form a metal ion and an electron, which leaves the anode via the electrical connection:

$$M_{(s)} \rightarrow M_{(aq)}^{(+n)} + ne^-$$
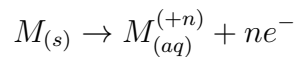
  The number of electrons liberated depends on the oxidation characteristics of the metal.

- At the cathode, the electrons re-enter the electrolyte after traveling through the electrical connection. The reaction is

$$O_2 + 2H_2O + 4e^- \rightarrow 4OH^- \text{And also} 2H^+ + 2e^- \rightarrow H_2$$
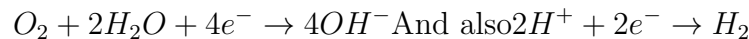
These reactions and the current path are illustrated in Figure 36 above, with copper forming the more-noble cathode and aluminum the more-active anode. The two metals are termed a "galvanic couple", and the further the metals are from each other in a galvanic series the more corrosion will occur. In the context of our turbine project, it is important to avoid use of
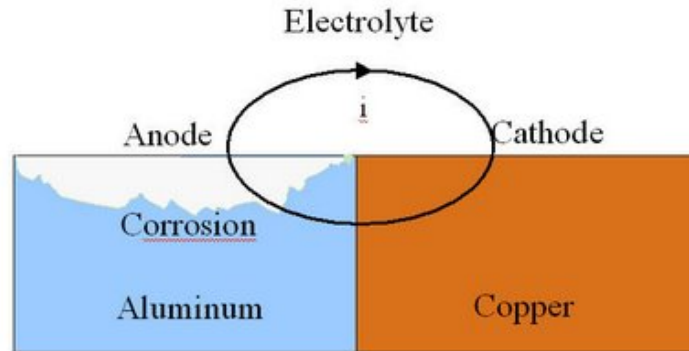
Figure 36: An example of galvanic corrosion

metals which are far apart on the galvanic series and may be in electrical contact. Specifically, the use of carbon fiber composites with metallic fasteners presents a challenging problem, as the highly cathodic graphite fibers will vigorously corrode most metals. The best metal for such fasteners may be platinum, but a more economically realistic material is titanium.

Biological activity can also influence the galvanic potential of some materials. Slime films of marine bacteria can bring the fasteners to a higher potential than the graphite, in which case carbon fibers become the sacrificial anode, which is undesirable as it is far easier to replace fasteners than to rebuild the carbon fiber composites.

To prevent this type of corrosion from damaging the turbine components, dissimilar materials must be avoided as much as possible, and if they must be used, they must be electrically isolated as much as possible. Additionally, maintaining as small an exposed surface area as possible of the cathodic material is desirable, since the rate of the corrosion is limited by how fast electrons can re-enter the solution at the cathode. Therefore, a small area will increase
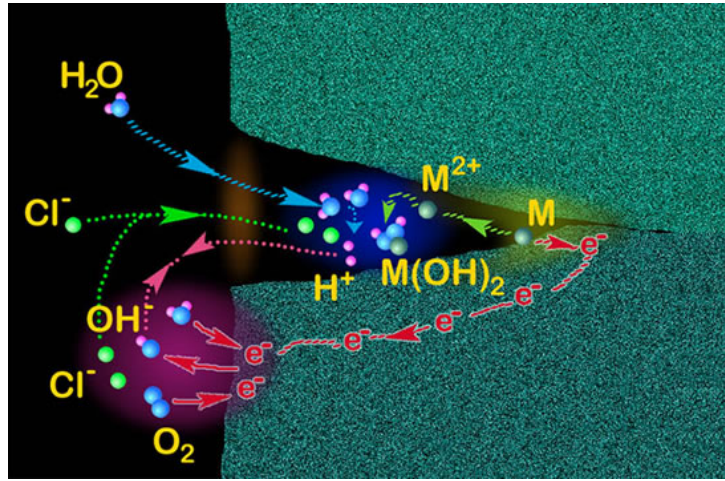
Figure 37: An example of crevice corrosion

the resistance of this connection and prevent the reactions from proceeding
as fast. Practically speaking, the cathodic material should be painted or
insulated from the electrolyte more strongly than the anodic material- this
is counterintuitive, since we would seem to want to reduce the "rusting" of
a surface. However, we must remember that this is not a general attack
mechanism, such as rust, and therefore different measures must be taken.

B.3   Crevice Corrosion

This mechanism is perhaps the most insidious and worrisome of the forms
of corrosion which will be present in the tidal turbine. Crevice corrosion is
extremely destructive and generally not visibly detectable until failure occurs,
since the primary area of attack is within an enclosed area. This type of
corrosion attacks most materials, and ironically, one of the most powerful
and corrosive electrolytes for this mechanism is seawater. An schematic of
the crevice corrosion process is shown in Figure 37.

The mechanism is that a small crevice or space may exist at a mechanical joint between two similar metals. Water enters the crevice, and due to random chemical interactions, ionization of the metal occurs inside the crack, similar to the anode reaction seen in galvanic corrosion. Reduction occurs elsewhere in the crack, resulting in a buildup of hydroxide ions. Oxygen, initially present the seawater, is slowly depleted according to the above equation. Once this occurs, the metal ions begin to build up in the crevice, generating a positively charged region. This pulls negatively charged ions into the crevice, such as chlorine, which is more mobile than oxygen. For reasons that are not fully understood [14], the resulting metal-chloride salts vigorously accelerate the corrosion in the crevice, creating an autocatalytic reaction that quickly destroys the integrity of the metal.

Although all metals are susceptible to crevice attack to a degree, common austenitic stainless steels (300-series) are extraordinarily sensitive to this mechanism. Stainless steel acquires its corrosion resistance by the surface oxidation of chromium and nickel within the metal bulk, forming an adherent protective layer of oxide on the surface. The presence of oxygen in the environment is necessary to maintain this oxide layer. In a crevice situation, the lack of oxygen causes this oxide layer can break down and expose the iron in the bulk, allowing rapid attack of the metal from the inside out. The danger of this attack is confounded since the material appears normal on the outside. Therefore, for our purposes, we will avoid stainless steels as much as possible in the construction of the turbine. Acceptable corrosion resistance and strength can be achieved with aluminum or composite parts.

Property	Value	Units
Elastic Modulus	7.20E+10	$\frac{N}{m^2}$
Poisson's ratio	0.22	N/A
Shear Modulus	2.95E+10	$\frac{N}{m^2}$
Density	2600	$\frac{Kg}{m^3}$
Tensile Strength	3.45E+09	$\frac{N}{m^2}$
Compressive Strength in X	1.08E+09	$\frac{N}{m^2}$
Yield Strength	3.45E+09	$\frac{N}{m^2}$

C   Stress analysis in a helical blade

In this section, the blade as a whole will be analyzed with Solidworks Simulation to obtain the maximum stress value and the Von Mises plot of the stress. Figure 38 below shows the 3-D model of the helical blade. The analyses will be done twice, once for each side of the blade. The analyses started by dividing the blades into 8 sections with the help of "split" feature in Solidworks to helps visualize the way of the water flow act as forces that hitting the blade. However, there are uncertainties on which directions that the flow will hit the blade since there is not enough detail information collected. Therefore, both sides of the blade will be analyzed to compare if there is any difference in the value of maximum stress. Table 9 summarizes the material properties for the blade and the total force of 4045.69 N used to represent the amount of force that the flow produced.

Figure 39 shows the von mises plot for the first analysis or the analysis of the outer side of the blade. Similar to the frame analysis, the green arrows represent fixture part of the blade, and the purple arrows represent the forces or the direction of the water flow. Additionally from Figure 39, the maximum stress shown is 23.1 MPa. Even though the value of maximum stress seems
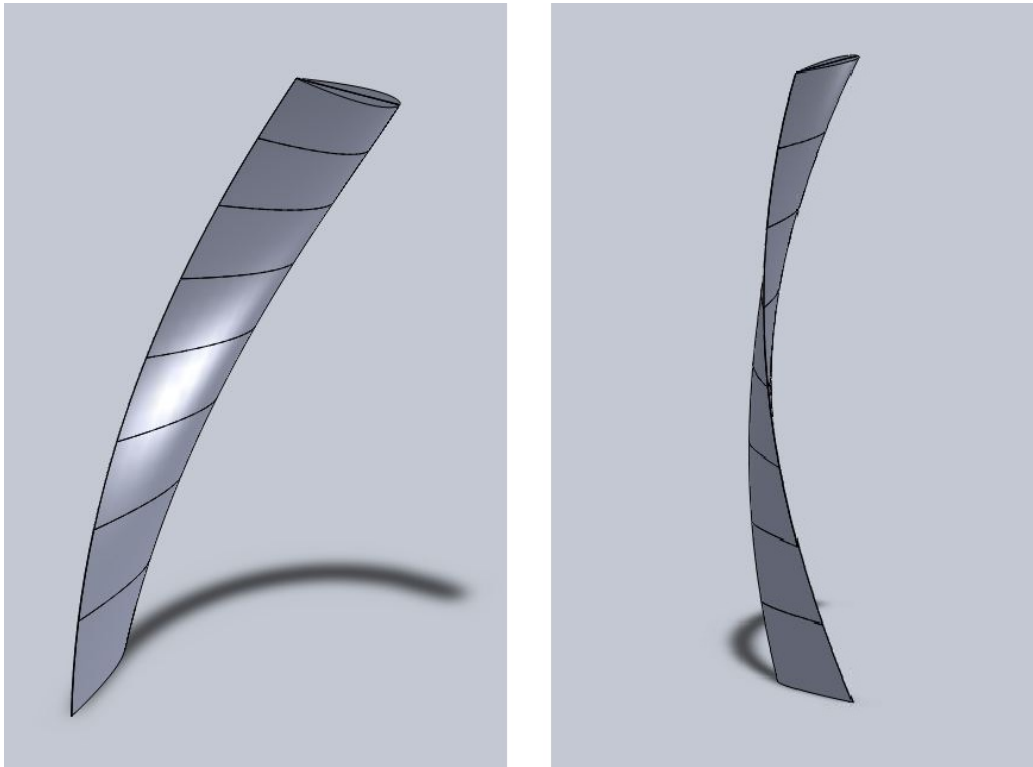
Figure 38: 3-D model of the helical blade

high, it is really not that much in comparison with the yield strength of fiberglass as also supported with the continuous blue color along the blade structure. This way the design of the blade will be sturdy since there are still lots of uncertainty on the unknown components in the real environment.

Figure 40 shows the von mises plot for the second analysis or the analysis of the inner side of the blade. In this analysis, the maximum stress obtained is 22.8 MPa and as before the plot still showing continuous blue color along the blade structure. Therefore, it can be concluded that the value of maximum stress in the blade is 23.1 MPa and it is obtained from the analysis where the force acting at the outer side of the blade structure. Something to be noted,
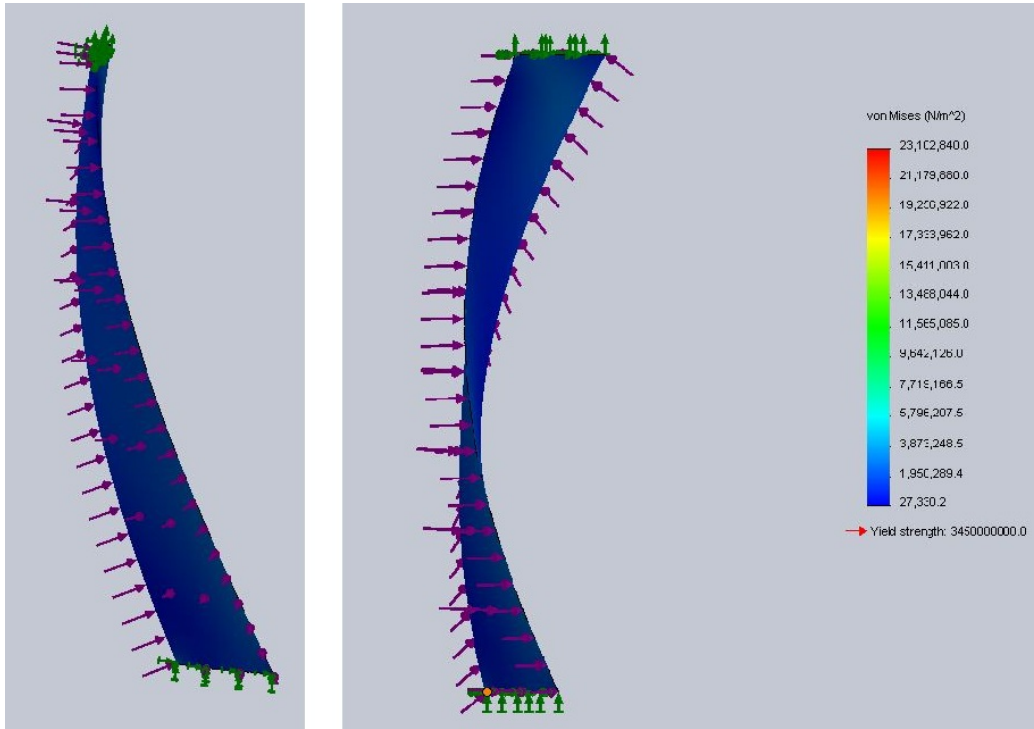
Figure 39: Von Mises plot for the outer side of the blade

the analysis being done here is only for pure fiberglass without any density of the resin being considered and most likely the volume ratio of the resin is much more in comparison to the volume ratio of fiber. Thus, this might lower the value of yield strength of the material by little bit.

D   VAWT angle, force and torque code

A matlab script was developed to generalize the BEMT calculations found in section 5.3. This script calculates the magnitude and angle of the relative velocity (the velocity "seen" by the foil) for various user supplied values of tip speed ratio and incident water velocity. It then uses a look-up ta-
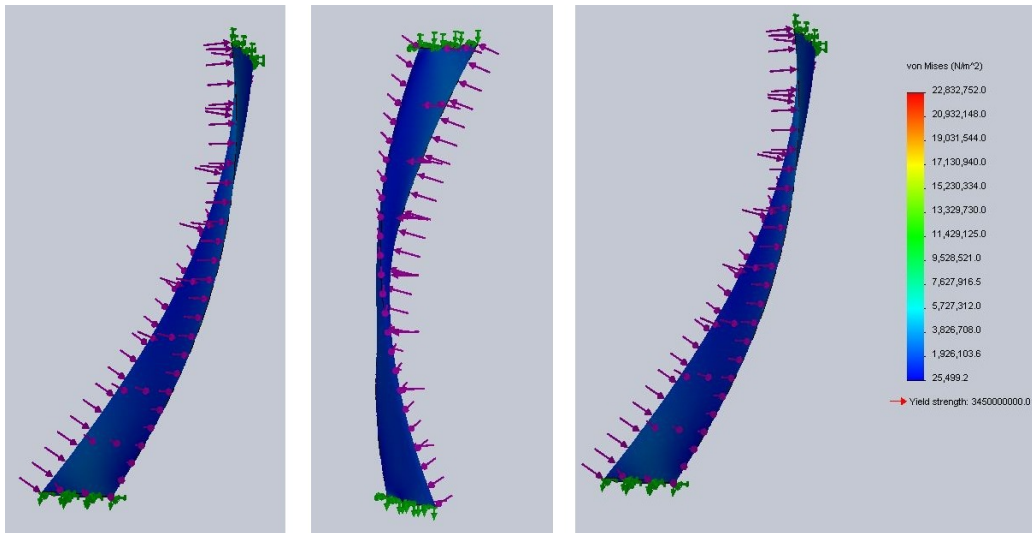
Figure 40: Von Mises plot for the inner side of the blade

ble to calculate lift and drag forces, as well as torque. The coefficients of lift and drag in the look-up table are taken from experimental values reported from work done at Sandia National Laboratory, and can by found here: http://www.cyberiad.net/library/airfoils/foildata/n0018cd.htm.

It is important to note that this script is a work in progress, and its results are tentative. For example, there is no axial induction factor included in the calculation, so it is possible to find coefficients of power that are physically meaningless (above 1). Figures 41-44 show script output that illustrates how some VAWT parameters change with tip speed ratio.

```
1 % Script to find velocities, angles and forces on a VAWT, ...
      version 2.1
2 % Nick Stelzenmuller, 5/21/11
3 % Script needs lift.mat and drag.mat in order to run properly
4 % lift.mat and drag.mat are lift and drag coefficients are ...
```
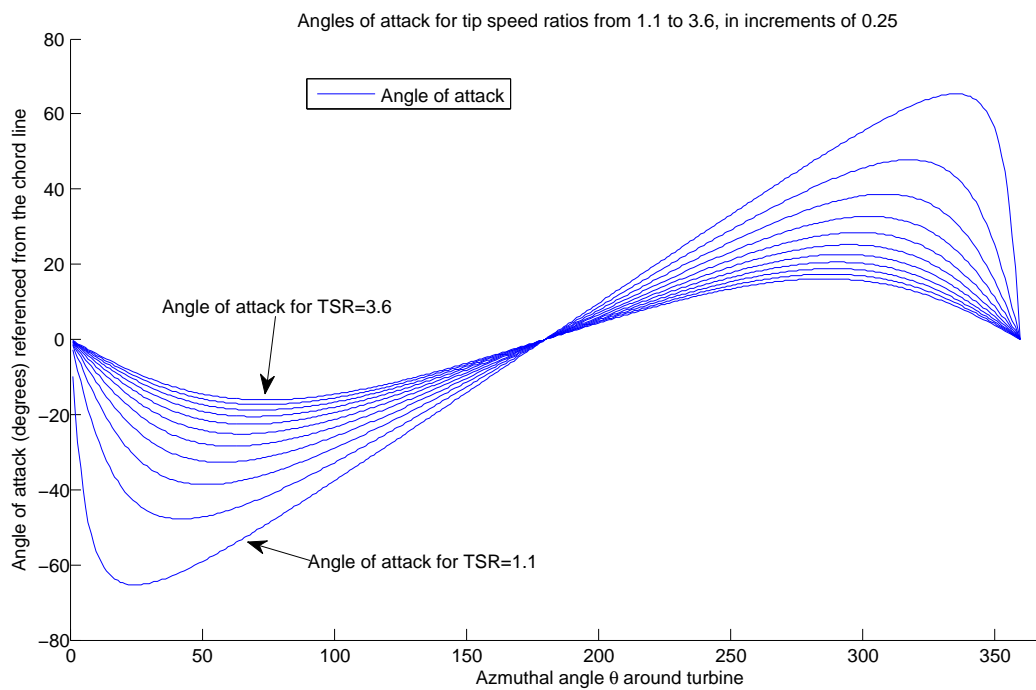
Figure 41: Plot of angles of attack around the turbine circle for various TSR's. Plot generated by the matlab script VAWT calculator ver 2.m
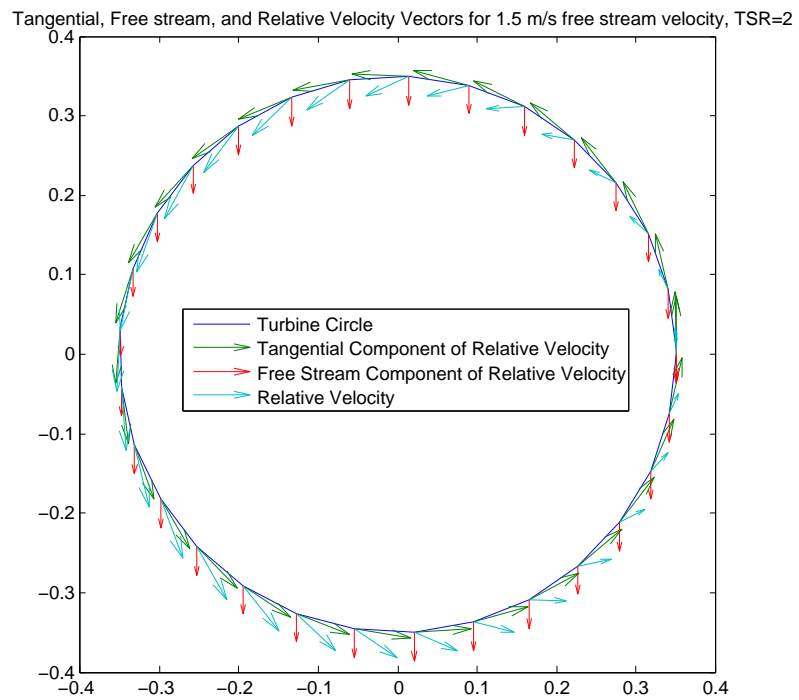
Figure 42: Plot of incident, tangential, and relative velocity vectors around the turbine circle for various TSR's. Plot generated by VAWT calculator ver 2.m

Lift and drag force vectors, plotted with relative velocity for 1.5 m/s free stream velocity and TSR=2
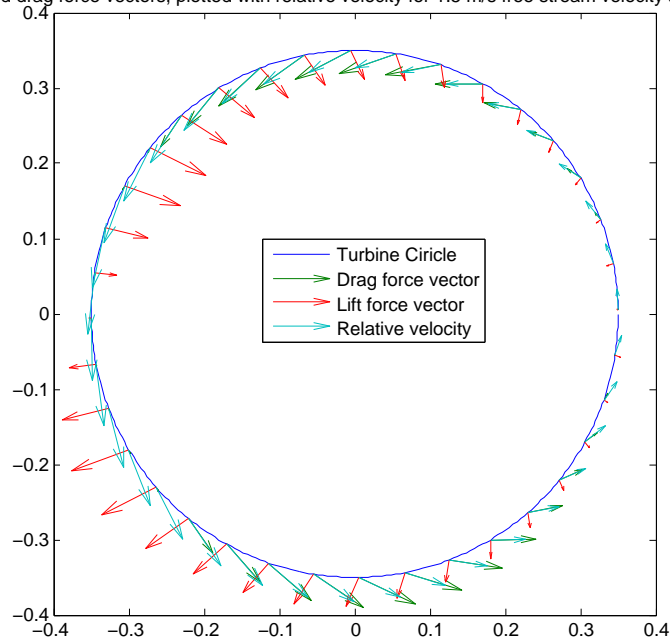
Figure 43: Plot of lift and drag forces around the turbine circle for various TSR's. Plot generated by VAWT calculator ver 2.m
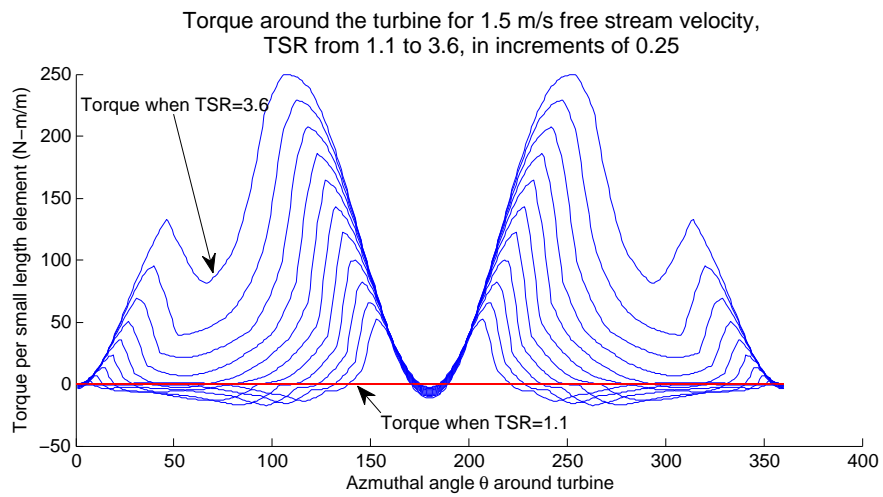
Figure 44: Plot of torque around the turbine circle for various TSR's. Plot generated by VAWT chalculator ver 2.m

```matlab
       taken from
5  % experimental data from
6  % http://www.cyberiad.net/library/airfoils/foildata/n0018cd.htm
7  % for angles of attack from 0 deg to 200 deg
8  % and Reynolds numbers from 40,000 to 5,000,000
9  % Turbine is assumed to be rotating clockwise.
10 clear all; close all; clc;
11 lambdavec=1.1:.1:3.6;
12 for l=1:length(lambdavec)
13
14 %Set the following parameters
15
16 lambda=lambdavec(l);        % Set tip speed ratio
17 FreeStream=1.5;  % Set free stream velocity (m/s)
18 turb_R=.35;      % Set turbine radius (m)
19 turb_H=1;        % Set turbine height (m)
20 N=360;           % Set number of blade positions for which ...
       to solve (KEEP AT 360!)
21 C=.165;          % Set chord length (m)
22 rho=1025;        % Set fluid density (kg/m^3)
23 eta=1.07*10^-3;  % Set dynamic viscocity of fluid (Pa*s)
24
25 %%%%%%%%%%%%%%%%%%%%%%%%%%%%%%%%%%%%%%%%%%%%%%%%%%%%%%%%%%%%%%%%%%%%
26 %%%%%%%%%%%%%%%%%%%%%%%%%%%%%%%%%%%%%%%%%%%%%%%%%%%%%%%%%%%%%%%%%%%
27
28 Re=rho*FreeStream*C/eta;        % Calculate Reynolds number ...
       of flow conditions
29 omega=lambda*FreeStream/turb_R; % calculate rotational ...
       speed (rad/s)
30
31 theta=linspace(pi/180,2*pi,N);  % Generate points on a ...
       circle in polar coordinates
```

```matlab
32  R=ones(length(theta),1)'*turb_R;

33

34  V_t_theta=pi/2+theta;                      % Generate ...
        tangential component of velocity vector
35  V_t_R=ones(1,length(theta))*turb_R*omega;  % in polar ...
        coordinates
36  [circX,circY]=pol2cart(theta,R);           % Transform into ...
        cartesian coordinates

37

38  V_inf_U=zeros(1,length(theta));            % Generate "free ...
        stream component"
39  V_inf_V=ones(1,length(theta))*-FreeStream; %(in this case ...
        going in the negative Y direction)
40                                             %of the relative ...
                                                velcity vector)

41

42  [V_t_U,V_t_V]=pol2cart(V_t_theta,V_t_R); % Transform the ...
        tangential velocity vector in cart. coord.

43

44  figure;
45  plot(circX,circY)
46  title('Tangential, Free stream, and Relative Velocity ...
        Vectors for 1.5 m/s free stream velocity, TSR=2')
47  set(gca,'DataAspectRatio',[1 1 1])  % Plot both vectors with ...
        true aspect ratio
48  hold on
49  quiver(circX,circY,V_t_U,V_t_V,.4)
50  hold on
51  quiver(circX,circY,V_inf_U,V_inf_V,.4/lambda)
52  V_r_U=V_t_U+V_inf_U;
53  V_r_V=V_t_V+V_inf_V;                       % Find the relative ...
        velocity (vector sum of V_t and V_inf
```

```matlab
54                                          %and plot it as well
55 V_r=sqrt(V_r_U.^2+V_r_V.^2);
56 hold on
57 quiver(circX,circY,V_r_U,V_r_V,0.45)
58 legend('Turbine Circle','Tangential Component of Relative ...
       Velocity','Free Stream Component of Relative ...
       Velocity','Relative Velocity')
59 %%%%%%%%%%%%%%%%%%%%%%%%%%%%%%%%%%%%%%%%%%%%%%%%%%%
60 %%%%%%%%%%%%%%%%%%%%%%%%%%%%%%%%%%%%%%%%%%%%%%%%%%
61
62 % Angles
63 V_r_angle=atan2(V_r_V,V_r_U);   % Find angle of relative ...
       velocity wrt theta
64 for i=1:length(theta)            % Fix the atan2 results ...
       (atan2 gives angles for -pi:pi, this puts them from 0:pi)
65     if V_r_angle(i)<0
66         V_r_angle(i:length(theta))=V_r_angle(i:length(theta))+2*pi;
67     end
68 end
69 figure;
70 plot(theta*180/pi, ...
       V_t_theta*180/pi,theta*180/pi,V_r_angle*180/pi)
71 legend('Chord angle', 'V_r','Location', 'Best')
72 xlabel 'Azmuthal angle \theta around turbine refreneced from ...
       horizontal'
73 ylabel 'Chord and Relative Velocity angles as referenced ...
       from    '\theta''
74
75 alpha=V_t_theta-V_r_angle;  % Angle of attack is calculated ...
       as the angle between the
76 %                             chord line (V_t) and the ...
       relative velocity
```

```matlab
77 %                                (V_r). It is negative on the ...
      upstream side
78 %                                and positive on the downstream ...
      side.
79
80 hold on
81 plot(theta*180/pi,alpha*180/pi)
82 legend 'Angle of attack'
83 xlabel 'Azmuthal angle \theta around turbine'
84 ylabel 'Angle of attack (degrees) referenced from the chord ...
      line'
85 title 'Angles of attack for tip speed ratios from 1.1 to ...
      3.6, in increments of 0.25'
86 %%%%%%%%%%%%%%%%%%%%%%%%%%%%%%%%%%%%%%%%%%%%%%%%%%%%%%%%%%%%%%%%%
87 %%%%%%%%%%%%%%%%%%%%%%%%%%%%%%%%%%%%%%%%%%%%%%%%%%%%%%%%%%%%%%%%%
88 % Lift and Drag
89
90 alpha_table=cat(2,0:22,25:5:200);        % Generate list of ...
      alphas and Reynolds number that
91 Re_table=[40000,80000,160000,360000,700000,1000000,2000000,5000000]; ...
      % have been used by Xfoil to find corresponding
92 load lift.dat                            % lift and drag ...
      coefficients (which are contained in
93 load drag.dat                            % lift.mat and drag.mat)
94
95 Re2=rho*V_r*C/eta;
96 Re_vec=ones(1,length(theta)).*Re2;                          ...
      % This code interpolates lift and
97 alpha_vec=abs(alpha)*180/pi; ...
                                 % drag coefficients ...
      from the lift
98 Cl=interp2(Re_table,alpha_table,lift,Re_vec,alpha_vec);    % ...
```

```matlab
                                      and drag tables for given Reynolds
99   Cd=interp2(Re_table,alpha_table,drag,Re_vec,alpha_vec);   % ...
                                      numbers and alphas. We assume symmetry
100  figure;                                                   % ...
                                      so −alpha=alpha
101  hold on
102  plot(theta*180/pi,Cl,theta*180/pi,Cd)
103  legend 'Cl' 'Cd'
104  xlabel('Azmuthal angle \theta around turbine')
105  ylabel('Lift and drag coefficients')
106  title('Lift and drag coefficients around the turbine for tip ...
                                      speed ratios from 1.1 to 3.6, in increments of 0.25')
107
108  F_l=.5*rho*C*V_r.^2.*Cl;                          % Calculate lift ...
                                      and drag forces (N/m)
109  F_d=.5*rho*C*V_r.^2.*Cd;                          % with standard ...
                                      equation
110
111  %  Generate lift and drag vectors by defining them in polar ...
                                      coordinates
112  %  (e.g magnitude=F_d, angle = angle of chord line)
113  %  The lift vector needed some fiddling, i.e. it is inward ...
                                      on the upstream
114  %  side and outward on the downstream side
115  [F_d_U,F_d_V]=pol2cart(V_r_angle,F_d);   % Drag force vector
116
117  %Lift force vector
118  [F_l_U_upstream,F_l_V_upstream]=pol2cart(V_r_angle(1:length(theta)/2)−3*pi/2,F_l(1:l
119  [F_l_U_downstream,F_l_V_downstream]=pol2cart(V_r_angle((length(theta)/2+1):end)−pi/2
120  F_l_U=cat(2,F_l_U_upstream,F_l_U_downstream);
121  F_l_V=cat(2,F_l_V_upstream,F_l_V_downstream);
122
```

```matlab
123  figure;
124  plot(circX,circY)
125  set(gca,'DataAspectRatio',[1 1 1])
126  title('Lift and drag force vectors, plotted with relative ...
          velocity for 1.5 m/s free stream velocity and TSR=2')
127  hold on
128  quiver(circX(1:10:end),circY(1:10:end),F_d_U(1:10:end),F_d_V(1:10:end),0.5)
129  hold on
130  quiver(circX(1:10:end),circY(1:10:end),F_l_U(1:10:end),F_l_V(1:10:end),0.5)
131  hold on
132  quiver(circX(1:10:end),circY(1:10:end),V_r_U(1:10:end),V_r_V(1:10:end),.5)
133  legend('Turbine Ciricle','Drag force vector','Lift force ...
          vector','Relative velocity', 'Location','BestOutside')
134
135  F_l_U_special=cat(2,F_l_U,F_l_U);
136  F_d_U_special=cat(2,F_d_U,F_d_U);
137  F_l_V_special=cat(2,F_l_V,F_l_V);
138  F_d_V_special=cat(2,F_l_V,F_l_V);
139  for i=1:360
140
141
142      F_l_U_sum=sum(F_l_U_special(i:90+i)*turb_H/N);   % This ...
              code sums the x and y components of the
143      F_d_U_sum=sum(F_d_U_special(i:90+i)*turb_H/N);   % lift ...
              and drag forces along one blade for
144      F_l_V_sum=sum(F_l_V_special(i:90+i)*turb_H/N);   % all ...
              of the blade positions around the
145      F_d_V_sum=sum(F_d_V_special(i:90+i)*turb_H/N);   % ...
              turbine circle
146
147      F_U_sum=F_l_U_sum+F_d_U_sum;                 % This block ...
              sums all of the x and y forces
```

```matlab
148     F_V_sum=F_l_V_sum+F_d_V_sum;              % and calculates ...
           the vector sum
149     F_sum(i)=sqrt(F_U_sum^2+F_V_sum^2);
150 end
151
152 [Largest_force_on_blade,I]=max(F_sum)            % This is ...
       the largest force on a blade
153 t_force_y/turb_H
154 figure;
155 plot(circX(I:90+I),circY(I:90+I))
156 set(gca,'DataAspectRatio',[1 1 1])
157 title('Lift and drag force vectors, on blade when blade is ...
       in max force position')
158 hold on
159 quiver(circX(I:90+I),circY(I:90+I),F_d_U(I:90+I),F_d_V(I:90+I),0.5)
160 hold on
161 quiver(circX(I:90+I),circY(I:90+I),F_l_U(I:90+I),F_l_V(I:90+I),0.5)
162
163 %Spoke_drag=mean(.5*rho*.64*0.006*turb_R/3*8*V_r.^2);
164 Torque=(F_l.*sin(abs(alpha))-F_d.*cos(abs(alpha)))*turb_R;   ...
       % Calculate the torque
165 hold on
166 plot(theta*180/pi,Torque)
167 xlabel('Azmuthal angle \theta around turbine')
168 ylabel('Torque per small length element (N-m/m)')
169 title('Torque around the turbine for 1.5 m/s free stream ...
       velocity, TSR from 1.1 to 3.6, in increments of 0.25')
170 plot([0 360],[0 0],'r')
171 Total_torque(l)=sum(Torque*turb_H/N)%-Spoke_drag;    % Sum ...
       the torques around all positions
172 Cp=Total_torque(l)*omega/(rho*turb_R*turb_H*(FreeStream*1).^3);
173 Cp_vec(l)=Cp;
```

```
174  end
175  figure;
176  plot(lambdavec,Total_torque)
177  xlabel '\lambda'
178  ylabel 'Torque (N-m)'
179  figure;
180  plot(lambdavec,Cp_vec)
181  xlabel '\lambda'
182  ylabel 'Cp'
```

E   Drag force code

The drag force on the turbine was modeled in a MATLAB script using a simple drag model. This model used a coefficient of drag = 1, and an rough estimate of the frontal area of the Sea Spider, turbine frame, buoys and instruments. The drag on the turbine was based on linear momentum theory, which gives drag as a function of turbine efficiency. These models need to be refined, both by a more accurate estimate of frontal area and a better estimate of C_F. Total drag on the structure may be able to be modeled in a CFD program.

```
1  function h = Turbine_force_calculator(sz)
2
3
4  %if user doesn't specify size, use the following as default
5  if nargin < 1;sz = [800 600];end
6  myGUI_width = sz(1);%GUI width (pixels)
7  myGUI_height = sz(2);%GUI height (pixels)
8
```
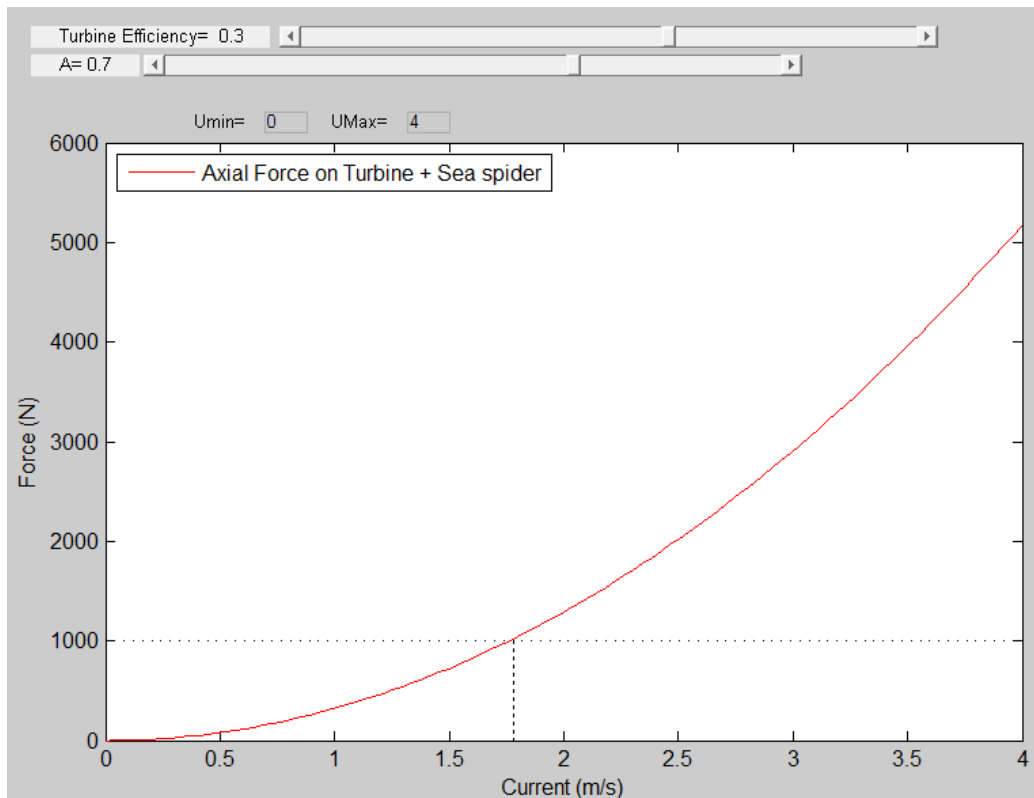
Figure 45: Plot of drag force as a function of free stream current velocity. This plot was generated by the following script.

```
9   padx = 50;%x pading for everything relative to main figure
10  pady = 45;
11  ipadx = 5;%x pading between items within the main figure
12  ipady = 5;
13  widgetH = 16;%height to make widgets (ie controls)
14
15  %add data that needs to be shared and accessed by different ...
        controls
16  %and function to the handles structure "h". This structure ...
        will passed
17  %to each control Callback when executed.
```

```matlab
18
19  h.Umin = 0;%min U value to plot
20  h.Umax = 4;%max U value to plot
21
22  h.a =.3; % a, axial induction factor
23  h.b = 0.7; % A, turbine swept area
24
25
26  %=======================BEGIN CREATING ...
        LAYOUT=============================
27  %To set the position of a control, you need to specify the ...
        following:
28  %[distance_from_left_edge distance_from_bottom_edge width ...
        height]
29
30  %create the main figure (mainFig) in middle of screen.
31  %Store all control handles in structure "h"
32  scrsz = get(0,'ScreenSize');%get screen size
33  h.mainFig = figure('Position',[ ...
34      (scrsz(3)-myGUI_width)/2, ...
35      (scrsz(4)-myGUI_height)/2, ...
36      myGUI_width, ...
37      myGUI_height]);
38  set(h.mainFig,'MenuBar','None')%Remove default figure menubar
39  set(h.mainFig,'ToolBar','None')%Remove default figure toolbar
40  set(h.mainFig,'Resize','off')%prevent window from being resized
41  set(h.mainFig,'Name','Axial Force calculator') %prevent ...
        window from being resized
42  %I could have placed all of these inside the above statement ...
        where I
43  %set the position, but prefer this method as it is easier to ...
        read.
```

```
44
45  %add some axes to plot on
46  %I have used pixels as the units to describe the position so the
47  %padding between the axes and other controls does not change ...
        if a
48  %bigger window size is used for mainFig
49  h.axes = axes('Unit','pixel','Position',[padx+5 pady ...
        myGUI_width-2.5*padx myGUI_height-160]);
50
51  %add labels for sliders
52  h.txt_a = uicontrol('style','text','Position',[padx-30 ...
        (myGUI_height-pady-0*(widgetH+ipady)) 11*widgetH ...
        widgetH], ...
53      'string',['Turbine Efficiency=  ' num2str(h.a)]);
54  h.txt_b = uicontrol('style','text','Position',[padx-30 ...
        (myGUI_height-pady-1*(widgetH+ipady)) 5*widgetH widgetH], ...
55      'string',['A= ' num2str(h.b)]);
56  % h.txt_c = uicontrol('style','text','Position',[padx ...
        (myGUI_height-pady-2*(widgetH+ipady)) 3*widgetH widgetH], ...
57  %      'string',['c= ' num2str(h.c)]);
58
59  %create sliders
60  %slider StepSize = (max-min)/number_of_steps    ==>(use 40 ...
        steps)
61  slider_width = myGUI_width-(2*padx+3*widgetH+ipadx);%all ...
        sliders to be this long
62  h.slider_a = uicontrol('style','slider', ...
63      'Position',[(3*padx+3*widgetH+ipadx) ...
            (myGUI_height-pady-0*(widgetH+ipady)) ...
            0.75*slider_width widgetH], ...
64      'Min',0,'Max',0.5,'Value',h.a,'SliderStep',[0.025 0.025]);
65  h.slider_b = uicontrol('style','slider', ...
```

116

```matlab
66      'Position',[(padx+3*widgetH+ipadx) ...
            (myGUI_height-pady-1*(widgetH+ipady)) ...
            0.75*slider_width widgetH], ...
67      'Min',0.1,'Max',1,'Value',h.b,'SliderStep',[0.025 0.025]);
68 % h.slider_c = uicontrol('style','slider', ...
69 %      'Position',[(padx+3*widgetH+ipadx) ...
        (myGUI_height-pady-2*(widgetH+ipady)) slider_width ...
        widgetH], ...
70 %      'Min',-10,'Max',10,'Value',h.c,'SliderStep',[0.025 ...
        0.025]);
71
72 editH = (myGUI_height-pady-3*(widgetH+ipady));%height to ...
        place edit boxes at
73
74 %create lables for edit boxes for Umin Umax
75
76 boxColour = get(h.mainFig,'Color');%set the background of ...
        these boxes the same as mainFig
77 h.txt_xmin = ...
        uicontrol('style','text','Position',[(3*padx+-1*(widgetH+ipadx)) ...
        editH 3*widgetH widgetH], ...
78      'string','Umin=','HorizontalAlignment','right','BackgroundColor',boxColour);
79 h.txt_xmax = ...
        uicontrol('style','text','Position',[(3*padx+4*(widgetH+ipadx)) ...
        editH 3*widgetH widgetH], ...
80      'string','UMax=','HorizontalAlignment','right','BackgroundColor',boxColour);
81
82 %create  edit boxes for Umin Umax
83 h.edit_xmin = ...
        uicontrol('style','edit','Position',[(3*padx+2*(widgetH+ipadx)) ...
        editH 2*widgetH widgetH], ...
84      'string',h.Umin,'HorizontalAlignment','left','BackgroundColor',boxColour);
```

```matlab
85  h.edit_xmax = ...
        uicontrol('style','edit','Position',[(3*padx+7*(widgetH+ipadx)) ...
        editH 2*widgetH widgetH], ...
86      'string',h.Umax,'HorizontalAlignment','left','BackgroundColor',boxColour);

87

88  %======================END CREATING ...
        LAYOUT=============================

89

90  %======================BEGIN SETTING ...
        CALBACKS============================
91  %set callbacks for sliders
92  set(h.slider_a,'callback',{@slider_a_Callback h});
93  set(h.slider_b,'callback',{@slider_b_Callback h});

94

95  %set callbacks for edit boxes
96  set(h.edit_xmin,'callback',{@edit_xmin_Callback h});
97  set(h.edit_xmax,'callback',{@edit_xmax_Callback h});

98

99  %======================END SETTING ...
        CALBACKS============================

100

101 guidata(h.mainFig,h)%update the entire handle structure to ...
        include everything defined above
102 updatePlot(h);%plot the default values initially

103

104 %======================BEGIN DEFINING ...
        CALBACKS============================
105 function slider_a_Callback(hObject, eventdata, h)
106 h = guidata(hObject);%get the entire handle structure for ...
        the GUI
107 val = get(hObject,'Value');%get the value from the slider
108 str = sprintf('Turbine efficiency=%0.2f',val);%create a string
```

```matlab
109  set(h.txt_a,'String',str);%put string in text box for a
110  h.a = val;%update handles
111  guidata(hObject,h);%update entire handle structure
112  updatePlot(h);%replot
113
114  function slider_b_Callback(hObject, eventdata, h)
115  h = guidata(hObject);
116  val = get(hObject,'Value');
117  str = sprintf('A=%0.2f',val);
118  set(h.txt_b,'String',str);
119  h.b = val;
120  guidata(hObject,h);
121  updatePlot(h);
122
123
124  function edit_xmin_Callback(hObject, eventdata, h)
125  h = guidata(hObject);%get the entire handle structure for ...
          the GUI
126  Umin = str2double(get(hObject,'String'));%get the value of ...
          the box
127  h.Umin = Umin;%update handles
128  guidata(hObject,h)%update entire handle structure
129  updatePlot(h);%replot
130
131  function edit_xmax_Callback(hObject, eventdata, h)
132  h = guidata(hObject);
133  Umax = str2double(get(hObject,'String'));
134  h.Umax = Umax;
135  guidata(hObject,h)
136  updatePlot(h);
137
```

```matlab
138  %======================END DEFINING ...
         CALBACKS==============================

139

140  function updatePlot(h)

141  %This is the function that that makes use off all data that

142  %has been stored by the controls in the GUI

143  h = guidata(h.mainFig);%get the entire handle structure for ...
         the GUI

144  U = linspace(h.Umin,h.Umax,100); % Range of current velocities

145   a=fsolve(@(a)4*a*(1-a)^2-h.a, 0.3); % Solves for a from ...
         user-defined turbine efficiency

146  Cf=4*a*(1-a);      % Calculate drag coefficient from linear ...
         momentum theory (crude, needs refining)

147  rho=1025;

148

149  A_ss=0.4;  % Area of the sea spider (very rough ballpark)

150  Cf_ss=1; % Drag coefficient for sea sider. Again, an ...
         educated guess

151

152  F_t=0.5*Cf*rho*h.b*U.^2; %  Drag force on turbine

153  F_ss=0.5*Cf_ss*rho*A_ss*U.^2;  %Drag force on sea spider

154  F=F_t+F_ss;   %Total drag force

155

156  axes(h.axes)%set axis to plot on

157

158  % To resist this force there needs to be a suffcent ...
         friction force between

159  % the sea spider and the sea floor

160  mu=0.8;  % Coefficient of static friction (depends on type ...
         of sea bed, probably close to 1?)

161  M_lead=272; % Added lead mass (in kg), ¬600 lbs

162  M_ss=50;  % Mass of sea spider (just a guess)
```

```
163  M_turbine=10; % Mass of turbine (again, guess)
164  M=M_ss+M_lead+M_turbine;  % Overall mass
165  D=0.2; % Total displacement of everything (m^3)....guess
166  g=9.81;
167  max_F=mu*g*(M—D*rho);   % Max frictional holding force, this ...
         is plotted as a horizontal line
168  i=find(F>max_F,1,'First');        % A sloppy, sloppy way to ...
         get a vertical line from the x—axis to the intersection ...
         of the
169  hline=linspace(0,max_F,1000);    % force curve and the max ...
         force line
170  vline=ones(1000)*U(i);
171  plot(U,F,'r',U,max_F,'—k',vline,hline,':k' );%plot data
172  xlabel('Current (m/s)')
173  ylabel ('Force (N)')
174  legend('Axial Force on Turbine + Sea spider', 'Location', ...
         'NorthWest')
```

F   Tipping moment code

The tipping moment of the Sea Spider with the turbine was modeled in a
MATLAB script using a simple drag model. This model neglected the drag
on the turbine frame (which will be considerable), and considered the drag
on the Sea Spider and the turbine as two point forces acting at the center
of frontal area of the Sea Spider and turbine, respectively. It was further
assumed that the Sea Spider was oriented to the flow such that the Sea Spider
would tip back evenly on two legs. The resistance to this overturning moment
is modeled as the weight [4] acting vertically through the center of mass, and

---

[4]Weight under water is simply weight in air minus the weight of the displaced water.
This was calculated from rough estimates of weight and volume of the Sea Spider and
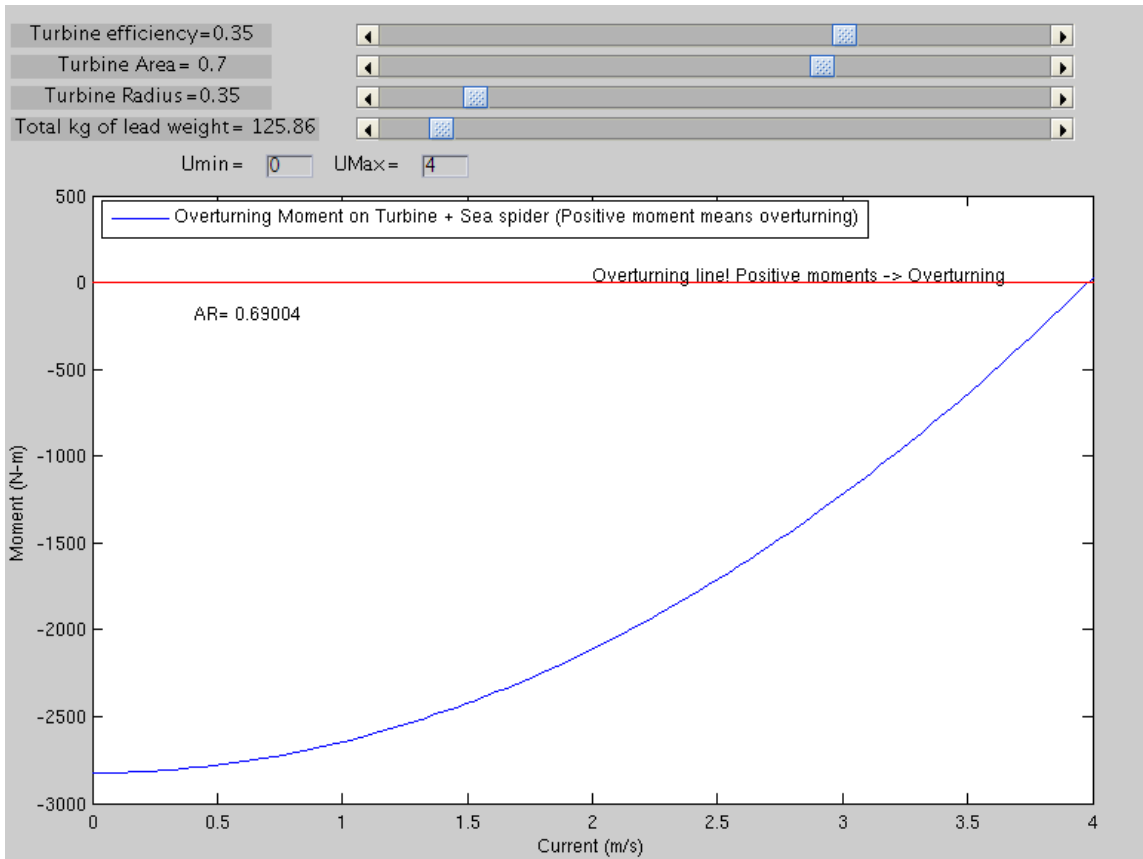
Figure 46: Plot of tipping moment as a function of free stream current velocity. A positive tipping moment implies the structure has tipped over. This plot was generated by the following script.

the weight of one lead block acting vertically through that block. This model is crude, and needs refining before the results can be used. Specifically, the assumption of perfectly horizontal flow is not valid, and current with an upward angle will increase the tipping moment. The drag forces should be more accurately modeled, as discussed in Appendix E.

---

turbine

```matlab
1  function h = moment_calculator(sz)
2  % Fuction to caclculate overturning moments
3
4  %if user doesn't specify size, use the following as default
5  if nargin < 1;sz = [800 600];end
6  myGUI_width = sz(1);%GUI width (pixels)
7  myGUI_height = sz(2);%GUI height (pixels)
8
9  padx = 50;%x pading for everything relative to main figure
10 pady = 45;
11 ipadx = 5;%x pading between items within the main figure
12 ipady = 5;
13 widgetH = 16;%height to make widgets (ie controls)
14
15 %add data that needs to be shared and accessed by different ...
       controls
16 %and function to the handles structure "h". This structure ...
       will passed
17 %to each control Callback when executed.
18
19 h.Umin = 0;%min U value to plot
20 h.Umax = 4;%max U value to plot
21
22 h.a =.3; % a, axial induction factor
23 h.b = 0.7; % A, turbine swept area
24 h.c=0.3; % Radius of turbine
25 h.d=600; % Total kg of lead attached to sea spider legs
26
27 %=======================BEGIN CREATING ...
       LAYOUT=============================
28 %To set the position of a control, you need to specify the ...
       following:
```

123

```matlab
29  %[distance_from_left_edge distance_from_bottom_edge width ...
        height]
30
31  %create the main figure (mainFig) in middle of screen.
32  %Store all control handles in structure "h"
33  scrsz = get(0,'ScreenSize');%get screen size
34  h.mainFig = figure('Position',[ ...
35      (scrsz(3)-myGUI_width)/2, ...
36      (scrsz(4)-myGUI_height)/2, ...
37       myGUI_width, ...
38       myGUI_height]);
39  set(h.mainFig,'MenuBar','None')%Remove default figure menubar
40  set(h.mainFig,'ToolBar','None')%Remove default figure toolbar
41  set(h.mainFig,'Resize','off')%prevent window from being resized
42  set(h.mainFig,'Name','Overturning moment calculator') ...
        %prevent window from being resized
43  %I could have placed all of these inside the above statement ...
        where I
44  %set the position, but prefer this method as it is easier to ...
        read.
45
46  %add some axes to plot on
47  %I have used pixels as the units to describe the position so the
48  %padding between the axes and other controls does not change ...
        if a
49  %bigger window size is used for mainFig
50  h.axes = axes('Unit','pixel','Position',[padx+5 pady ...
        myGUI_width-2.5*padx myGUI_height-190]);
51
52  %add labels for sliders
53  h.txt_a = uicontrol('style','text','Position',[padx-30 ...
        (myGUI_height-pady-0*(widgetH+ipady)) 11*widgetH ...
```

124

```matlab
        widgetH], ...
54       'string',['Turbine Efficiency=  ' num2str(h.a)]);
55  h.txt_b = uicontrol('style','text','Position',[padx-30 ...
         (myGUI_height-pady-1*(widgetH+ipady)) 11*widgetH ...
         widgetH], ...
56       'string',['Turbine Area= ' num2str(h.b)]);
57  h.txt_c = uicontrol('style','text','Position',[padx-30 ...
         (myGUI_height-pady-2*(widgetH+ipady)) 11*widgetH ...
         widgetH], ...
58       'string',['Turbine Radius= ' num2str(h.c)]);
59  h.txt_d = uicontrol('style','text','Position',[padx-30 ...
         (myGUI_height-pady-3*(widgetH+ipady)) 13*widgetH ...
         widgetH], ...
60       'string',['Total kg of lead weight= ' num2str(h.d)]);
61
62  %create sliders
63  %slider StepSize = (max-min)/number_of_steps    ==>(use 40 ...
         steps)
64  slider_width = myGUI_width-(2*padx+3*widgetH+ipadx);%all ...
         sliders to be this long
65  h.slider_a = uicontrol('style','slider', ...
66       'Position',[(4*padx+3*widgetH+ipadx) ...
             (myGUI_height-pady-0*(widgetH+ipady)) ...
             0.75*slider_width widgetH], ...
67       'Min',0,'Max',0.5,'Value',h.a,'SliderStep',[0.025 0.025]);
68  h.slider_b = uicontrol('style','slider', ...
69       'Position',[(4*padx+3*widgetH+ipadx) ...
             (myGUI_height-pady-1*(widgetH+ipady)) ...
             0.75*slider_width widgetH], ...
70       'Min',0.1,'Max',1,'Value',h.b,'SliderStep',[0.025 0.025]);
71  h.slider_c = uicontrol('style','slider', ...
```

```matlab
72      'Position',[(4*padx+3*widgetH+ipadx) ...
            (myGUI_height-pady-2*(widgetH+ipady)) ...
            0.75*slider_width widgetH], ...
73      'Min',0.1,'Max',2,'Value',h.c,'SliderStep',[0.025 0.025]);
74  h.slider_d = uicontrol('style','slider', ...
75      'Position',[(4*padx+3*widgetH+ipadx) ...
            (myGUI_height-pady-3*(widgetH+ipady)) ...
            0.75*slider_width widgetH], ...
76      'Min',0,'Max',1600,'Value',h.d,'SliderStep',[0.025 0.025]);
77
78
79  editH = (myGUI_height-pady-3*(widgetH+ipady));%height to ...
        place edit boxes at
80
81  %create lables for edit boxes for Umin Umax
82
83  boxColour = get(h.mainFig,'Color');%set the background of ...
        these boxes the same as mainFig
84  h.txt_xmin = ...
        uicontrol('style','text','Position',[(3*padx+-1*(widgetH+ipadx)) ...
        editH-25 3*widgetH widgetH], ...
85      'string','Umin=','HorizontalAlignment','right','BackgroundColor',boxColour);
86  h.txt_xmax = ...
        uicontrol('style','text','Position',[(3*padx+4*(widgetH+ipadx)) ...
        editH-25 3*widgetH widgetH], ...
87      'string','UMax=','HorizontalAlignment','right','BackgroundColor',boxColour);
88
89  %create  edit boxes for Umin Umax
90  h.edit_xmin = ...
        uicontrol('style','edit','Position',[(3*padx+2*(widgetH+ipadx)) ...
        editH-25 2*widgetH widgetH], ...
91      'string',h.Umin,'HorizontalAlignment','left','BackgroundColor',boxColour);
```

```matlab
92  h.edit_xmax = ...
        uicontrol('style','edit','Position',[(3*padx+7*(widgetH+ipadx)) ...
        editH—25 2*widgetH widgetH], ...
93      'string',h.Umax,'HorizontalAlignment','left','BackgroundColor',boxColour);
94
95  %=====================END CREATING ...
        LAYOUT=============================
96
97  %=====================BEGIN SETTING ...
        CALBACKS============================
98  %set callbacks for sliders
99  set(h.slider_a,'callback',{@slider_a_Callback h});
100 set(h.slider_b,'callback',{@slider_b_Callback h});
101 set(h.slider_c,'callback',{@slider_c_Callback h});
102 set(h.slider_d,'callback',{@slider_d_Callback h});
103
104 %set callbacks for edit boxes
105 set(h.edit_xmin,'callback',{@edit_xmin_Callback h});
106 set(h.edit_xmax,'callback',{@edit_xmax_Callback h});
107
108 %=====================END SETTING ...
        CALBACKS============================
109
110 guidata(h.mainFig,h)%update the entire handle structure to ...
        include everything defined above
111 updatePlot(h);%plot the default values initially
112
113 %=====================BEGIN DEFINING ...
        CALBACKS============================
114 function slider_a_Callback(hObject, eventdata, h)
115 h = guidata(hObject);%get the entire handle structure for ...
        the GUI
```

```matlab
116  val = get(hObject,'Value');%get the value from the slider
117  str = sprintf('Turbine efficiency=%0.2f',val);%create a string
118  set(h.txt_a,'String',str);%put string in text box for a
119  h.a = val;%update handles
120  guidata(hObject,h);%update entire handle structure
121  updatePlot(h);%replot
122
123  function slider_b_Callback(hObject, eventdata, h)
124  h = guidata(hObject);
125  val = get(hObject,'Value');
126  str = sprintf('Turbine Area=%0.2f',val);
127  set(h.txt_b,'String',str);
128  h.b = val;
129  guidata(hObject,h);
130  updatePlot(h);
131
132  function slider_c_Callback(hObject, eventdata, h)
133  h = guidata(hObject);
134  val = get(hObject,'Value');
135  str = sprintf('Turbine Radius=%0.2f',val);
136  set(h.txt_c,'String',str);
137  h.c = val;
138  guidata(hObject,h);
139  updatePlot(h);
140
141  function slider_d_Callback(hObject, eventdata, h)
142  h = guidata(hObject);
143  val = get(hObject,'Value');
144  str = sprintf('Total kg of lead weight= %0.2f',val);
145  set(h.txt_d,'String',str);
146  h.d = val;
147  guidata(hObject,h);
```

```matlab
148  updatePlot(h);
149
150  function edit_xmin_Callback(hObject, eventdata, h)
151  h = guidata(hObject);%get the entire handle structure for ...
         the GUI
152  Umin = str2double(get(hObject,'String'));%get the value of ...
         the box
153  h.Umin = Umin;%update handles
154  guidata(hObject,h)%update entire handle structure
155  updatePlot(h);%replot
156
157  function edit_xmax_Callback(hObject, eventdata, h)
158  h = guidata(hObject);
159  Umax = str2double(get(hObject,'String'));
160  h.Umax = Umax;
161  guidata(hObject,h)
162  updatePlot(h);
163
164  %=======================END DEFINING ...
         CALBACKS=============================
165
166  function updatePlot(h)
167  %This is the function that that makes use off all data that
168  %has been stored by the controls in the GUI
169  h = guidata(h.mainFig);%get the entire handle structure for ...
         the GUI
170  U = linspace(h.Umin,h.Umax,100); % Range of current velocities
171   a=fsolve(@(a)4*a*(1-a)^2-h.a, 0.3); % Solves for a from ...
         user-defined turbine efficiency
172  Cf=4*a*(1-a);     % Calculate drag coefficient from linear ...
         momentum theory (crude, needs refining)
173  rho=1025;
```

129

```matlab
174  A=h.b; % Turbine area
175  A_ss=0.4;  % Area of the sea spider (very rough ballpark)
176  Cf_ss=1; % Drag coefficient for sea sider. Again, an ...
         educated guess
177
178  F_t=0.5*Cf*rho*A*U.^2; %  Drag force on turbine
179  F_ss=0.5*Cf_ss*rho*A_ss*U.^2;  %Drag force on sea spider
180  F=F_t+F_ss;  %Total drag force
181
182
183
184  % To resist this force there needs to be a suffcient ...
         friction force between
185  % the sea spider and the sea floor
186  mu=0.8;  % Coefficient of static friction (depends on type ...
         of sea bed, probably close to 1?)
187  M_lead=h.d; % Added lead mass (in kg), ¬600 lbs
188  M_ss=50;  % Mass of sea spider (just a guess)
189  M_turbine=10; % Mass of turbine (again, guess)
190  M=M_ss+M_lead+M_turbine;  % Overall mass
191  Disp=0.2; % Total displacement of everything (m^3)....guess
192  g=9.81;
193  max_F=mu*g*(M—Disp*rho);   % Max frictional holding force, ...
         this is plotted as a horizontal line
194
195  % Defining some sea spider and turbine geometry
196
197  R=h.c; %radius of turbine
198  D=2*R; % Diameter of turbine
199  Ht=A/D; % Height of turbine
200  AR=D/Ht; %Definition of aspect ratio
201
```

```matlab
202  h_offset=0.1; % Distance bottomof turbine is from top of sea ...
         spider
203
204  CF_ss=(14-5.76)*0.0254;  % Height from ground of the center ...
         of force from
205                                                %drag on sea ...
                                                      spider.
206                                                % Defined in ...
                                                      inches from ...
                                                      Nick's sketch
207
208
209  CF_turbine=14*0.0254+h_offset+Ht/2; % Height above ground of ...
         center of force of
210                                                              % ...
                                                       turbine ...
                                                       drag
211
212  L_ss=35*0.254; % Distance between sea spider legs (lever arm ...
         for lead weight)
213
214  Wt=g*(M-Disp*rho);   % Weight of entire structure
215  Wt_oneleg=g*M_lead/3; % Weight force of one weighted leg
216  cg=L_ss/2; % Lever arm gravity force
217
218  M=F_t*CF_turbine+F_ss*CF_ss-Wt*cg-Wt_oneleg*L_ss;
219
220  % i=find(F>max_F,1,'First');        % A sloppy, sloppy way ...
         to get a vertical line from the x-axis to the ...
         intersection of the
221   hline=linspace(0,h.Umax,1000);    % force curve and the max ...
          force line
```

131

```
222  hline2=zeros(1000);
223  axes(h.axes)%set axis to plot on
224  plot(U,M,hline,hline2,'r');%plot data
225  xlabel('Current (m/s)')
226  ylabel ('Moment (N)')
227  legend('Overturning Moment on Turbine + Sea spider (Positive ...
          moment means overturning)', 'Location', 'NorthWest')
228  str=['AR= ' num2str(AR)];
229  text(0.1,0.8, str,'Units','Normalized')
230  text(2,20,'Overturning line! Positive moments -> Overturning')
```

G   Turbine efficiency code

The turbine extracts power from the tidal current according to $P = C_p \frac{1}{2} \rho A U^3$.
In order to understand how much energy the turbine extracts over the course
of a day or a month the tidal current velocity must be accurately pre-
dicted. Fortunately predictability is one of key advantage of the tidal current
resource—tides can be modeled accurately years into the future. The follow-
ing MATLAB script calculates the tidal cycle by superposition of the tidal
effects of the Sun and the Moon. Plotting these constituents reveals a two
primary tidal frequencies: a diurnal cycle and a biweekly cycle called the
spring/neap cycle. A mean power over 90 days was calculated based on the
mean U^3 over those 90 days. This calculation was used to find the mini-
mum efficiency of the turbine necessary to produce an average of 20 W of
electrical power, based on assumptions of drivetrain and generator efficiency.
It was found that in order to produce 20 W of electricity averaged over 90
days, with battery, generator, and drivetrain efficiencies of 0.8, 0.8, and 0.9,
respectively, and a turbine swept area of 0.7 m^2. a turbine efficiency of 25%
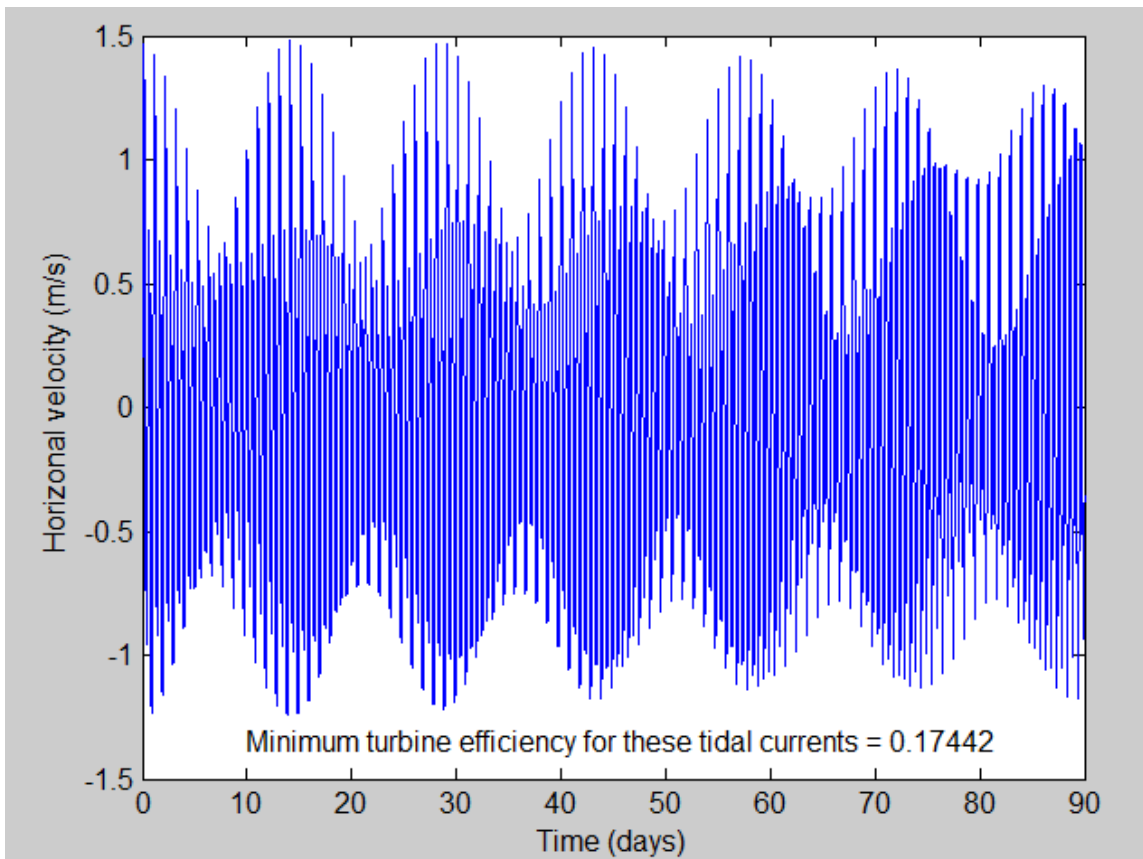
Figure 47: Plot of tidal current velocities over 90 days. The efficiency of the turbine given on this plot, 17.4%, was calculated by assuming a swept area of 1 m^2, and generator, drivetrain, and battery efficiencies of 0.8, 0.9, and 0.8, respectively

is necessary for this tidal current regime. Figure 47 show the tidal current history and gives a value for minimum turbine efficiency for a swept area of 1 m^2.

```
1  %Brian Polagye
2  %October 20, 2010
3
```

```matlab
%Description: routine to test capabilities for a micropower ...
    system

clear

%% Setup

%M2 constituent
A(1) = 0.85;          %amplitude (m/s)
phi(1) = 0;           %phase (degrees)
w(1) =0.0805114*2*pi;        % frequency (1/h)  Brian's
%w(1)=0.5058681;
%  Alternate freq  (Nick's) from ...
    http://marine.rutgers.edu/dmcs/ms503/2007/Tides1.htm


%S2 constituent
A(2) = 0.25;
phi(2) = 10;
w(2) = 0.0833333*2*pi;
%w(2)=0.52359878;

%K1 constituent
A(3) = 0.25;
phi(3) = 20;
w(3) = 0.0417807*2*pi;
%w(3)=0.2625158;


%O1 constituent
A(4) = 0.15;
phi(4) = 30;
```

```matlab
34  w(4) = 0.0387307*2*pi;
35  %w(4)=0.24335227;
36
37  P_target = 20;   %average watts continuous supply
38  rho = 1024;      %density
39
40  A_turbine = 1;            %turbine swept area
41
42  eta_b = 0.8;
43  eta_g = 0.8;
44  eta_d = 0.9;
45
46  n_days = 90;     %number of days in time series
47
48  %% Generate time series
49
50  dt = 10/60;              %time increment (hours)
51  t = [0:dt:n_days*24]';   %time series (hours)
52
53  u = zeros(size(t));
54  % u = calculate velocity time series
55  for i=1:4;
56  u(:,i)=A(i)*sin(w(i)*t+phi(i)*(pi/180));
57  end
58  u=sum(u,2);
59
60
61  %% Calculate efficiency
62
63  % calculate eta to meet minimum specs
64
65  eta_t=2*P_target./(rho*A_turbine*eta_b*eta_g*eta_d*mean(abs(u).^3));
```

```
66
67  %eta_t_correction_factor=0.7;
68  % Fudge factor to estimate :
69  %   1) Not producing power at all speeds (cut-in speeds),
70  %   2) operating below peak efficiency for some speeds
71  %eta_t=eta_t/eta_t_correction_factor;
72
73
74  % figure to check that velocity calculation makes sense
75  figure(1)
76  plot((t-t(1))/24,u,'-b')
77  str1=['Minimum turbine efficiency for these tidal currents = ...
         ' num2str(eta_t)];
78  text(10,-1.35,str1)
79  xlabel('Time (days)')
80  ylabel('Horizonal velocity (m/s)')
```

H Cost of Materials and Machining

Table 9: Cost of materials and machining for turbine construction. Not comprehensive.

Item	Details	Cost	Source	Comments
Stainless steel center shaft	diameter = 1" length = 3 ft	$71.85	speedymetals.com	Cost of $8.98/lb for 8 lbs
Stainless steel framework	diameter = 1.5"; length = 6 ft	$247.68	speedymetals.com	Cost of $3.44/in; 0.188" thick
Stainless steel framework	thickness = 0.25" width = 1.25"	$99.80	speedymetals.com	Cost of $9.98/ft
Marine bearings	2 bearings with 1" ID; length = 3"	$105.98		Cost of $ 52.99 each
Blade mold	Performed on 5 axial CNC machine	$1,820.29	Turn Point Design	
Blade core material	1 sheet 1/2" Baltek	$105.51	Fiberlay	Rigid; 48" x 58" sheet
Blade resin system	Resin and hardener (West 105 and 206)	$69.40	Fisheries Supply	
Blade prepreg graphite cloth	4 layers/ surface for 4 blades	$291.68	Fiberlay	Cost of $72.92/ 50"; x Yd
Mold release wax	Grignard Mold Magic	$15.50	Fiberlay	
Safety supplies; solvents; etc		$50.00	Fiberlay	
Total	**Only costs for turbine construction**	**$2,877.69**		**Additional funding will be required for generator and coupling.**

TURN POINT DESIGN

Turn Point Design
2320 South Park Ave.
Port Townsend, WA 98368

Estimate

Date	Estimate #
2/22/2011	92

Name / Address
Browyn Hughes

	Project

Item	Description	Qty	Cost	Total
	Turbine Blade Tooling--- Single sided tool - second side machined post lamination			
CAD Design	create cutting geometry and cutting regions	2.4	85.00	204.00T
CNC Programming	Programming of milling operations and cutting sub routines to create a part	3.2	85.00	272.00T
Misc. materials	Particle board -- tool base substrate	3	25.99	77.97T
Misc. materials	Baltic Birch Plywood --- tool surface substrate	1	49.99	49.99T
Misc. materials	Tooltec -- Tool surface coat -- applied to cut tool to create a non-stick mold surface		105.99	105.99T
Misc. Labor	fixture parts onto machine,prep mold surface, apply tooltec fabric	3.8	65.00	247.00T
5 axis CNC	CNC cutting time 5-axis	2.9	99.00	287.10T
	SUBTOTAL---Tooling costs			1,244.05
	Cost to machine second side of parts-- post lamination-- 4 blades total			
CNC Programming	Programming of milling operations and cutting sub routines to create a part	1.2	85.00	102.00T
5 axis CNC	CNC cutting time 5-axis	1.9	99.00	188.10T
Misc. Labor	fixture parts onto machine, load tooling, clean up and misc. CNC operation	2.4	65.00	156.00T
	SUBTOTAL-- Machine second side of blades			446.10

Subtotal	$1,690.15
Sales Tax (7.7%)	$130.14
Total	$1,820.29

TURN POINT DESIGN

Turn Point Design
2320 South Park Ave.
Port Townsend, WA 98368

Estimate

Date	Estimate #
2/22/2011	93

Name / Address
Browyn Hughes

	Project

Item	Description	Qty	Cost	Total
CAD Design	Turbine Blade Tooling--- Two mold halves create cutting geometry and cutting regions	3.1	85.00	263.50T
CNC Programming	Programming of milling operations and cutting sub routines to create a part	4.9	85.00	416.50T
Misc. materials	Particle board -- tool base substrate	6	25.99	155.94T
Misc. materials	Baltic Birch Plywood --- tool surface substrate	2	49.99	99.98T
Misc. materials	Tooltec -- Tool surface coat -- applied to cut tool to create a non-stick mold surface		211.98	211.98T
Misc. Labor	fixture parts onto machine,prep mold surface, apply tooltec fabric	7.6	65.00	494.00T
5 axis CNC	CNC cutting time 5-axis	5.8	99.00	574.20T
	SUBTOTAL---Tooling costs			2,216.10

Subtotal	$2,216.10
Sales Tax (7.7%)	$170.64
Total	$2,386.74

References

[1] Northwest National Marine Renewable Energy Center. `http://depts.washington.edu/nnmrec/about.html`.

[2] Outside the box. *Professional Boatbuilder*.

[3] Tidal Turbines. `http://www.soue.org.uk/souenews/issue7/tidalturbines.html`, March 2008.

[4] Marine Current Turbines. `http://www.marineturbines.com`, March 2011.

[5] McMaster-Carr. `http://www.mcmaster.com/#bearings/=bgltif`, March 2011.

[6] McMaster-Carr. `http://www.mcmaster.com/#ball-and-roller-bearings/=bgm3xv`, March 2011.

[7] Open Centre Turbine Technology Overview. `http://openhydro.com/techOCT.html`, March 2011.

[8] Verdant Power, LLC. Free Flow System. `http://verdantpower.com/what-systemsint/`, March 2011.

[9] Sylvain Antheaume, Thierry MaÃ®tre, and Jean-Luc Achard. Hydraulic darrieus turbines efficiency for free fluid flow conditions versus power farms conditions. *Renewable Energy*, 33(10):2186 – 2198, 2008.

[10] A.S. Bahaj, A.F. Molland, J.R. Chaplin, and W.M.J. Batten. Power and thrust measurements of marine current turbines under various hydrodynamic flow conditions in a cavitation tunnel and a towing tank. *Renewable Energy*, 32(3):407 – 426, 2007.

[11] W.M.J. Batten, A.S. Bahaj, A.F. Molland, and J.R. Chaplin. Hydrodynamics of marine current turbines. *Renewable Energy*, 31(2):249 – 256, 2006. Marine Energy.

[12] Michael M. Bernitsas, Kamaldev Raghavan, Y. Ben-Simon, and E. M. H. Garcia. Vivace (vortex induced vibration aquatic clean energy): A new concept in generation of clean and renewable energy from fluid flow. *Journal of Offshore Mechanics and Arctic Engineering*, 130(4):041101, 2008.

[13] C.A. Consul, R.H.J Willden, E. Ferrer, and M.D. McCulloc. Influence of solidity on the performance of a cross-flow turbine. Department of Engineering Science, University of Oxford, Oxford, UK.

[14] Mars G Fontana. *Corrosion Engineering*. McGraw-Hill.

[15] Chris Garrett and Patrick Cummins. Generating power from tidal currents. *Journal of Waterway, Port, Coastal, and Ocean Engineering*, 2004.

[16] Andrei-Mugur Georgesc, Sanda-Carmen Georgesc, Mircea Degerat, Sandor Berand, and Costin Ioan Cosoiu. Numerical modelling comparison between airflow and water flow within the achard-type turbine. In *2nd IAHR International Meeting of the Workgroup on Cavitation and Dynamic Problems in Hydraulic Machinery and Systems*.

[17] Alexander Gorlov. Development of the helical reaction hydraulic turbine. Technical report, MIME Department of Northeast University, 1998.

[18] Sang-Hun Han, Kwang-Soo Lee, Ki-Dai Yum, Woo-Sun Park, and Jin-Soon Park. Evaluation of helical turbine efficiency for tidal current power plant based on in-situ experiment. In *Asian and Pacific Coasts.*

[19] G P Hoya and A Guha. The design of a test rig and study of the performance and efficiency of a Tesla disc turbine. *Proceedings of the Institution of Mechanical Engineers, Part A: Journal of Power and Energy*, 2009.

[20] M.A. Kamoji, S.B. Kedare, and S.V. Prabhu. Performance tests on helical Savonius rotors. *Renewable Energy*, 34(3):521 – 529, 2009.

[21] Yusaku Kyozuka. An experimental study on the darrieus-savonius turbine for the tidal current power generation. *Journal of Fluid Science and Technology*, 2008th ser.(3.3), 2008.

[22] Verdant Power LLC and GCK Technology Inc. Intergration of the Gorlov helical turbine into an optimized hardware/software system platform. Technical report, Amesbury Tidal Energy Project, 2005.

[23] S. Mazumdar. *Composites Manufacturing: Materials, Product, and Process Engineering.* CRC Press LLC.

[24] I G Bryden Owen, A. Prototype support structure for seabed mounted tidal current turbines. *Proceedings of the Institute of Mechanical Engineers*, 219(4), 2005.

[25] Mitsuhiro Shiono, Katsuyuki Suzuki, and Seiji Kiho. Output characteristics of Darrieus water turbine with helical blades for tidal current generations. In *Proceedings of The Twelfth (2002) International Offshore and Polar Engineering Conference*, 2002.

[26] Tetsuya Wakui, Yoshiaki Tanzawa, Takumi Hashizume, and Toshio Nagao. Hybrid configuration of Darrieus and Savonius rotors for stand-alone wind turbine generator systems. `http://www2.iee.or.jp/ver2/honbu/14-magazine/log/2004/2004_02b_11.pdf`, 2004.

[27] D Wang, M Atlar, and R Sampson. An experimental investigation on cavitation, noise, and slipstream characteristics of ocean stream turbines. *Proceedings of the Institution of Mechanical Engineers, Part A: Journal of Power and Energy*, 2007.

[28] J. Zanette, D. Imbault, and A. Tourabi. A design methodology for cross flow water turbines. *Renewable Energy*, 35(5):997 – 1009, 2010.